PhD degree in Molecular Medicine (curriculum in Molecular Oncology)

European School Of Molecular Medicine (SEMM),

University of Milan and University of Naples "Federico II"

Settore disciplinare: Bio/10

The role of miR-340 in post-transcriptional regulation of the uPA-system in breast cancer

Valentina Buttiglione

IFOM, Milan

Matricola n. R09866

Supervisor: Dr. Nicolai Sidenius

IFOM, Milan

Anno accademico: 2014-2015

To Isabella Di Nanna, the who made me love this discipline and

Ezio Minervini, my scientific mentor, who always believed in me

“Ogni mio atomo è una festa di elettroni,

è la fisica delle emozioni,

è la scienza bellezza,

si procede per intuizioni”

Lorenzo Cherubini

TABLE OF CONTENTS

1. LIST OF ABBREVIATIONS

18S = 18S ribosomal RNA
α-SMA = α-smooth muscle actin
α2AP = α2-antiplasmin
ACTA2 = actin, alpha 2, smooth muscle, aorta
AGO = Argonaute
Ang-1 = angiotensin-1
AP1 = activation protein 1
AREs = AU-rich elements
ATF = amino terminal fragment
ATF1 = activating transcription factor 1
ATP = adenosine triphosphate
B2M = beta-2-microglobulin
BCL-2 = B-cell lymphoma 2
BrdU = thymidine analog 5-bromo-2'-deoxyuridine
BSA = bovine serum albumin
CAFs = cancer-associated fibroblasts
cAMP = cyclic adenosine monophosphate
CAV1 = caveolin 1
CCL2 = chemokine (C-C motif) ligand 2
CDK12 = cyclin-dependent kinase 12
CI = cell index
CIMPR/IGH-II = cation-independent mannose 6-phosphate/insulin-like growth factor-II receptor
CIS = carcinoma in situ
COL1A1 = collagen, type I, alpha 1
COM = cooperation region
CREB = cAMP response element-binding protein
CSF-1 = colony stimulating factor 1
CTCs = circulating tumour cells
CTF = CCAAT-binding transcription factor
CTF/NF-I = CCAAT-binding transcription factor nuclear factor I
CTGF = connective tissue growth factor
CXCL12 = chemokine (C-X-C motif) ligand 12
DCIS = ductal carcinoma *in situ*
DELFIA® = enzyme-linked immunosorbent assay
DFS = disease free survival
DGCR8 = Di George syndrome critical region gene 8
DHX36 = DEAH box protein 36
DMEM = Dulbecco's modified Eagle's medium
DTT = dithiothreitol
E_2 = oestradiol
ECM = extracellular matrix
EDTA = ethylenediaminetetraacetic

EGF = epidermal growth factor
EGFR = epidermal growth factor receptor
EGR = early growth response protein
ELISA = enzyme-linked immunosorbent assay
ER = oestrogen receptor
ERBB2 = Erb-B2 receptor tyrosine kinase
ERK = extracellular-signal-regulated kinase
Ets = E26 transformation-specific
FAK = focal adhesion kinase
FBS NA = foetal bovine serum north American
FBS SA = foetal bovine serum south American
fc = fold change
FGF = fibroblast growth factor
FGF-2 = fibroblast growth factor-2
FISH = fluorescence *in situ* hybridization
FN = fibronectin
GAPDH = glyceraldehyde-3-phosphate dehydrogenase
GFD = growth factor-like domain
GFP = green fluorescence protein
GPCR = G-protein-coupled receptor
GPI = glycosylphosphatidylinositol
GRE = glucocorticoid response element
HB-EGF = heparin-binding EGF-like growth factor
hCG = human chorionic gonodotropin
HCC = hepatocellular carcinoma
HEK = human embryonic kidney
HEPA = high-efficiency particulate arrestance
HGF = hepatocyte growth factor
HIF-1 = hypoxia-inducible factors 1
HMBS = hydroxymethylbilane synthase
hnRNP C = heterogeneous ribonuclear protein C
HOXD10 = homeobox D10
HPRT1 = hypoxanthine phosphoribosyltransferase 1
HPV = human papillomavirus
HR = hazard ratio
HRE = hypoxia-responsive element
HRP = horseradish peroxidase
IC = invasive carcinoma
ICAM1 = intercellular-adhesion molecule 1
IF = immunofluorescence
IGF = insulin growth factor
IHC = immunohistochemistry
IL-1β = interleukin-1β
IP = intraperitoneal injection
ISH = *in situ* hybridization
IVC = individually ventilated cages

JNK = Jun N-terminal kinase
KD = kringle domain
KLF4 = Kruppel-like factor 4
LFA-1 = lymphocyte-function-associated antigen-1
LN = laminin
LNA = locked nucleic acid
LOE = level of evidence
LOX = lysyl oxidase
LPS = lipopolysaccharide
LRP = low density lipoprotein receptor
Mac1 = macrophage I antigen
MAGP = microfibril-associated glycoprotein
MAPK = mitogen-activated protein kinase
microRNA = miRNA
MK2 = mitogen-activated protein kinase-activated protein kinase 2
MKI67 = marker of proliferation Ki-67
MMP = metalloproteinase
MNNG = methylnitronitrosoguanidine
MQ = Milli-Q
NF-κB = kappa-light-chain-enhancer of activated B cells
NFAR = nuclear factors associated with dsRNA
NGF = nerve growth factor
OS = overall survival
p = p value
PA-system = plasminogen activation system
PAI-1 = plasminogen activator inhibitor 1
PAI-2 = plasminogen activator inhibitor 2
CRS = cAMP-responsive element
PARN = deadenylase poly(A)-specific ribonuclease
PBS = phosphate buffered saline
PBS-T = phosphate buffered saline-Tween
PCI = protein C inhibitor
PCR = polymerase chain reaction
PDGF = platelet-derived growth factor
PDGFR = platelet-derived growth factor receptor
PFA = paraformaldehyde
PGK = phosphoglyceraldeide kinase
PI = propidium iodide
PI3K = phosphatidylinositol-3-kinases
PK = proteinase K
PKC = protein kinase C
PLAU = plasminogen activator, urokinase
PLAUR = plasminogen activator, urokinase receptor
Plg = plasminogen
Pli = plasmin
PMA = phorbol 12-myristate 13-acetate

PMSG = pregnant mare serum gonadotropin
PN-1 = protease nexin-1
PR = progesterone receptor
qPCR = quantitative polymerase chain reaction
Raf = rapidly accelerated fibrosarcoma
RCL = reactive centre loop
RGD = Arg-Gly-Asp
RHAU = DExH RNA helicase associated with AU-rich element
RNP = ribonucleoprotein
ROCK1 = Rho-associated, coiled-coil containing protein kinase 1
ROS = reactive oxygen species
rpm = revolutions per minute
RPMI = Roswell Park Memorial Institute
rt = room temperature
RT = reverse transcription
RTCA = label-free real-time cell-based assay
RTK = receptor tyrosine kinase
S100A4 = S100 calcium binding protein A4
SD = standard deviation
SDS = sodium dodecyl sulphate
SDS-PAGE = sodium dodecyl sulphate-polyacrylamide gel electrophoresis
SEM = standard error of the mean
SERPINE1 = serpin peptidase inhibitor, clade E member 1
SLRP = small leucine-rich proteoglycan
SMB = somatomedin B domain
SNAI1 = snail family zinc finger 1
SP-1 = specificity protein 1
SPARC = secreted protein acidic and rich in cysteine
suPAR = soluble urokinase-type plasminogen activator receptor
SW1/SNF = switch/sucrose non-fermentable
TAE = Tris-acetate-EDTA
TALEN= transcription activator-like effector nuclease
TAZ = tafazzin
TBE = Tris-borate-EDTA
TBS-T = Tris-buffered saline-Tween
TCDD = 2,3,7,8-tetrachlorodibenzo-p-dioxin
TERT = telomerase reverse transcriptase
TFE3 = transcription factor E-box 3
TGF-β = transforming growth factor, beta
TN = tenascin
TN = triple negative
TNF-α = tumour necrosis factor, alpha
TPs = touch preps
tPA = tissue-type plasminogen activator
TRBP = = TAR RNA binding protein
TRF = time-resolved fluorescence

TRS = TGF-β responsive sequence
TSP-1 = thrombospondin-1
TSS = transcriptional start site
UEF = urokinase enhancer factors
uPA = urokinase-type plasminogen activator
uPA-system = urokinase-type plasminogen activator system
uPAR = urokinase-type plasminogen activator receptor
USF-2a = upstream stimulatory factor-2a
VCAM = vascular-cell adhesion molecule 1
VEGF = vascular endothelial growth factor
VLDLR = very low density lipoprotein receptor
VN = vitronectin
WNT1 = wingless-type MMTV integration site family, member 1
YAP1 = yes-associated protein 1
ZNFs = zinc fingers

2. FIGURES INDEX

3. TABLES INDEX

4. ABSTRACT

The urokinase-type plasminogen activator system (uPA-system), whose main components are the serine protease uPA (*PLAU*), the cell surface receptor uPAR (*PLAUR*) and the uPA inhibitor PAI-1 (*SERPINE1*), has been extensively studied for its involvement in cancer pathogenesis. Specifically, nowadays the components of the uPA-system are well-characterised determinants for the prognosis of breast cancer. The regulation of the gene expression of the uPA-system components is very complex and depends on a plethora of stimuli acting both at transcriptional and post-transcriptional level. The uPA-system components are often over expressed in breast cancer but the detailed molecular mechanisms regulating the expression are still to uncover. In an expression analysis conducted on a cohort of unselected breast cancer patients, we found that the expression of *PLAU* and *PLAUR* is highly correlated. Meta-analyses of published experimental data and *in silico* studies pointed out the possibility that *PLAU*, *PLAUR* and also *SERPINE1* might be negatively regulated at post-transcriptional level by a microRNA, the miR-340. We experimentally validated the role of miR-340 as negative regulator of the expression of the three uPA-system components using MDA-MB-231, a triple negative breast cancer cell line. Microarray experiments, performed to characterise the global transcriptome changes induced by miR-340 in MDA-MB-231 cells, showed that miR-340 down regulates also the expression of desmoplastic reaction-related genes underlining a possible role of miR-340 in regulating tumour-associated genes. Notably, most of the identified miR-340 target genes were found indeed to be associated with poor clinical outcome in breast cancer. Functional studies carried out in MDA-MB-231 cells suggested that miR-340 might modulate cell proliferation, even if this effect was not confirmed *in vivo*. In order to better define the functional role of miR-340, we generated a miR-340 deficient mouse model, taken advantage of the zinc finger nuclease technology. Overall these data identify, for the first time, a single microRNA that is able to down regulate the expression of the three main

components of the uPA-system together with desmoplastic reaction and breast cancer prognosis-related genes, thus representing a new potential player in the pathogenesis of breast cancer.

5. INTRODUCTION

Breast cancer is the most common cancer in women worldwide. Despite the progresses in early diagnosis, surgical techniques and therapies, breast cancer is still the second cause of death in women (reviewed in[1]). The complexity in developing efficacious therapies that completely eradicate the disease is mainly due to the great heterogeneity of the neoplasm and the plasticity of the tumour microenvironment.

The main constituent of the microenvironment is the extracellular matrix (ECM). The ECM is a network of fibrous structural proteins embedded in a visco-elastic gel of glycosaminoglycans, proteoglycans and glycoproteins. In addition, a meshwork of secreted proteins and numerous stromal cells, including endothelial and immune cells, fibroblasts and adipocytes, complete the microenvironment composition. The communication between the microenvironment and the epithelial compartment is essential for many biological functions such as cell adhesion, proliferation, polarity, differentiation and apoptosis. The microenvironment may communicate to the epithelial compartment by changing structural properties and via transmembrane receptors. In the same way, secreted proteins derived from the epithelium, like growth factors and cytokines, binding ECM through glycosaminoglycans, can influence microenvironment remodelling altering matrix stiffness and/or inducing ECM proteolysis (reviewed in[2]). A proper regulation of the networks between the microenvironment and the epithelium is important for the correct homeostasis of tissues. The knowledge of the molecular mechanisms, which regulate genes acting on the microenvironment architecture and signalling, may be useful to define how these mechanisms are altered during tumour formation and progression.

The urokinase-type plasminogen activator system (uPA-system) is an important player in the homeostasis of the microenvironment both in normal and in pathological conditions. In the context of pathological conditions, it participates in the tumour microenvironment remodelling and in mediating the signalling between epithelium and stroma (reviewed in[3]).

In breast cancer the expression levels of the components of the uPA-system are associated with the outcome of the disease. Therefore, the characterisation of the molecular mechanisms regulating the uPA-system expression might disclose new cues to understand the machinery, which govern the plasticity of the microenvironment during breast cancer pathogenesis.

5.1 MAMMARY GLAND MICROENVIRONMENT

5.1.1 The extracellular matrix

The ECM of the mammary gland can be divided into three structurally different layers: the highly specialised basal lamina, bordering the basal membrane of mammary epithelial cells, the intra- and interlobular stroma, neighbouring the alveoli and lobules respectively and the fibrous connective layer.

5.1.1.1 Basal lamina

The basal lamina is the most specialised ECM compartment that directly underlies the mammary glands epithelium. The main components of the basal lamina are laminins, collagen IV, nidogens and perlecan (fig. 1).

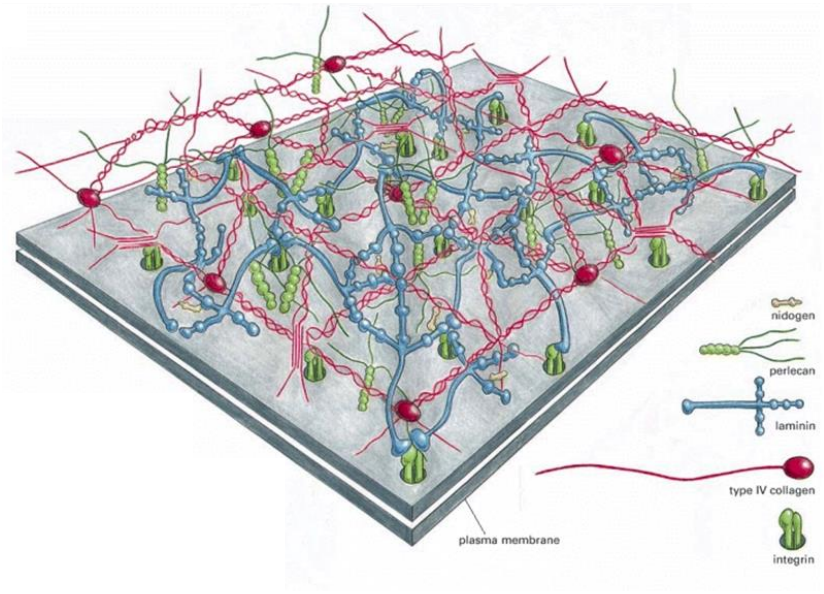

Adapted from figure 19-43 "Molecular Biology of the Cells" 5/e (© Garland Science 2008)

Figure 1: basal lamina.

The main components of the basal lamina: laminins (blue), collagen IV (red), nidogens (yellow) and perlecan (green) are schematically depicted.

Laminins (LNs) are large heterotrimeric glycoproteins present in 15 different combinations, according to five α, three β and three γ subunits. LNs are in physical contact with epithelial cells acting as critical mediator of ECM-epithelium interactions. In mammary microenvironment the most abundant LN is LN111 (previously named LN1), which is mainly released by myoepithelial cells[4]. LN111 is one of the major components of the basal lamina. It participates in the maintenance of the breast tissue (reviewed in[5]) especially in mammary cells differentiation[6], polarization[7] and acinar formation[8].

Collagen IV is a network-forming collagen consisting of heterotrimer comprised of six possible genetically distinct α chains distributed in a tissue-specific manner[9]. Specifically in the mammary glands, collagen IV has been supposed to be the primary scaffold protein of the basal lamina (reviewed in[10]), which provides the principal mainstay for mammary epithelial cells[11,12]. Furthermore cryptic domain of collagen IV fragments might show anti-angiogenic effects (reviewed in[13]).

Nidogens are sulphated glycoproteins, synthesised by fibroblasts in different tissues[14,15], which are incorporated into the basal lamina upon secretion[15]. They are present in 1:1 ratio with LNs and in the mammary microenvironment they act as stabiliser of the basal lamina creating a bridge between LN111 and collagen IV[16].

Perlecan is a proteoglycan composed of a core protein covalently linked to the proteoglycan heparin sulphate. The mammary epithelial cells themselves can secrete heparin sulphate behaving as a source of perlecan. Perlecan is essential for the assembly of basal lamina in several organs[17] and for the bone marrow matrix functions[18]. Moreover perlecan can also synergise the biological effect of the fibroblast growth factor (FGF) family[19]. A perlecan soluble C-terminal fragment, called endorepellin, is able to inhibit endothelial cell migration and angiogenesis altering the morphogenesis of capillaries[20].

5.1.1.2 Intra- and interlobular stroma

The intralobular stroma is a collagen-rich structure adjacent to the basal lamina, which surrounds the alveoli; the interlobular stroma refers to band of stroma, which envelopes cluster of alveoli composing a single lobule (fig. 2). The principal constituents of this layer are the fibrillar collagen and several ECM components such as fibronectin, tenascin family proteins, secreted protein acidic and rich in cysteine (SPARC) and small leucine-rich proteoglycan family proteins (reviewed in[2]).

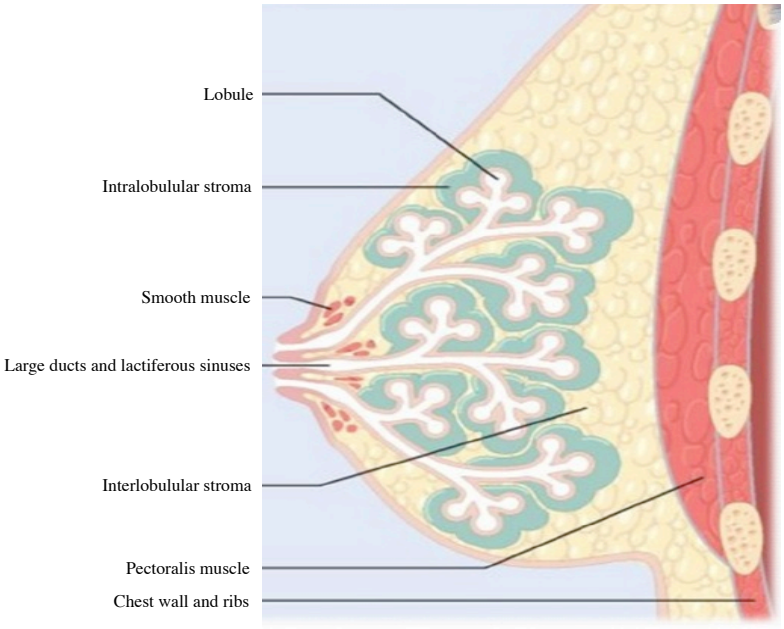

Figure 2: anatomic distribution of the intra- and interlobular stroma.

The intralobular stroma (light green) surrounds the alveoli; whereas the interlobular stroma (yellow) envelopes cluster of alveoli, which compose a single lobule.

The main collagen molecule involved in the fibrillar collagen is collagen I together with collagen III and V. Fibrillar collagen I is considered the stroma backbone of mammary glands, it is mainly produced by mesenchymal cells as fibroblasts, chondroblasts, osteoclasts and odontoblasts, during normal development, and by activated fibroblasts in the wound healing process. The collagen I synthesis is a multi-step process starting from a collagen precursor. The precursor is assembled in a triple helix procollagen structure, which is further arranged by different peptidases in the mature form. The mature form is stabilised by covalent intra- and intermolecular cross linking by the lysyl oxidase (LOX) resulting in the basic fibrillar structure (reviewed in[21]). In the mammary tissue the interplay between fibrillar collagen, integrins and growth factors is necessary to the mammary duct development[22] and evolution[23,24].

Fibronectin (FN) is a dimeric glycoprotein implicated in cell adhesion, migration, proliferation and branching morphogenesis. During the involution of the mammary gland, high level of a specific class of endopeptidases, known as metalloproteinases (MMPs),

highly correlates with FN fragments suggesting a positive feedback loop between these two players. This feedback loop is usually aimed to the clearance of epithelium since the MMPs can remodel the ECM and FN fragments are able to induce apoptosis[25].

The tenascin (TN) family consists of five members: TN-C, TN-R, TN-W, TN-X and TN-Y, which generally mediate anti-adhesive phenotype interfering with the interaction between the transmembrane heparin sulphate receptor synden-4 and the FN receptor $\alpha_5\beta_1$ integrin[26]. In mammary glands the most abundant TN isoforms are the TN-C and TN-X. Up regulation of TN-C has been observed in breast cancer (reviewed in[27]). As opposed to TN-C, TN-X seems to have a role in the maintenance of tissue elasticity[28].

SPARC is a secreted glycoprotein that mediates cell-matrix interaction binding collagen I and LN111 (reviewed in[29]). SPARC exhibits anti-adhesive properties causing cell rounding[30]; in contrast SPARC positively regulates FN assembly and integrin-linked kinase activity eliciting FN-induced stress fiber formation[31].

The small leucine-rich proteoglycan (SLRP) family members were initially associated to structural support participating in collagen fiber formation; recent findings have shown that SLRPs are implicated in signal transduction and cellular processes binding directly cell surface receptors and growth factors (reviewed in[32]). In the mammary glands the most abundant SLRPs are decorin and biglycan (reviewed in[33]). Decorin is a secreted glycoprotein composed of a core protein covalently bound to a single chondroitin sulphate or dermatan sulphate (reviewed in[34]). Different biological functions have been conferred to decorin. It is involved in the proper spatial alignment of stroma collagen fibers[35], in inhibiting epidermal growth factor receptor (EGFR) signalling through EGFR internalization and degradation by caveolar endocytosis[36] and in sequestering the transforming growth factor beta (TGF-β)[37]. In breast cancer decorin has the ability to suppress the Erb-B2 receptor tyrosine kinase 2 (ERBB2) signalling both *in vitro* and *in vivo*[38]; furthermore decorin negative affects angiogenesis since it is able to down regulate vascular endothelial growth factor (VEGF) expression in tumour cells[39]. Biglycan, as

decorin, is a glycoprotein composed of a core protein covalently bound to two glycosaminoglycans[34]. Biglycan may be hormonally regulated[40,41] and may participate in elastic fiber formation[42].

5.1.1.3 Fibrous connective tissue

The third layer of ECM consists of acellular fibrous connective tissue characterised by the absence of epithelium and the presence of fibroblasts, immune cells and high fibrillar collagen amount. This layer shares many ECM proteins with the other layers such as fibrillar collagen, FN, TNs, SLRPs and SPARC; the unique feature of fibrous connective tissue is the presence of the elastic fibers (reviewed in[2]).

The elastic fibers provide structural support and elasticity to different tissues. As for collagen I, the elastic fibers formation is a multi-step process starting with the binding of a secreted protein called microfibril-associated glycoprotein (MAGP) with the glycoprotein fibrillin. Several MAGP/fibrillin complexes are firstly assembled into 10- to 20 nm microfibrils and subsequently the microfibrils are associated with elastin, fibulins and proteoglycans. Also in this case the stabilization of the elastic fibers occurs through LOX-mediated cross linking (reviewed in[2]). The function of elastic fibers in mammary glands is still not clear. A correlation between mammary density, tissue tension and increase of breast cancer risk has been observed[43].

5.1.2 The stroma cells

The microenvironment is not only made up of structural acellular components but also of stromal cells. Different cell populations are present in the ECM meshwork including endothelial, immune and stem cells, pericytes, fibroblasts and adipocytes. The fibroblasts are the stroma cells that mainly orchestrate the ECM functions and regulate the recruitment of the other cellular components.

5.1.2.1 Fibroblasts

As described by Maller *et al.*[2] fibroblasts are the main components of the connective tissue. They are elongated cells with extended cell protrusions located within the fibrillar matrix. They represent a very heterogeneous family and different fibroblast phenotypes have been identified according with their secretome. Although several fibroblast markers have been identified, the classification of the different fibroblasts phenotype is not straightforward since none of the markers are exclusive. Fibroblasts synthesise many ECM components such as type I, III, IV and V collagen, LNs and FN, thus contributing to the formation of the basal lamina[44]. Fibroblasts secrete also ECM-degrading proteins, whose best example is represented by the MMPs, suggesting their role in the regulation of ECM homeostasis. Fibroblasts not only exert a role in the ECM homeostasis but also affect the epithelium compartment through both paracrine factors and mesenchymal-epithelial interaction, as it has been demonstrated in the development of mammary glands (reviewed in[45]). Fibroblasts play a prominent role also in pathological conditions such as wound healing (reviewed in[46]) and fibrosis (reviewed in[47]) sustaining the production of ECM components. Fibroblasts participating to wound repair and fibrosis are different from those present in normal conditions and are defined "activated". The activated fibroblasts are characterised by the expression of α-smooth muscle actin (α-SMA) and called myofibroblasts. Fibroblast activation may be induced by different stimuli released from injured tissue including TGF-β, epidermal growth factor (EGF), platelet-derived growth factor (PDGF) and FGF-2 (reviewed in[48]) or by direct cell-cell communication with leukocytes through adhesion molecules such as intercellular-adhesion molecule 1 (ICAM1) and vascular-cell adhesion molecule 1 (VCAM)[49]. As for resting fibroblasts, also activated fibroblasts may secrete different factors. They are still able to secrete MMPs to facilitate ECM turnover and remodelling[50]. In addition, they secrete a great amount of growth factors such as hepatocyte growth factor (HGF), insulin growth factor (IGF), nerve growth factor (NGF), wingless-type MMTV integration site family, member 1 (WNT1), EGF and FGF-2

providing proliferative signals to the surrounding epithelial cells (reviewed in[51]). The activated fibroblasts can also communicate with immune cells through the release of cytokines such as chemokine (C-C motif) ligand 2 (CCL2, also known as MCP1)[52]. Once the wound is repaired, the number of activated fibroblasts decreases and the resting phenotype is restored. During fibrosis activated fibroblasts create a self-perpetuating autocrine loop, which stimulates the activation of other fibroblasts often until organ death. This phenomenon has been also observed in activated fibroblasts, which make up the tumour microenvironment.

5.2 TUMOUR MICROENVIRONMENT

One of the first definition of tumour described it as "a wound that do not heal" forewarning the role of tumour microenvironment in cancer progression[53]. Nowadays the role of the microenvironment is well established in each step of tumourigenesis. Indeed, tumour microenvironment, dynamically arranging its composition, creates a proper milieu for tumour implantation, progression and metastases (reviewed in[54]) (fig. 3). These changes require heterotypic signalling and back-and-forth reciprocal interaction between the tumour parenchyma and the stroma (fig. 4).

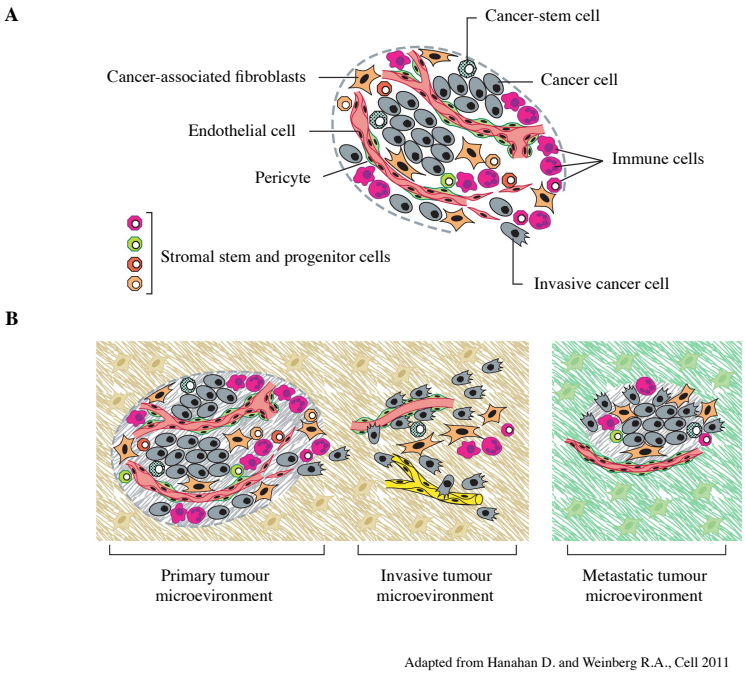

Figure 3: tumour microenvironment.

(A) Cellular components of the tumour microenvironment. (B) During cancer progression the transition from *in situ* to invasive carcinoma is characterised by the degradation of the basal lamina and the desmoplasia reaction. The microenvironment of a metastatic tumour has to sustain tumour migration, adhesion and homing of the tumour cells in a distant organ.

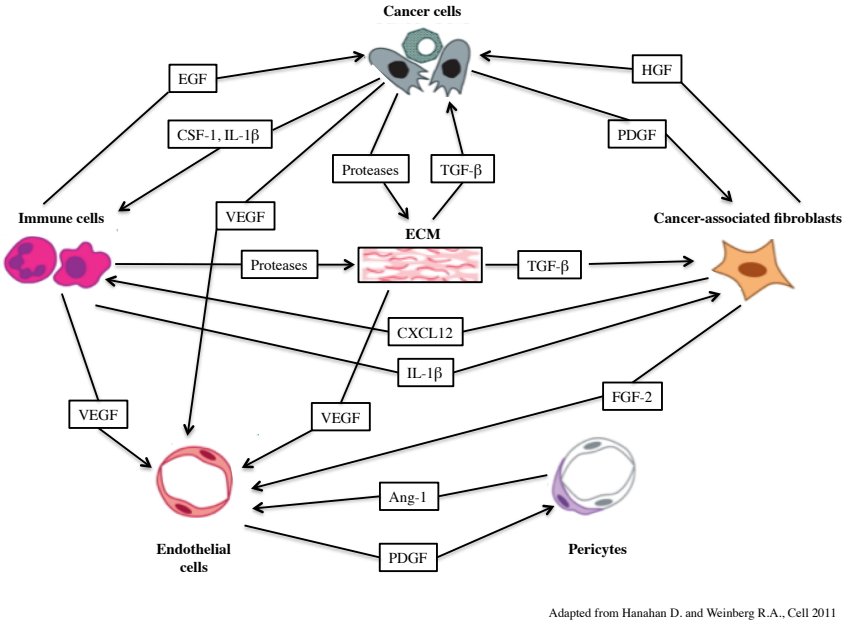

Figure 4: cross talk between tumour and stroma.

The main heterotypic signals between the tumour parenchyma and the stromal cells are schematically represented.

In the early stage of tumourigenesis, cancer cells form a neoplastic lesion embedded in an organ-specific microenvironment within the basal lamina but separated from the healthy epithelium. This tumour stage is called carcinoma *in situ* (CIS). CIS is associated with a tumour microenvironment similar to those observed during wound healing, characterised by an increased number of fibroblasts, enhanced capillary density and a high amount of collagen I and fibrin deposition[55]. Furthermore, the tumour microenvironment may sustain different pro-migratory pathways modulating the release and availability of growth factors by direct interaction with tumour cells through integrins (reviewed in[56]).

In the transition from CIS to invasive carcinoma (IC), the tumour cells invade the surrounding stroma. The evolution to invasive carcinoma is characterised by the degradation of basal lamina (reviewed in[57]). Furthermore, the invasive tumours show an abnormal tumour stroma and increased deposition of ECM (reviewed in[58]). This phenomenon is known as desmoplastic reaction, distinguished by an increased amount of fibrillar collagen, fibronectin, proteoglycans and TN-C[55].

The cellular components that mainly orchestrate the dynamic plasticity of the tumour microenvironment are the cancer-associated fibroblasts.

5.2.1 Cancer-associated fibroblasts

As described by Xing *et al.*[59], a specific group of fibroblasts, called cancer-associated fibroblasts (CAFs), is well established to actively participate to tumour progression and invasion providing a highly specialised tumour microenvironment. CAFs, as the normal counterpart, are highly heterogeneous and morphologically similar to myofibroblasts, even if perpetually activated. They may derive from resident fibroblasts, bone marrow, epithelial and endothelial cells after the acquisition of genetic or epigenetic alterations that may be induced by tumour-secreted paracrine factors. CAFs contribute to every step of tumourigenesis. In the early stages, tumour cells need specific pro-proliferative factors to

sustain their growth. CAFs secrete various growth factors and cytokines that support the proliferative rate of tumours including TGF-β, HGF, S100 calcium binding protein A4 (S100A4) and chemokine (C-X-C motif) ligand 12 (CXCL12). CAFs may enhance tumour growth also inducing mutations in cancer cells secreting the highly mutagen reactive oxygen species (ROS) under acidic conditions (reviewed in[60]). Furthermore, CAFs may affect cancer growth interfering with their metabolic pathways sustaining the switching to the faster anaerobic glycolysis, even in presence of oxygen[61]. CAFs are also involved in promoting tumour invasion and metastasis formation through transient heterotypic cell-cell contacts or secreting paracrine factors (reviewed in[48]). Specifically, the cross talk between the cancer cells and CAFs can induce both types of cells to modify tumour epithelium and microenvironment respectively to favour metastasis formation. For this reason, CAFs can mediate both ECM proteolytic and structural modification to create a path for the cancer cells to invade a distant organ. To this purpose, CAFs may secrete various matrix-degrading proteases, as MMPs, and their activators such as the urokinase-type plasminogen activator (uPA) (reviewed in[59]). CAFs may support tumour also sustaining a chronic inflammatory microenvironment and immune tolerance (reviewed in[62]). CAFs may recruit immune cells, including macrophages, neutrophils and lymphocytes through direct or direct mechanisms. Directly, secreting specific chemoattractant factors as thrombospondin-1 (TSP-1), which affects both angiogenesis and immune cells recruitment (reviewed in[63]); indirectly, since the CAFs-secreted MMPs may degrade ECM components, such as FN and collagen, whose fragments display both chemotactic properties for leukocytes and the ability to modulate the proliferation of the immune cells (reviewed in[59]). CAFs are also present in the cancer stem cell niches where they may regulate the differentiation and proliferation of cancer stem cells providing a unique specialised microenvironment (reviewed in[59]). The tumour niche comprised of CAFs is molecularly different from that of a normal stroma, even if several tumour niche-secreted factors have been also found in the normal counterpart[64]. Further studies are needed to better define the

cancer stem cell niche composition, origin and the role of CAFs in this type of microenvironment.

5.3 THE UROKINASE-TYPE PLASMINOGEN ACTIVATOR SYSTEM

The urokinase-type plasminogen activator system (uPA-system) is an important player in the homeostasis of the microenvironment both in normal and in pathological conditions, including wound healing and tumours (reviewed in[65]). The main components of the uPA-system are the serine protease uPA, the cell surface receptor uPAR and the uPA inhibitor PAI-1. The uPA-system-mediated functions may be divided into two interconnected branches: the proteolytic and the non-proteolytic functions (fig. 5). The uPA-system was firstly studied for its involvement in the modulation of pericellular proteolysis since it triggers the generation of plasmin at the cell surface. The non-proteolytic functions are based instead on the ability of uPAR-initiated cell signalling to support a plethora of biological functions. uPAR-mediated signalling requires the cross talk of the receptor with different players in the pericellular space, such as vitronectin (VN) and several membrane signalling receptors including integrins, receptor tyrosine kinases (RTKs) and G-protein coupled receptors (GPCPs).

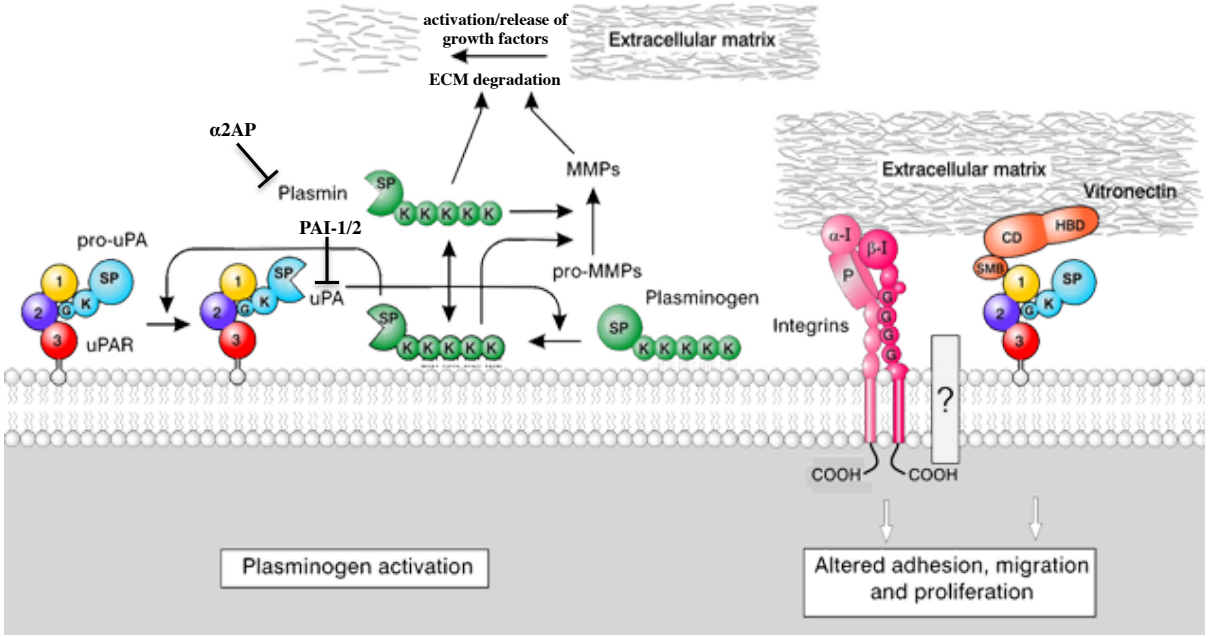

Adapted from Huret J.L., Extracellular - Atlas of Genetics and Cytogenetics in Oncology and Haematology

Figure 5: uPA-system functions.

The proteolytic and non-proteolytic functions of the uPA-system are schematically represented. The proteolytic function requires the activation of uPA, which in turn cleaves plasminogen thus to generate the active protease plasmin. In the ECM plasmin may cleave ECM components, promote the activation and release of growth factors and generate the active form of the MMPs, which further sustain matrix degradation. The proteolytic activities of uPA and plasmin are antagonised by PAI-1/PAI-2 and α2AP, respectively. uPAR-mediated cell signalling is mainly orchestrated by uPAR-VN interaction and the cross talk with integrins.

5.3.1 The urokinase-type plasminogen activator

The serine protease family is a class of proteases specialised in the degradation of peptide bonds through a serine residue located into the active site (reviewed in[66]). A member of this class of proteases is the urokinase-type plasminogen activator (uPA).

uPA is protease of 411 amino acids composed of two α helices and two anti-parallel β strands arranged into two disulphide bridge-linked polypeptide chains: the N-terminal A chain and the C-terminal B chain. The A chain harbours a kringle (KD) and a growth factor-like domain (GFD). The KD and the GFD domains, also denoted as amino terminal

fragment (ATF), are connected to the B chain through a linker region containing the activation site. The B chain contains the catalytic triad Asp[120], His[205] and Ser[356] [67].

As described by Andreasen *et al*.[68], cells release uPA as an inactive single-chain zymogen (pro-uPA), which is converted into the active two-chains uPA by plasmin-mediated cleavage of the peptide bond Lys[158]-Ile[159]. Active uPA in turn activates plasminogen (Plg), the zymogen form of plasmin (Pli), through the cleavage of the peptide bond Arg[506]-Val[561]. As a consequence, uPA and Pli create a positive feedback loop to active each other. This function is also ascribed to the homologue tissue-type plasminogen activator (tPA). While uPA-generated Pli is mainly involved in the pericellular proteolysis, tPA is believed primarily to mediate Pli generation in the fibrinolysis process. Despite the predominant role of plasmin, uPA may be cleaved by other proteases, which are involved in the activation process or in the generation of different uPA forms. Kallikrein, factor XIIa and cathepsins may activate uPA (reviewed in[69]). Indeed, *in vivo* experiments, conducted on a plasminogen deficient mouse model, demonstrated that a glandular kallikrein promotes the conversion of uPA into the active form[70]. Other proteases participate to the cleavage within the linker region generating instead the low molecular weight uPA, the N-terminal truncated variant[71,72].

Once Pli is generated, it may be involved in several ECM remodelling processes since it shows broad substrate specificity. Indeed, it may promote the cleavage of different extracellular matrix proteins such as LNs, FN and fibrin. Moreover, Pli may sustain both the conversion of the zymogen form of MMP-3, MMP-9, MMP-12 and MMP-13 into active MMPs and the activation and release of growth factors including FGF-2 and TGF-β. The involvement of uPA in promoting plasmin generation highlights the importance of uPA regulation for a balanced ECM remodelling.

5.3.2 The urokinase-type plasminogen activator receptor

The complexity of the uPA-system functions is mainly due to the great versatility of the urokinase-type plasminogen activator receptor (uPAR). uPAR is indeed not only involved in sustaining the uPA-mediated proteolytic functions but it is also able to orchestrate several signal transduction pathways interacting with the matricellular protein VN and different transmembrane signalling receptors.

uPAR is synthesised as a protein of 335 amino acids characterised by a 22 amino acids long-N-terminal secretion signal peptide and a 30 amino acids long-C-terminal, which is cleaved upon the attachment to the plasma membrane[73]. The mature form is a highly glycosylated protein of 283 amino acids composed of three homologous domains DI, DII and DIII, belonging to the Ly-6/uPAR protein domain family (reviewed in[74]), tethered to the plasma membrane by a glycosylphosphatidylinositol (GPI) anchor.

In normal conditions, uPAR is moderately expressed in various tissues including lungs, kidneys, spleen, vessels, uterus, bladder, thymus, heart, liver and testis. uPAR expression increases as a result of extensive tissue remodelling[75] or in pathological conditions such as cancer, inflammation and infections (reviewed in[76]). Two types of post-translational modifications are believed to globally and irreversibly regulate uPAR expression and activity: uPAR shedding and uPAR cleavage. The uPAR shedding consists of the release of the whole protein moiety from the cell surface. This process is mediated by phospholipases such as phosphatidylinositol-specific phospholipase D or by proteases including plasmin[77] and tissue kallikrein 4[78]. As a result a soluble form of uPAR, known as suPAR is released. uPAR shedding prevents most of cell surface uPAR activity but the soluble fragments may exert different functions, namely chemotactic mediators[79]. This mechanism allows a negative regulation of the number of receptor located at the cell surface. uPAR cleavage occurs in the linker region connecting the DI and DII and is mediated by several proteases including uPA[80], plasmin[80], neutrophil elastase (indicated in[74]) and different MMPs[81]. The cleavage causes the release of the N-terminal domain DI

thus inactivating uPAR binding with most of its ligands. Also in this case the generated fragments may acquire different biological activities as demonstrated both *in vitro*[82] and *in vivo*[83].

The first characterised role of uPAR is in regulating extracellular proteolysis acting as uPA receptor. In this context, it does not only cooperate with uPA for the conversion of plasminogen into active plasmin but it may also mediate the internalization of inactive uPA:PAI-1[84]/protease nexin-1 (PN-1)[85] complexes in collaboration with the low density lipoprotein receptor (LRP) family[86]. Subsequently, it was discovered that uPAR functions go beyond its role as a receptor for uPA. Many biological functions of uPAR occur indeed independently of uPA proteolytic activity. These functions are mainly related to the regulation of the cross talk between epithelium and the surrounding microenvironment through the physical or functional interaction with: VN[87], adhesion receptors belonging to the integrin family[88] and other interactors such as RTKs (e.g. EGFR[89] and platelet-derived growth factor receptor (PDGFR)[90]), caveolin[91], LRP family[86,92,93], GPCRs[94], the cation-independent mannose 6-phosphate/insulin-like growth factor-II receptor (CIMPR/IGH-II) implicated in the targeting of uPAR to lysosome[95]. All these interactions deeply affect cell proliferation, adhesion and migration, through the activation of signalling molecules including the proto-oncogene tyrosine-protein kinase Src, the serine kinase rapidly accelerated fibrosarcoma (Raf), the focal adhesion kinase (FAK), p130Cas and the extracellular-signal-regulated kinase (ERK)/mitogen-activated protein kinase (MAPK) (reviewed in[96]).

Despite the high number of uPAR interactors that have been proposed, uPA and VN are the only two binding partners that have been deeply characterised from a biochemical point of view.

5.3.2.1 uPAR-uPA binding

The uPA-uPAR binding is a high affinity interaction that does not involve additional co-factors. The resolution of the crystal structure of the uPA:uPAR complex has shown that the binding occurs between the GFD domain of uPA and a large hydrophobic pocket made up of all the three-uPAR domains[97,98]. As a consequence, the interaction is mainly dependent on the integrity of the three-domain structure of the receptor[99] but also on the type and degree of glycosylation[100].

5.3.2.2 uPAR-VN interaction

VN is an adhesive glycoprotein of 459 amino acids mainly expressed as soluble protein in the plasma as well as a multimeric form in the ECM. It consists of a N-terminal somatomedin B domain (SMB)[101] followed by a long connecting peptide harbouring the integrin binding site Arg-Gly-Asp (RGD)[102] and C-terminal hemopexin-like domains[103]. In the ECM, VN acts as matricellular protein, namely a protein that does not participate in the ECM structural arrangement but rather in the cross talk at the cell-matrix interface, binding ECM components, cell surface receptors (e.g. integrins, uPAR)[104] or other proteins present in the pericellular space such as PAI-1[105], uPA[106], Plg[107] and heparin[108].

The uPAR-VN interaction has been fully characterised. It consists of a high affinity binding[109], which requires the intact three-domain structure of the receptor[110]. Indeed the binding is mediated by a composite epitope on the DI/DII uPAR interface and the SMB domain of VN[111,112]. The binding of uPA to uPAR increases the affinity of uPAR for VN as a consequence of both uPA-induced uPAR conformational changes[113,114] as well as uPAR dimerization and/or oligomerization[115,116,117]. Trp^{32} and Arg^{91} were identified as uPAR key residues for the uPAR-VN interaction[99,111].

5.3.2.3 uPAR-integrins interaction

In addition to uPA and VN, important players of the uPAR-mediated non-proteolytic functions are integrins. Integrins are cell-surface adhesion receptors that anchor cells to the ECM and transduce signals between the microenvironment and the cells. Integrins influence cell shape and mediate intracellular signalling interacting with molecules that regulate cytoskeletal organization and signal transduction. Several studies associate integrins to uPAR-uPA-mediated cell migration, adhesion and proliferation[89,118,119]. The uPAR/integrin interaction is still mater of debate since conflicting results have been obtained. The interaction between uPAR and the FN receptor $\alpha_5\beta_1$[120] as well as the VN receptor $\alpha_v\beta_3$[121] and $\alpha_v\beta_5$[122] have been reported. Moreover, uPAR has also been shown to interact with integrin receptors expressed on the immune cells, such as the cell surface macrophage I antigen (Mac1, also known as $\alpha_M\beta_2$ integrin)[123]. Specific uPAR residues involved in the integrin binding have been proposed: Glu^{134}, Glu^{135}, Ser^{245}, His^{249} and Asp^{262} suggesting the existence of multiple and diverse binding sites. The binding requires the intact three-domain structure of uPAR[69] and is promoted by uPA and integrin ligand binding to uPAR and integrins, respectively[120]. In spite of these findings, a comprehensive study, aimed to specifically characterised the uPAR integrin-binding sites, failed to identify any of these sites[104]. Moreover, recently it has been shown that uPAR-mediated cell adhesion to VN triggers a novel type of integrin signalling that is independent of integrin–matrix engagement but dependent on membrane tensions supporting the hypothesis that uPAR and integrins are not necessarily in physical contact to mediate cell signalling[124].

5.3.3 The plasminogen activator inhibitor 1

The serpin (serine proteases inhibitor) family includes a wide range of serine protease inhibitors characterised by a globular structures consisting of three β-sheets and 9 α-helices and a common inhibition mechanism. Approximately 20 amino-acids-long reactive

centre loop (RCL) is the hub of the mechanism of inhibition of the serpine family. Indeed, the reactive centre peptide bond (P_1-P_1') within the RCL, is the part of the inhibitor which interacts with the specific protease by a 1:1 stable complex[125,126]. The P_1 residue confers the substrate specificity.

The plasminogen activator inhibitor-1 (PAI-1) and α2-antiplasmin (α2AP) belong to the serpine family and represent the main negative regulators of the Pli generation. While α2AP directly inhibits Pli, PAI-1 exerts the inhibitory effect on Pli generation targeting both uPA and tPA. Three other members of the serpin family, PAI-2, PN-1 and the protein C inhibitor (PCI) have also been shown to inhibit uPA and tPA at physiologically relevant rate (reviewed in[127]). Among these different serine protease inhibitors, PAI-1 is the fastest and specific inhibitor of uPA and tPA (reviewed in[128]).

PAI-1 is either 379 or 381 amino acids glycosylated protein due to the presence of two possible cleavage sites for the N-terminal signal peptide. PAI-1 is mainly released by endothelial cells, megakaryocytes as well as smooth muscle cells and stored in the platelets. After the release in the bloodstream, PAI-1 circulates as active form in complex with VN[129]. In order to inhibit uPA, PAI-1 binds active uPA generating a covalent uPA-PAI-1 complex. When bound to uPAR, this complex is internalised, through LRP-related protein family-mediated mechanism, into clathrin-coated vesicles[130]. uPA-PAI-1 complex is degraded into the lysosomes while uPAR is recycled back to the cell surface[131]. Specifically, as described by Dupont *et al.*[128], during the complex formation the P_1-P_1' bond of PAI-1 ($Arg^{348/358}$-$Met^{349/359}$) is inserted into the uPA active site, therefore uPA can cleave the P_1-P_1' bond and the P_1 residue is linked to the active site of uPA by an ester bond. The N-terminal of the RCL is inserted into the β-sheet A, relocating uPA to the opposite pole of PAI-1. The distortion of the active site completely impairs the catalytic activity of the enzyme. Premature RCL insertion into the β-sheet A results in the conversion of the active PAI-1 into the so-called latent state. *In vitro*, PAI-1 latency can be bypassed by denaturation and refolding of the inhibitor.

PAI-1 can bind VN not only in the blood but also in the pericellular space. The binding occurs within the SMB domain through an epitope, which overlaps with the uPAR binding site; therefore PAI-1 and uPAR may compete for the binding of VN[132]. In addition, the binding of PAI-1 with VN sterically prevents also the binding of integrins with the RGD motif of VN[133,134]. As a consequence, PAI-1 does not act only as negative regulator of plasmin generation but it is also involved in the modulation of cell adhesion and migration[132]. In addition, it has been shown that PAI-1 has a role in the negative regulation of apoptosis as well as PAI-2[135].

5.4 uPA-SYSTEM AND CANCER

The role of uPA-system in cancer is well established. Both branches of the uPA-system functions have a role in each step of tumourigenesis. It is widely believed indeed that the role of the uPA-system in promoting tumour growth and dissemination is mediated by its proteolytic activity capable of remodelling the ECM and generating pro-tumour factors. Additionally, important processes occurring in cancer such as cell migration, proliferation and release from states of dormancy have been linked to uPAR-initiated cell signalling independently of extracellular proteolysis.

5.4.1 Tumour formation

The tumour formation is enhanced by an uncontrolled cell proliferation sustained by an alteration of the apoptosis pathways. uPA-mediated Pli generation may support mitogenic pathways through the activation and release of growth factors that can act both on epithelial and endothelial cells. These factors include FGF-2 and VEGF, targeting the endothelial cells, and HGF and IGF-1, which affect the epithelial compartment (reviewed in[136]). uPAR-initiated cell signalling may also activate pathways involved in sustained proliferation. In MCF-7, an oestrogen positive breast cancer cell lines, PAI-1, uPA, uPAR

and very low density lipoprotein receptor (VLDLR) have been shown to cooperate in promoting ERK/MAPK signalling[137]. Furthermore, down regulation of uPAR results in cell dormancy in epidermoid carcinoma HEp cancer cells as a consequence of an impaired uPAR-$\alpha_5\beta_1$ integrin interaction which causes a reduction of ERK and FAK mediated-signalling[138]. A recent *in vivo* study provided direct evidence that the uPAR-VN interaction influences tumour growth likely because the interaction strengthens the uPAR-dependent adhesion and proliferation signalling[139].

5.4.2 Angiogenesis

Another important biological event necessary for tumour growth and invasion is angiogenesis. Angiogenesis requires the formation of new blood vessels, a process mediated by the migration of endothelial cells and new ECM synthesis (reviewed in[140]). In this context, the uPAR-uPA interaction is involved both in ECM remodelling (reviewed in[141]), allowing the flux of new endothelial cells in the tumour stroma, and in the activation and release of pro-angiogenic factors such as FGF-2, TGF-β and VEGF (reviewed in[136]). Moreover, angiostatin[142] and K1-5[143], products derived from plasmin proteolysis, can act as potent angiogenesis inhibitors. As a consequence, uPAR-uPA interaction may exert both pro- and anti-angiogenic effects that can be dependent on the stage of angiogenesis. Also PAI-1 shows a dual behaviour that may be related to the concentration of the inhibitor. It can sustain angiogenesis at basal concentration (nanomolar range) but an increase to a micromolar range results in an anti-angiogenic effect[144].

5.4.3 Invasion

The first characterised cancer-related uPA-system function is the trigger of pericellular proteolysis thus to support cancer invasion. During invasion cancer cells penetrate and remodel ECM according to the different tumour needs. As reviewed by Duffy[145], this demand is accomplished by different proteases such as MMPs, cathepsins, heparinases,

uPA and Pli. The positive feedback loop between uPA and Pli is fundamental to sustain ECM proteolysis. As already mentioned, despite uPA, Pli may sustain extensively ECM proteolysis degrading different ECM components including fibrin, LN, FN and perlecan. In addition, plasmin may further support ECM proteolysis activating the precursor form of MMPs, which in turn break down ECM components. The uPA-system proteolytic functions may also favour the release of pro-invasive factors. ECM-associated TGF-β may be released as a consequence of protease-dependent ECM degradation. Free TGF-β can exert a dual role in tumourigenesis, tumour suppressor in early stage and metastasis promoter in later steps[146]. Finally, ECM degradation products can acquire pro-tumour features as shown for LN5[147] and FN[148]. The role of uPA-system-mediated ECM remodelling to sustain invasion[149] and intravasation[150] has been also shown *in vivo* performing experiments in chicken embryos.

5.4.4 Metastasis

In order to metastasise, tumour cells migrate from their primary site to a distant organ. Therefore migration and adhesion are two important biological processes involved in the metastasis formation. Both branches of the uPA-system functions are involved in tumour metastases. The proteolytic functions may sustain migration through a limited ECM degradation and release of motility factors such as FGF-2 and TGF-β, while uPAR-initiated cell signalling can enhance cell adhesion in consequence of the cross talk with integrins (reviewed in[96]). It has been shown that the expression of uPA, Plg/Pli, uPAR and PAI-1 is up regulated during migration[151] and several studies have suggested the importance of the uPA-system components in this process. Indeed, antisense oligonucleotides against uPA inhibit migration *in vitro*[152] and Plg/Pli enhances cell migration since an enzymatically inactive uPA, but proficient for uPAR binding, inhibits cell migration of endothelial cells[153]. In monocytes a pro-migratory effect is also exerted by uPAR alone through the interaction with the integrin $\alpha_M\beta_2$[154]. PAI-1 inhibits instead cell

migration, independently of the inhibition of uPA, interfering in the binding of VN with integrins[133,134].

5.4.5 uPA-system in breast cancer

A great deal of effort was invested to determine the localisation of the uPA-system components in breast cancer tissue. Immunohistochemistry and *in situ* hybridization analyses conducted on breast cancer patients' tissues have shown that the uPA-system components are mainly localised in the stromal compartment[155,156,157]. Specifically, colocalisation experiments revealed that uPA is mainly expressed by a subset of myofibroblasts, macrophages and capillary endothelial cells[158]. Nevertheless, the expression of uPA in the tumour epithelial compartment is not completely ruled out[159,160]. uPAR expression in ductal breast carcinoma is particularly evident in macrophages[161]. Yet, the localisation of uPAR in a subpopulation of different type of cancers has been also proposed[159,160,162]. Subsequently, Nielsen *et al.*[163] unambiguously demonstrated the prominent localisation of both uPA and uPAR in myofibroblasts and macrophages in early invasive foci of ductal carcinoma *in situ* (DCIS). Also PAI-1 staining indicated a stromal localisation especially in a subpopulation of myofibroblasts, myoepithelial cells and endothelial cells[164] but the localisation in breast and skin tumour cells was also observed[159,160].

Breast cancer provided the first evidence of the role of uPA-system components as prognostic factors. The prognostic value of uPA and PAI-1 in breast cancer has been extensively studied along the years. Duffy *et al.*[165] firstly showed that in primary breast carcinoma elevated levels of uPA were associated with poor prognosis. Subsequently, Look *et al.*[166] revealed that high level of PAI-1 was also associated with poor outcomes in primary breast cancer. Nowadays uPA and PAI-1 are among the strongest independent breast cancer prognostic markers with the highest level of evidence (LOE-1)[167]. In lymph node-negative patients, the protein levels of uPA and PAI-1 are indeed useful to design

individualized treatment strategy. Specifically, the quantification of uPA and PAI-1 levels allows the identification of patients that may benefit from adjuvant chemotherapy[168]. High level of uPAR is also associated with negative outcome in breast cancer, even if the prognostic impact is less strong than uPA and PAI-1[169]. Interestingly, the mRNA level of a specific uPAR transcript variant, lacking the exons four and five (uPAR-del4/5), was significantly associated with disease-free survival (DFS)[170]. Both the wild type and uPAR-del4/5 have been reported to be independent prognostic markers in lymph node negative breast cancer[171]. The localisation of uPAR may influence its impact on breast cancer prognosis since, in invasive breast carcinoma, the level of uPAR expression in cancer cells, but not in stromal cells, was significantly associated with patients' prognosis, thus contributing to a more aggressive phenotype[172].

The widely adopted breast cancer classification, based on immunohistochemistry analysis, identifies three major breast cancer subtypes: hormone receptor positive (oestrogen and progesterone receptor positive, ER^+/PR^+), ERBB2 positive ($ERBB2^+$) and triple negative (TN). The uPA-system components show some controversial correlation with the hormone receptor status. *In vitro* studies conducted in human breast cancer cell lines reported an arguable association between oestrogens and uPA expression. On the one hand, oestradiol (E_2) was shown to enhance uPA expression in ER^+ breast cancer cell lines[173], on the other hand E_2 is able to reduce uPA expression both at mRNA and protein level in ER^+ MDA-MB-231 variant eliciting a reduction of invasive capacity[174]. Also PAI-1 expression was found to be negatively affected by E_2 in ER^+ MDA-MB-231 variant; while no effect was observed on uPAR expression[175]. *In vivo* experiments reported that progesterone inhibits tumour growth of the triple negative breast cancer cell line MDA-MB-231, which highly expresses uPA-system components[176]. Nevertheless, in breast cancer patients a negative correlation between high levels of uPA[177] and PAI-1[178] with the ER and PR status was shown. On the contrary, no correlation between uPAR level and ER/PR status was observed[179]. In spite of these divergences, uPA, uPAR, PAI-1 levels were shown to be

predictive for the benefit of hormone therapy[180,181]. The ERBB2$^+$ breast cancer represents approximately the 20% of breast cancer subtypes. It is characterised by the over expression of ERBB2 (also known as HER-2), which is associated with poor clinical outcomes. uPA/PAI-1 levels and ERBB2 status were considered independent prognostic markers, which provide complementary information about DFS, overall survival (OS) and therapy in lymph-node negative patients[182]. Several studies showed the co-amplification and co-expression of uPAR and ERBB2 in advanced breast cancer circulating tumour cells (CTCs), in touch preps (TPs) of frozen primary breast carcinomas[183,184] and in bone marrow micro metastatic cells[185]. The possibility of cooperation between uPAR and ERBB2 has been also supported *in vitro*. Different studies showed indeed the existence of a cross talk between EGFR family and uPAR in different cancer cell lines, which enhanced a proliferative signalling mainly by ERK and Src[89,186,187,188].

5.5 GENE REGULATION OF THE uPA-SYSTEM

The involvement of the uPA-system in a plethora of biological functions suggests a complexity in gene regulation both at gene and transcript level. The characterisation of the main players implicated in regulating the gene expression of the uPA-system components may be useful to define the molecular mechanisms, which alter the uPA-system expression during tumourigenesis.

5.5.1 Transcriptional regulation

5.5.1.1 *PLAU*

The uPA gene *PLAU* is located at the positive strand of chromosome 10q22.2. It is 6.4 kb long and encodes for two transcript variants: the preprotein isoform 1 and the isoform 2. The isoform 2 is alternatively spliced at the 5' end, as a result of an additional downstream

transcriptional start site (TSS), thus generating a shorter transcript, with a distinct N-terminal, compared to isoform 1. The two transcripts are translated into the same identical protein uPA.

PLAU is expressed endogenously at low level in a wide range of cells and its expression may be induced by various signalling molecules including growth factors, cytokines, peptide and steroid hormones, genotoxic agents and cell morphology changes (reviewed in[189]) .

The *PLAU* minimal promoter region contains a canonical TATA-box, a 200 bp GC-rich region and one copy of CAAT sequence (fig. 6). The GC-rich region and the CAAT sequence are targeted by two main transcription factors: specificity protein 1 (SP1) and CCAAT-binding transcription factor (CTF) respectively, which are involved in the basal expression of *PLAU*. SP1 may be recruited upon ERK/Jun N-terminal kinase (JNK)-mediated phosphorylation[190].

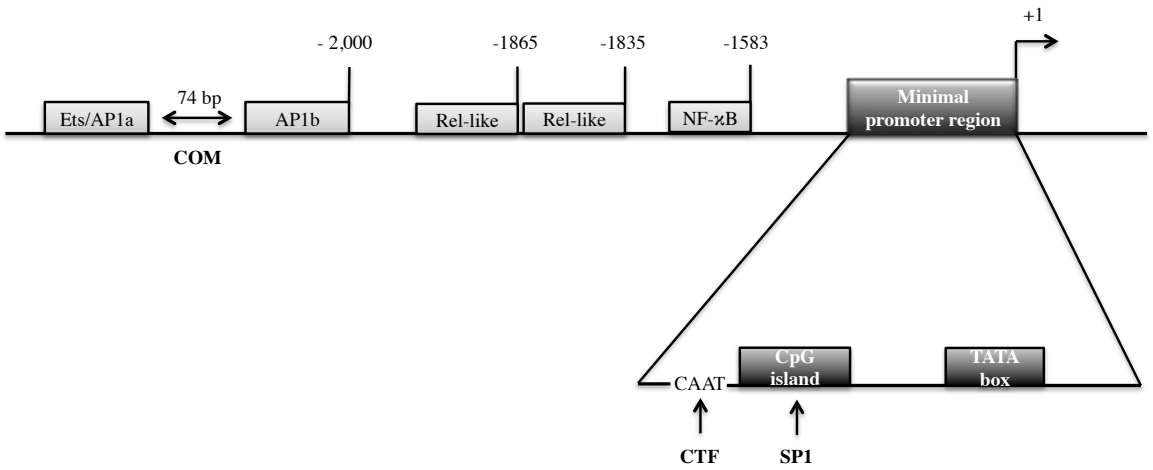

Figure 6: schematic representation of *PLAU* promoter.

PLAU minimal promoter region contains a canonical TATA-box, a 200 bp GC-rich region and one copy of CAAT sequence. The GC-rich region and the CAAT sequence are targeted by two main transcription factors: SP1 and CTF, respectively. Additional transcription factor binding sites are reported in the promoter region.

PLAU transcription may be also mediated by several enhancers located at -2.0 kb from the TSS[191]. Enhancer activity requires the cooperation with an upstream conserved composite

E26 transformation-specific (Ets)/activation protein 1a (AP1a) (Ets/AP1a) and a downstream AP1b sites. The two AP1 sites are separated by 74 bp long region, known as cooperation mediator (COM), containing binding sites for several urokinase enhancer factors (UEF) (fig. 6). In addition, another conserved Ets/AP1 site is present in the opposite orientation of the human uPA gene (reviewed in[189]).

The Ets sites, characterised by the minimal consensus sequence GGAA, may bind many Ets family members even if only Ets1[192,193,194,195] and Ets2[196,197] have been found to activate *PLAU* expression. The AP1 sites are recognised by the transcription factor complex AP1, consisting of either homodimer of Jun or heterodimer of Jun and Fos family members[198,199]. The transcription factors, that bind the Ets/AP1 sites, may be activated by several MAPK signalling-mediated intracellular stimuli. As a consequence, the *PLAU* transcription responds to several stimuli including phorbol 12-myristate 13-acetate (PMA)[200], okadaic acid[201], cytoskeletal reorganization[201], mechanical stimuli (e.g. laminar shear stress[202]), growth factors (e.g. FGF-2[203], HGF[204,205] and IGF[206]), oncogenes[207,208], genotoxic agents (e.g. UV[209] and methylnitronitrosoguanidine (MNNG)[210]) and cytokines (e.g. tumour necrosis factors-α (TNF-α)[211] and colony stimulating factor 1 (CSF-1)[212,213]). These signalling molecules mediate *PLAU* expression predominantly by ERK-induced signalling. On the contrary, genotoxic agents and TNF-α follow JNK-mediated *PLAU* promoter activation (reviewed in[189]). Furthermore, AP1 site may also mediate the repression of *PLAU* by the transcription factor E2F1[214].

The transcription of *PLAU* is also controlled by nuclear factor kappa-light-chain-enhancer of activated B cells (NF-κB) transcription factor since conserved NF-κB-like binding sequence at -1583 and two additional Rel-like binding sites in tandem repeats at -1865 and -1835 are located in *PLAU* human promoter[215] (fig. 6). The NF-κB binding sequences seem to be sensitive to PMA stimulation that lead to the generation of NF-κB heterodimeric complexes: c-Rel/p65 and p65/p50[215]. The NF-κB binding sites are required for the $\alpha_v\beta_3$/VN-induced down regulation of *PLAU*[216].

Cyclic adenosine monophosphate (cAMP) responsive enhancer was located in porcine uPA gene 3.4 kb upstream the cap site[217,218]. It is composed of three protein-binding domains, recognised by cAMP response element-binding protein (CREB), the activating transcription factor 1 (ATF1) and the LFB3 transcription factors[219]. cAMP-mediated *PLAU* activation in cell line derived from pig kidney epithelia has been shown to require physical interaction between CREB/ATF1 and LFB3 and to follow a tissue specific hormonal regulation[220]. In the end a negative regulator of the enhancer activity was found at -600 bp[221].

In tumours, it has been shown that the over expression of *PLAU* seems to be mediated by NF-κB through the constitutive expression of RelA in pancreatic adenocarcinomas[222]. β-catenin, instead, promotes *PLAU* expression in colorectal cancer through two different consensus motifs located at -737 (TBE1) and -562 (TBE2)[223]. The deregulation of *PLAU* expression has been also ascribed to changes in the methylation status of the promoter. Indeed, high *PLAU* expression is associated to a hypomethylation of the promoter in the triple negative breast cancer cell line MDA-MB-231[224]; while low *PLAU* expression, observed in the oestrogen receptor positive breast cancer cell line MCF-7, is due to the hypermethylation of the *PLAU* promoter[225].

5.5.1.2 *PLAUR*

The uPAR gene *PLAUR* is located at the negative strand of chromosome 19q13.31 and consists of seven exons. Exon 1 encodes the 5'UTR and the signal peptide while the exons 2-3, 4-5, 6-7 encodes the domains DI, DII and DIII, respectively[226]. Different splicing variants spanning 22 to 24 kb are reported, even if a complete characterisation has not been fully assayed yet[227]. Use of an alternative exon 7, lacking the GPI anchor, so as to encode for a soluble form of *PLAUR*, was documented both in mouse[228] and human[229]; variants lacking exon 5 and 4-5 have been also described[226,227]. The different transcript variants may

be translated in likewise different proteins, even if the most abundant is the one derived from the transcript variant 1[227].

PLAUR is expressed in many different cell types at low level in a tissue specific manner[230] (reviewed in[189]). Several stimuli may enhance *PLAUR* expression including oncogenes, cytokines, hormones and growth factors (reviewed in[189]).

A strong promoter regulates *PLAUR* expression. The promoter region, which shows the maximal activity, consists of 188 bp between -141 and +47 relative to the TSS[231]. It is characterised by the lack of conventional TATA and CAAT boxes but the presence of a short CpG-rich island, recognised by SP1 transcription factor[231]. Several sequences related to consensus cis-acting elements for AP1 (-70; -184)[232], AP2 (-170)[231], NF-κB (-45)[233] and SP1 transcription factors (-94; -103)[231], involved in the basal *PLAUR* expression (reviewed in [189]) have also been identified (fig. 7). The Kruppel-like factor 4 (KLF4) has been also identified as new transcription factor, which promotes *PLAUR* expression[234].

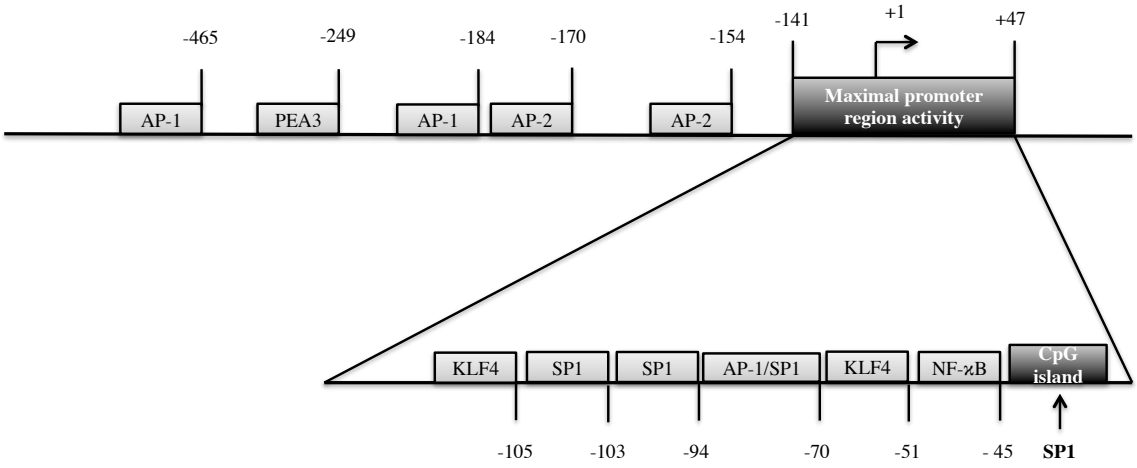

Figure 7: schematic representation of *PLAUR* promoter.

The promoter region, which shows the maximal activity, consists of 188 bp between -141 and +47. It is characterised by the lack of conventional TATA and CAAT boxes but the presence of a short CpG-rich island recognised by SP1 transcription factor. The additional transcription factor binding sites are reported in the promoter region.

Different studies provided some biological mechanisms involved in *PLAUR* transcription. Namely, PMA[235,236] and Ras-dependent[237] *PLAUR* expression involves a combination of

downstream ERK/JNK activation, which elicits the nucleus translocation of c-Jun/JunD heterodimers; in turn c-Jun/JunD activates *PLAUR* expression binding the AP1 site. Furthermore, it has been shown that TGF-β promotes *PLAUR* transcription through the binding of SP1 at -70 bp from the TSS in human monocyte-like cells U937[238]. A silencing motif has been also identified at -249 bp consisting of PEA3/Ets binding site[239] (fig. 7). PEA3 is involved in the silencing of *PLAUR* upon uPAR-β_3 integrin interaction[239], thus supporting the hypothesis of a feedback loop between uPAR-mediated adhesion and proteolysis. In addition, over expression of the integrin binding protein β_3-endonexin decreases *PLAUR* expression through the binding with the p50/p65 transactivation complex thus inhibiting the association of the κB site to the NF-κB transcription factor[240].

PLAUR is highly expressed in almost all cancer tissue[241,242,160] and a predominant expression in stroma compartment has been observed[163]. Tumour-specific transcription factors binding a AP2/SP1 site have been identified in gastrointestinal tumours[243]. Moreover, two AP1 consensus motifs have been shown to be required for the PMA-inducible *PLAUR* expression in colon cancer cells[235,232]. Recently, it has been observed that the over expression of B-cell lymphoma 2 (BCL-2) in breast cancer cells, in hypoxia condition, provokes SP1-mediated *PLAUR* expression induced by ERK1/2 signalling[244].

5.5.1.3 *SERPINE1*

The PAI-1 gene *SERPINE1* is located at the positive strand of chromosome 7q22.1. It is transcribed into a single pre-mRNA, which may generate two different transcripts: a long isoform 3.2 kb long and a short one 2.2 kb long. The two mRNAs codify for the same protein since they differ only for the polyadenylation site, which confers a more extended 3'UTR to the long transcript[245,246].

SERPINE1 is expressed in almost all cell types but mainly in adipocytes, hepatocytes and endothelial cells and the expression may be induced by different stimuli including growth factors, inflammatory cytokines and hormones (reviewed in[189]).

SERPINE1 promoter is characterised by a consensus TATA box and the presence of several binding sites for AP1, AP2, CCAAT-binding transcription factor nuclear factor I (CTF/NF-1) and SP1 transcription factors (reviewed in[189]) (fig. 8).

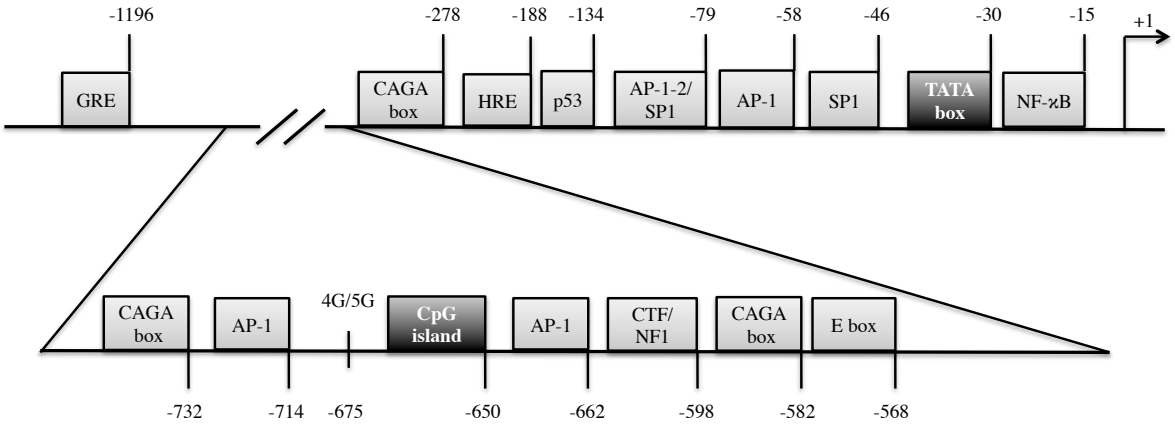

Figure 8: schematic representation of *SERPINE1* promoter.

SERPINE1 promoter is characterised by a consensus TATA box and is responsive to several stimuli. The main transcription factor biding sites, together with the polymorphism 4G/5G are reported.

*SERPINE*1 transcription is susceptible to PMA stimulation, which enhances the binding of c-Jun homodimers to AP1 sites[247,248]. Transcription factors, belonging to switch/sucrose non-fermentable (SW1/SNF) family of proteins, have been identified to induce *SERPINE*1 transcription both in human[249] and mouse[250].

An extracellular signal particularly involved in the induction of *SERPINE1* expression is TGF-β. In the human hepatocellular carcinoma cell line HepG2, sequences displaying high homology to the consensus binding sites for CTF/NF-I and the ubiquitous factor E-box have been identified as TGF-β responsive elements[251]. Thereafter, in the same cell line other three TGF-β responsive elements, termed CAGA boxes, have been found (fig. 8). They cooperate for TGB-β-mediated *SERPINE1* expression through the interaction with SMAD3/SMAD4 heterodimers[252]. In human hepatoma Hep3B cell line a 12 bp-long sequence, called TGF-β responsive sequence (TRS), which overlaps with the CAGA box, has been reported to mediate a strong transcriptional activation upon TGF-β binding when multiple copies are located upstream of the promoter[253]. In fibrosarcoma-derived HT 1080

cells, it has been shown that the transcription factor E-box 3 (TFE3)-binding protein synergises with SMAD3/SMAD4 complex to mediate TGF-β induction of *SERPINE1* in a SMAD3 phosphorylation-dependent manner. This synergism acts through the simultaneous binding of TFE3 with an E-box spanning -568 to -563 bp, and of the SMAD3/SMAD4 with a sequence immediately upstream the CAGA boxes (-590 to -572)[254]. Another example of TGF-β regulation of the *SERPINE1* expression has been proposed: TGF-β is able to elicit the interaction between SMAD3 and SP1 through two SP1-binding sites[255]. This new mechanism might underline the predominance of SP1 site in TGF-β-dependent *SERPINE1* expression against the TGF-β-responsive elements. Indeed, SP1 mediates *SERPINE1* transcriptional activation by other mediators including glucose/glucosamine[256,257], fatty acids[258] and angiotensin II[259].

Another important signal implicated in the regulation of *SERPINE1* expression is cAMP. Indeed, an increase of intracellular cAMP level promotes a decrease of *SERPINE1* expression[260]. The mechanism proposed hypothesises that cAMP inhibits PMA-induced transcription via the proximal AP1 site interfering with the c-Jun homodimer binding[261].

Glucocorticoids are potent promoters of *SERPINE1* expression in different cells and tissues (reviewed in[262]). Two glucocorticoid-responsive elements have been identified in *SERPINE1* promoter between positions -100 to +75 and -800 to -549[263] but show little homology with the standard glucocorticoid response element (GRE) consensus sequence suggesting an indirect mechanism of activation.

SERPINE1 may be responsive also to the glucose; indeed high level of *SERPINE1* has been observed in diabetes[264]. Glucose regulates *SERPINE1* expression through two SP1 sites located between -85 to -42 bp in vascular smooth muscle cells[265]. The exact mechanism involved in the glucose-mediated *SERPINE1* expression has not been fully understood. In pathological conditions such as obesity and insulin-resistance an increase of PAI-1, TNF-α, TGF-β and insulin levels has been observed. In this context, *SERPINE1* promoter activation seems to be mediated by TNF-α via, at least partially TGF-β

activation [266]; indeed a functional NF-ϰB binding site responsive to TNF-α has been located at -15 kb in *SERPINE1* promoter [267] (fig. 8). The over expression of *SERPINE1* may be also due to insulin[268]. Ligand-bound insulin receptor can trigger the activation of both ERK and phosphatidylinositol-3-kinases (PI3K) and the former sustains *SERPINE1* expression through AP1 transcription factor[269]. Finally, *SERPINE1* gene may be also negatively regulated by the E2F family members[214] that are transcription factors known to regulate cell-cycle-related genes.

An unusual mechanism of increase in basal transcription of *SERPINE1* is based on the allele-specificity. One polymorphism of *SERPINE1*, consisting of a single nucleotide insertion/deletion (4G/5G), is identified in the promoter region (fig. 8). The 4G allele has been associated with higher plasma PAI-1 activity[270]. Transcriptional studies have shown that both alleles bind a specific transcription factor but only the allele 5G is also able to interact with a repressor protein[271].

Other mediators of *SERPINE1* expression include the serum in quiescent cells[272], endotoxin[273] and lipopolysaccharide (LPS)[274] in endothelial liver cells and growth factors such as EGF[275], heparin-binding EGF-like growth factor (HB-EGF)[276], VEGF[277,278] and FGF-2[279].

Malignant and invasive tumours show an up regulation of PAI-1. The expression of *SERPINE1* may be related to the onco-suppressor p53 through the binding with a p53-binding site located at -159 to -134 on the *SERPINE1* promoter[280] (fig. 8). In addition, *SERPINE1* expression is regulated by hypoxia. Hypoxia is a phenomenon occurring in different pathological condition including tumour (reviewed[281]). This condition supports the activation of several genes through an increase of the hypoxia-inducible factors 1 (HIF-1) transcription factor level[282]. *SERPINE1* is strongly positively regulated by hypoxia in human endothelial cells[283] and different mechanisms have been suggested. In rat hepatoma cells putative hypoxia-responsive elements (HRE) 1 and HRE2 have been characterised[284]. Yet the upstream stimulatory factor-2a (USF-2a) interacts with HRE1 down regulating

SERPINE1 expression[285]. Therefore HIF-1 and USF-2a balance the effect of hypoxia on *SERPINE1* expression. Also in HepG2 cells HIF-1-dependent *SERPINE1* expression is mediated by a HRE (fig. 8); furthermore, in the same cells, it has been reported that hypoxia-mediated *SERPINE1* induction may be suppressed by p38MAPK and PI3K inhibitors[286]. A similar behaviour has been also observed in freshly prepared human keloid-derived fibroblasts[287].

5.5.2 Regulation of mRNA stability

5.5.2.1 *PLAU*

PLAU mRNA stability is dependent on either positive or negative regulators, which have been characterised over the last years.

In LLC-PK_1 pig kidney epithelial cells, it has been observed that *PLAU* mRNA, induced by cAMP or PMA, shows a short half-life of 70 minutes but the inhibition of the protein synthesis by cycloheximide, puromycin or pentamycin stabilises *PLAU* mRNA[288,289]. In the same cells, it has been observed that *PLAU* mRNA half-life can be prolonged by down regulation of the protein kinase C (PKC)[290] and Ca^{2+} [291]. In addition, in human colon cancer cells HCT116, PMA and cycloheximide increase *PLAU* mRNA accumulation acting both at transcriptional and post-transcriptional level[292]. The metastatic rat mammary tumour cell line MAT 13762 shows high *PLAU* level that may be affected upon dexamethasone treatment[293]; in human transformed keratinocyte cell line, 2,3,7,8,-tetrachlorodibenzo-p-dioxin (TCDD) stabilises *PLAU* mRNA[294].

The finding that the insertion of *PLAU* 3'UTR upstream the poly(A) of a stable globin mRNA makes it unstable suggested that the main determinants of *PLAU* mRNA instability are located within the 3'UTR[295]. Three regions have been found to contribute to the instability of *PLAU* mRNA: a sequence with a stem-structure, a region requiring on going transcription to destabilise the mRNA and the ARE sequences[295]. The latters are the most

important defined mRNA instability elements. They consist of AU-rich sequences defined as AU-rich responsive elements (AREs). The AREs are characterised by pentameric (AUUUA) or nonameric (UUAUUUAUU) sequences[296,297] and are classified into three classes (I, II, III) according to the presence or not of the pentamer and how these motifs are arranged[298]. *PLAU* 3'UTR harbours 50 nt long highly conserved class I ARE characterised by two distinct AUUUA and AUUUUUA motifs[295]. It was firstly defined as the region responsible for *PLAU* mRNA stabilisation induced by the down regulation of PKC[295]. The increase of *PLAU* expression observed in breast cancer cells is mainly due to an impairment of ARE-mediated mRNA degradation that results in a longer mRNA half-life[299]. The ARE-mediated *PLAU* mRNA degradation mechanism has been found to depend *in vitro* on the binding of the heterogeneous ribonuclear protein C (hnRNP C) to the AREs sequence[299]. On the contrary, the constitutive activation of mitogen-activated protein kinase-activated protein kinase 2 (MK2) sustains *PLAU* mRNA stability[300,301] likely through the cytoplasmic accumulation of the ARE-binding protein HuR, whose interaction with the AREs stabilises *PLAU* mRNA[300]. Other AREs binding proteins have been identified: nuclear factors associated with dsRNA (NFAR) and DExH RNA helicase associated with AU-rich element (RHAU) (also known as DEAH box protein 36 (DHX36))[302]. The latter provided a mechanism for the ARE-dependent degradation of *PLAU* mRNA. Namely, DHX36 recruits the deadenylase poly(A)-specific ribonuclease (PARN) and exosomes to *PLAU* 3'UTR AREs. DHX36 and PARN synergise the degradation of mRNA through the PARN-mediated deadenylation and the displacement of the mRNA stabiliser AREs binding proteins HuR and NFAR by a DHX36-adenosine triphosphate (ATP)-dependent mechanism. The hydrolysis of ATP elicits the association of exosomes to the AREs thus directing the mRNA degradation[302].

5.5.2.2 *PLAUR*

The first characterised post-transcriptional stabilisers of *PLAUR* mRNA were pro-inflammatory agents such as PMA, LPS and TGF-β in lung carcinoma cells[303,304]. Subsequently, phosphoglyceraldeide kinase (PGK), a *PLAUR* mRNA binding protein, which binds a 51 nt long sequence within the coding region, has been identified. Over expression of PGK in lung carcinoma cells line results in a decrease of *PLAUR* mRNA level and cell surface uPAR protein expression[305].

In line with *PLAU* regulation of mRNA stability, also *PLAUR* 3'UTR harbours an approximately 50 nt conserved class I ARE, marked by the nonameric motif (UUAUUUAUU)[306]. Indeed, experiments conducted in Jurkat T and HeLa cells showed that this region confers instability to a β-globin mRNA suggesting that *PLAUR* 3'UTR is fundamental for the regulation of mRNA instability. In addition, it has been found that the lymphocyte-function-associated antigen-1 (LFA-1) induces *PLAUR* mRNA stabilisation[306] as well as the AREs binding protein HuR[300]. In *PLAUR* transfected kidney cells[307] and in non-small cell lung cancer primary cells[308], it has instead been reported that uPA acts at *PLAUR* post-transcriptional level increasing the activity of a novel unknown factor. The binding of this factor to the coding region of *PLAUR* mRNA seems to stabilise the transcript.

5.5.2.3 *SERPINE1*

In line with the other uPA-system components, *SERPINE1* mRNA stability depends on both AREs within the 3'UTR and several different signalling molecules.

As reviewed by Nagamine *et al*.[189], the 3'UTR of the longest *SERPINE1* transcript shows one copy of the AUUUA, which confers less stability compared to the shorter counterpart. On the other hand, the signalling molecules able to affect *SERPINE1* mRNA stability include growth factors, cytokines and hormones. In human HepG2 hepatoma cell line, TGF-β[309] and insulin[310] increase the 3.2 kb transcript half-life but no effect is observed in

the 2.2 kb transcript. Conversely, IGF-1 stabilises both *SERPINE1* transcripts[310]. 8-bromo-cAMP, a cyclic nucleotide analogous, causes a decrease of *SERPINE1* mRNA level in HTC rat hepatoma cells; while *SERPINE1* 3'UTR may affect the instability of a β-globin mRNA in a cAMP-dependent manner[311]. This observation suggests that PAI-1 cAMP-responsive elements (PAI-CRS) might be located within *SERPINE1* 3'UTR, as it has been later demonstrated[311,312]. Even if PAI-CRS binding proteins have been isolated, their role in *SERPINE1* mRNA level regulation has not been completely elucidated yet. Other regulators of *SERPINE1* mRNA half-life have been defined including the osteogenic protein-1[313], angiotensin II[314,315] and *Rickettsia rickettsii* infection[316].

5.6 uPA-SYSTEM AND microRNAs

5.6.1 microRNAs

microRNAs (miRNAs) are a class of small, approximately 21 nt-long, non-coding RNAs involved in the post-transcriptional regulation of gene expression. The majority of microRNAs are encoded from dedicated miRNA gene loci whereas roughly the 30% derived from introns of protein-coding genes. The process of miRNA biogenesis is schematically illustrated in fig. 9. In the nucleus the microRNA sequence is transcribed by a RNA polymerase II (Pol II) into a capped, spliced and polyadenylated primary double strand miRNA (pri-miRNA)[317], which may give rise to a single miRNA or cluster of miRNAs. The pri-miRNA is folded into a hairpin structure characterised by an imperfect base-paired stem and is processed into a mature miRNA by the RNase III type endonucleases DROSHA and DICER in a two-steps mechanism. Specifically, the DROSHA and Di George syndrome critical region gene 8 (DGCR8) form a complex (called microprocessor), which fosters the DROSHA-mediated cleavage of one strand portion of the pri-miRNA thus generating 60-70 nucleotides-long hairpin double strand precursor miRNA (pre-miRNA)[318,319]. The pre-miRNA is exported into the cytoplasm by

exportin 5[320] where it is further cleaved by the RNAse III DICER, complexed with the TAR RNA binding protein (TRBP), to generate the mature double strand miRNA[321]. Subsequently, one strand, generally the 3', is degraded while the 5' end is selected as functional mature miRNA[322]. In order to induce repression of the gene expression, the mature miRNA is assembled into the ribonucleoprotein (RNP) complex micro-RNPs (miRNPs), also known as miRNA-induced silencing complex (miRISCs), through the interaction with the Argonaute (AGO) family protein, key components of the miRISCs, together with GW182 family proteins (Gregory 2005).

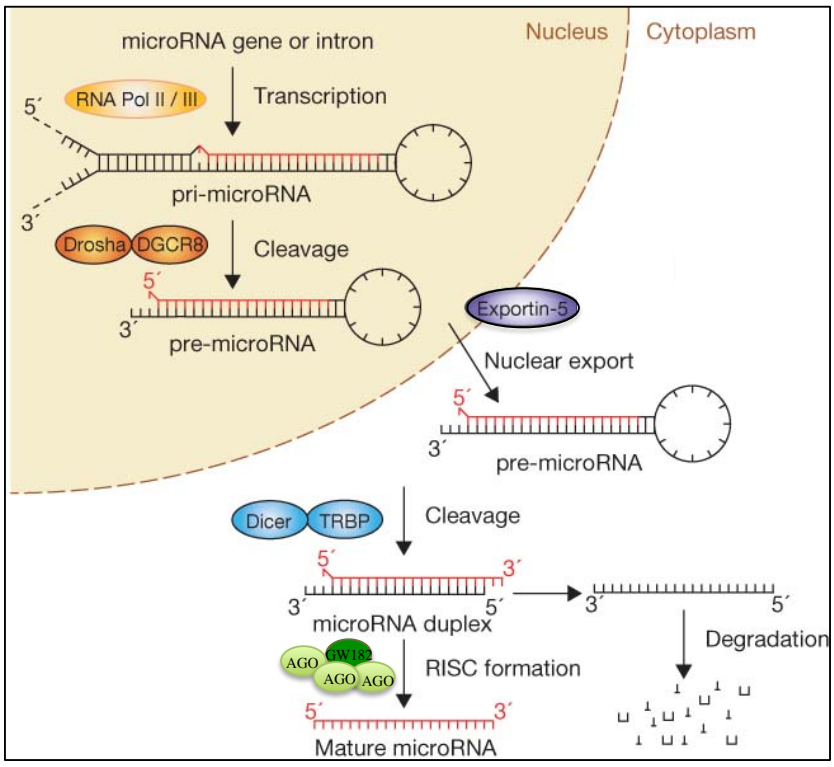

Adapted from Winter J., Nat Cell Biol. 2009

Figure 9: miRNA biogenesis.

The figure summarises the miRNA biogenesis. In the nucleus the microRNA sequence is transcribed by a RNA polymerase II in a double strand pri-RNA. The pri-miRNA is converted in a double strand precursor, the pre-miRNA, by DROSHA together with DGCR8. The pre-miRNA is exported into the cytoplasm and converted into the mature form by the complex DICER/TRPB. The functional strand of the mature miRNA is loaded, through the interaction with the AGO proteins, into the RISC complex to silence target mRNAs through inhibition of mRNA translation or mediating mRNA degradation.

The miRNA-mediated repression of gene expression is mainly based on an imperfect binding between the miRNA and the 3'UTR of the target mRNA. Nevertheless, a continuous and perfect base pairing between a 2-8 nucleotides-long miRNA sequence, called seed region, and the 3'UTR is a stringent requirement[323]. The binding of a miRNA to the target mRNA elicits either inhibition of mRNA translation or mRNA degradation, on the one hand interfering with the translational machinery[324,325,326], on the other hand sustaining the destabilisation of the mRNA through a miRNA-mediated mRNA deadenylation and decay[327,328,329]. According to these mechanisms, miRNAs may target hundreds of different mRNAs and a single mRNA may be regulated by different miRNAs. Several miRNAs are involved in the regulation of tumour-promoting or tumour-suppressor genes; as a consequence, an alteration of the miRNA levels may exert a role in the tumourigenesis process.

5.6.2 miRNAs-mediated post-transcriptional regulation of the uPA-system components

The post-transcriptional regulation of the uPA-system components is also dependent on several microRNAs. Defects of this mechanism of gene regulation may be associated to the tumour-promoter function of this system.

PLAU expression is mainly modulated by miR-193a/b in breast[330,331,332,333], prostate[334] and liver cancer[335]. In hepatocellular carcinoma (HCC) *PLAU* expression is also regulated by miR-23b[336] as also in human papillomavirus (HPV)-mediated cervical cancer[337] and in the angiogenesis process[338]. miR-181 family members have also been shown to influence *PLAU* expression in breast cancer[332,333] and fibrosis[339]. In addition, an indirect mechanism has been proposed to stabilise *PLAU* mRNA through miR-29a-mediated HuR expression in breast cancer[340].

Different miRNAs may also directly target *PLAUR* mRNA[341,342,343,344]. Moreover, the indirect regulation of *PLAUR* may also occur through the targeting of transcription factors, as shown for miR-10b-mediated homeobox D10 (HOXD10) inhibition in glioma cells[345,346]

and HCC[347] and for miR-155-mediated indirect AP1 activation in breast cancer cell lines by a miR-155/MAPK/AP1 mechanism[348]. Finally, through an indirect mechanism miR-146a is able to target both *PLAUR* and *PLAU* in mouse brain metastases[349].

Consistently with the versatility of *SERPINE1* in different biological functions, it is targeted by a plethora of miRNAs. miR-30 family is involved in *SERPINE1* regulation during adipocyte differentiation[350,351], endothelium formation[352] and gastric cancer[353]. miR-34 family regulates *SERPINE1* directly in human choriocarcinoma cell line[354] and in lung epithelium[355], indirectly through the repression of an inhibitor of KLF4 transcription factor during endothelium formation[356].

5.7 AIM

In the last years the microenvironment is emerging as a new important hallmark of cancer. During tumourigenesis, the microenvironment continuously arranges itself in order to support tumour onset and progression. The study of the determinants, which might have a role in the plasticity of the tumour microenvironment, has been receiving increasing attention. The uPA-system is an important player in the homeostasis of the microenvironment sustaining both ECM proteolysis and the cross talk between the microenvironment and the epithelium compartment. The uPA-system has been extensively studied for its involvement in cancer pathogenesis. Indeed, both uPA-system-mediated pericellular proteolysis and signalling may sustain tumour growth, invasion and dissemination. In breast cancer the uPA-system components are often co-over expressed and high levels are associated with poor clinical outcomes. Specifically, uPA and PAI-1 are among the strongest prognostic markers whereas uPAR has been proposed to cooperate with ERBB2 in the aggressiveness of the $ERBB2^{+}$ breast cancer subtype.

The regulation of the gene expression of the uPA-system components is very complex and depends on a plethora of stimuli acting both at transcriptional and post-transcriptional level. In the promoter region, specific enhancers and responsive-elements have been

characterised for each uPA-system component. Studies on the post-transcriptional regulation reported that the mRNA half-life is mainly dependent on “instability elements”, known as AU-rich elements (AREs). Furthermore microRNAs, which modulate directly or indirectly the expression of the uPA-system components are emerging.

Taken into account the relevance of uPA-system in tumourigenesis, the aim of the present study is to characterise the molecular mechanisms that orchestrate the coordinated over expression of the uPA-system components in the context of breast cancer.

6. MATERIALS AND METHODS

6.1 PATIENTS AND MATERIALS

DNA and cDNA samples of an unselected cross-section of 133 primary breast cancer patients were kindly provided by Dr. Paul N. Span (Radboud University Nijmegen Medical Centre, NL). Scramble lentiviral vector (SBI) and the packaging vectors VSV-G, pMDL and REV (Addgene) were kindly gifted by Dr. P.P. Di Fiore (IFOM, Milan) and Dr. F. D'Adda di Fagagna (IFOM, Milan), respectively. suPAR used for the immunoassay standard curve was produced in our laboratory according to the protocol described in Resnati *et al*.[79]; uPA and PAI-1, employed for the immunoassay standard curve, were kindly provided by Dr. J. Henkin (Abbott Laboratories Abbott Park, IL, USA) and Dr. P.A. Andreasen (Århus University, Denmark), respectively. α-uPAR monoclonal antibody R2 and α-PAI polyclonal antibody are a kind gift of Dr. G. Høyer-Hansen (Finsen Laboratory, Denmark) and Dr. P.A. Andreasen (Århus University, Denmark), respectively. α-uPAR and biotinylated α-uPAR polyclonal antibody SI369 and α-uPA and biotinylated α-uPA polyclonal antibody SI367 were generated in IFOM Antibody Facility immunising rabbits with the following made in house antigens:

human pro-uPA:

SNELHQVPSNCDCLNGGTCVSNKYFSNIHWCNCPKKFGGQHCEIDKSKTCYEGNG
HFYRGKASTDTMGRPCLPWNSATVLQQTYHAHRSDALQLGLGKHNYCRNPDNR
RRPWCYVQVGLKPLVQECMVHDWADGKKPSSPPEELKFQCGQKTLRPRFKIIGGE
FTTIENQPWFAAIYRRHRGGSVTYVCGGSLISPCWVISATHCFIDYPKKEDYIVYLG
RSRLNSNTQGEMKFEVENLILHKDYSADTLAHHNDIALLKIRSKEGRCAQPSRTIQ
TICLPSMYNDPQFGTSCEITGFGKENSTDYLYPEQLKMTVVKLISHRECQQPHYYG
SEVTTKMLCAADPQWKTDSCQGDSGGPLVCSLQCRMTLTGIVSWGRGCALKDKP
GVYTRVSHFLPWIRSHTKEENGLVL

human suPAR:

LRCMQCKTNGDCRVEECALGQDLCRTTIVRLWEEGEELELVEKSCTHSEKTNRTL

SYRTGLKITSLTEVVCGLDLCNQGNSGRAVTYSRSRYLECISCGSSDMSCERGRHQ

SLQCRSPEEQCLDVVTHWIQEGEEGRPKDDRHLRGCGYLPGCPGSNGFHNNDTFH

FLKCCNTTKCNEGPILELENLPQNGRQCYSCKGNSTHGCSSEETFLIDCRGPMNQC

LVATGTHEPKNQSYMVRGCATASMCQHAHLGDAFSMNHIDVSCCTKSGCNHP

6.2 CELL CULTURE

6.2.1 Cell lines

The human embryonic kidney (HEK) 293 cell line and the variant expressing the large T antigen HEK 293T were purchased from DSMZ and ICLC, respectively. They are cultured in Dulbecco's modified Eagle's medium (DMEM) (Lonza) supplemented with 10% foetal bovine serum south American (FBS SA) (Biowest), 5 mM L-glutamine (Microtech®), 100 U/mL penicillin (Microtech®), 100 U/mL streptomycin (Microtech®) in humidified cell culture incubator (Galaxy S RSBiotech, Scientific Laboratory Supplies) at 37 °C, 5% CO_2. The NCI-60 panel cell lines were purchased from the National Cancer Institute (Bethesda, MD) and cultured in Roswell Park Memorial Institute (RPMI) 1640 (Lonza) supplemented with 10% FBS north American (NA) (Sigma-Aldrich®), 5 mM L-glutamine (Microtech®), 100 U/mL penicillin (Microtech®), 100 U/mL streptomycin (Microtech®) in humidified cell culture incubator (Galaxy S RSBiotech, Scientific Laboratory Supplies) at 37 °C, 5% CO_2.

6.2.2 Transfections

MDA-MB-231 cells (NCI-60), cultured in antibiotics-free medium, were reverse transfected for 48 h with 10 nM oligonucleotides [miR-340 mimic/control (Life Technologies), esiRNAs/controls (Sigma-Aldrich®)] mixed with Lipofectamine®

RNAiMAX transfection reagent (Life Technologies) diluted in Opti-MEM® (Life Techologies). The transfection mix was incubated at room temperature (rt) 20' in the dark before transfecting cells.

6.2.3 Infections

Viral particles were produced co-transfecting $5*10^5$ HEK 293T cells, plated in complete medium, with the packaging vectors VSV-G, pMDL and REV (Addgene) and either the miR-340 precursor construct pMIRNA1 (SBI) or scramble lentiviral vector (SBI). The supernatant containing the virus particles was collected, filtered and added to MDA-MB-231 cells in order to generate the stable over expression of the miR-340 precursor or scramble miRNA.

6.3 MOLECULAR BIOLOGY

6.3.1 Nucleic acid extraction and cDNA synthesis

6.3.1.1 DNA extraction

IFOM Cell Biology Unit provided $2*10^6$ cell pellet of MCF10A (ATCC®) and $3.2*10^6$ of MDA-MB-231 (ATCC®) cell lines. The genomic DNA was extracted using Genomic DNA Buffer Set with Genomic-tip 20/G (QIAGEN) following the manufacturer's instructions. The DNAs were suspended in Tris-HCl pH 8.5 at 55 °C 2 h in Thermomixer compact (Eppendorf) and quantified by a microvolume UV spectrophotometer (NanoDrop® ND-1000). The plasmidic DNA was extracted using Wizard® *Plus* SV Minipreps DNA purification system (Promega) or QIAGEN® Plasmid Maxi Kit (QIAGEN) according to the manufacturer's instructions. Murine DNAs were extracted from tail biopsies stored in ethanol at rt. Tails were digested in 50 µl of lysis buffer [0.1 M Tris-HCl, 5 mM ethylenediaminetetraacetic acid (EDTA), 0.2% sodium dodecyl sulphate

(SDS), 0.2 M NaCl] supplemented with 0.1 mg/ml proteinase K (PK) (Roche) at 55 °C over night (o/n) in Thermomixer compact (Eppendorf). The PK was inactivated incubating at 95 °C for 5' in Thermomixer compact (Eppendorf). The DNAs were suspended in 600 µl of Milli-Q (MQ) H_2O (Q-POD® Element, Merck Millipore).

6.3.1.2 RNA extraction and cDNA synthesis

Cells were rinsed twice with sterile 1X phosphate buffered saline (PBS) and detached incubating with 1X trypsin-EDTA (Microtech®) in 1X PBS at 37 °C. Cell suspension was collected and centrifuged at 1200 revolutions per minute (rpm) for 5'. The supernatant was discarded and the cell pellet collected. RNAs were extracted using miRNeasy Mini Kit (QIAGEN) following the manufacturer's instructions. Possible DNA contamination was removed by 15' of incubation with DNAse (QIAGEN) according to the manufacturer's instructions. RNAs were eluted in 30 µl of MQ H_2O (Q-POD® Element, Merck Millipore) and quantified by a microvolume UV spectrophotometer (NanoDrop® ND-1000). The RNA quality control was carried out by agarose gel electrophoresis.

The complementary DNA (cDNA) was obtained by reverse transcription (RT) following the manufacturer's instructions of the reverse transcriptase SuperScript II® (Life Technologies) for the random primers method[357]. RNA (1 µg) was mixed with 3 µg/µl of random primers (Life Technologies) diluted in MQ H_2O (Q-POD® Element, Merck Millipore) and incubated at 65 °C for 5' in a thermal cycler GeneAmp® PCR System 9700 (Life Technologies). Subsequently a master mix composed of 5X Buffer FS, 10 mM dNTPs mixture (Promega), 100 mM dithiothreitol (DTT), 40 U/µl RNAse OUT™ and 200 U/µl SuperScript II® was added. Different incubation steps were performed in thermal cycler GeneAmp® PCR System 9700 (Life Technologies) according to the following protocol: 25 °C, 5'; 50 °C, 50' and 72 °C, 15'. All the reagents of the master mix were purchased from Life Technologies, except the dNTPs mixture. The cDNA for miR-340 expression analysis was obtained using High-Capacity cDNA Reverse Transcription Kit

(Life Technologies) starting from 10 ng of 2 ng/µl RNA and following the manufacturer's instructions. Different incubation steps were performed in Applied Biosystems® 2720 Thermal Cycler (Life Technologies): 16 °C, 30'; 42 °C 30' and 85 °C 5'.

6.3.2 Genotyping

The genotype of the mice was assayed by polymerase chain reaction (PCR) on genomic DNA extracted from mouse tail biopsies. PCR reaction was performed according to the manufacturer's instructions of Go Taq G2 (Promega) and is composed of 10 µl of 5X buffer (Promega), 1 µl of 10 mM dNTP mixture (Promega), 2.5 µl each of 10 µM forward and reverse primer (Sigma Aldrich®), 0.25 µl of 5 U/µl Go Taq G2 (Promega) and 1 µl of DNA. Amplification protocol: initial denaturation 95 °C, 4'; denaturation 95 °C, 30''; annealing 55 °C, 1'; extension 72 °C, 10'; final extension 72 °C, 10'; 35 cycles in thermal cycler GeneAmp® PCR System 9700 (Life Technologies).

forward primer (Sigma-Aldrich®): 5' – AATTAAATTTTTCTTTCCCAAACA – 3'

reverse primer (Sigma-Aldrich®): 3' – TCTAATAAAGTGAATAAACCGTTTTGA – 5'

6.3.3 Agarose gel electrophoresis

Separation of DNA fragments by size was solved by agarose gel electrophoresis[358] in Tris-acetate-EDTA (TAE) 1X buffer. The agarose gel was obtained dissolving agarose (0.7-2%) (GellyPhor^{LE}, EuroClone®) in TAE 1X and 1X GelRed™ nucleic acid gel stain (Biotium). The size of fragments was determined by a 100 bp or 1 kb DNA ladder (Promega) and visualised in an UV trans illuminator (EuroClone®). The separation of RNA fragments was performed using the same procedure described above but using Tris-borate-EDTA (TBE) 1X as electrophoresis buffer.

6.3.4 Quantitative polymerase chain reaction (qPCR)

6.3.4.1 Copy number variation

TaqMan® probe sets (Life Technologies) for *PLAUR* Hs02762685_cn (intron 1 - exon 2) or *ERBB2* Hs02416554_cn (exon 18 – intron 18) and endogenous copy number reference, the telomerase reverse transcriptase (TERT) were mixed with 20 ng of genomic DNA samples and TaqMan® Universal PCR Master Mix, no AmpErase® UNG (Life Technologies) according to the manufacturer's instructions. Each sample was analysed in triplicate in standard 96-well plates (Life Technologies) according to the following amplification protocol: initial denaturation 95 °C, 10'; denaturation 95 °C, 15"; annealing/extension 60 °C 1'; 40 cycles and analysed on a 7900HT Fast real-Time PCR System (Life Technologies). *PLAUR* and *ERBB2* copy number was calculated as relative quantification ($RQ = 2^{-\Delta\Delta Ct}$) according to the ΔΔCt method[359].

6.3.4.2 Gene expression analysis

Gene expression analyses on breast cancer patients and cell lines were conducted by reverse transcriptase quantitative polymerase chain reaction (RT-qPCR) using Taqman® low-density arrays (Life Technologies) or standard 96-well plates (Life Technologies), respectively. cDNA quality control was evaluated measuring the expression level of 18S, mixing 5 ng of cDNA with TaqMan® Universal PCR Master Mix, no AmpErase® UNG (Life Technologies) with the specific 18S Taqman® probe set (Life Technologies), in technical duplicates (breast cancer patients) or triplicates (cell lines) according to the manufacturer's instructions and following the amplification protocol: initial denaturation 95 °C, 10'; denaturation 95 °C, 15"; annealing/extension 60 °C, 1'; 40 cycles and analysed on a 7900HT Fast real-Time PCR System (Life Technologies). qPCR reactions, containing 5 ng of cDNA, or 2 ng for miR-340 quantification, mixed with Taqman® Universal PCR Master Mix, no AmpeErase® UNG (Life Technologies) and the specific Taqman® probe

set (Life Technologies), were analysed on a 7900HT Fast real-Time PCR System (Life Technologies) according to the manufacturer's instructions and using the previous amplification protocol. The expression levels were calculated according to the ΔΔCt method [359].

The following Taqman® probe sets (Life Technologies) were used: 18S: Hs99999901_s; *ACTA2*: Hs00426835_g1; *B2M*: Hs99999907_m1; *CAV1*: Hs00971716_m1; *CDK12*: Hs00212914_m1; *COL1A1*: Hs00164004_m1; *CXCL12*: Hs00171022_m1; *CTGF*: Hs00170014_m1; *ERBB2*: Hs01001580_m1; *FN1*: Hs00365052_m1; *GAPDH*: Hs99999905_m1; *HGF*: Hs00300159_m1; *HMBS*: Hs00609293_g1; *HPRT1*: Hs02800695_m1; *LOX*: Hs00942480_m1; miR-340: TM 002258; *MKI67*: Hs01032443_m1; *PLAU*: Hs01547054_m1; *PLAUR*: Hs00182181_m1; *ROCK1*: Hs01127699_m1; *SERPINE1*: Hs01126606_m1; *SNAI1*: Hs00195591_m1; *TAZ*: Hs00794094_m1; *YAP1*: Hs00902712_g1.

6.3.5 Cloning

The ambiguous rearrangements obtained during the generation of the Mir340 knock out mouse were solved cloning the genotyping PCR products using TOPO® TA Cloning® Kit (Life Technologies) in one shot® TOP10 chemically competent *E.Coli* (Life Technologies) and following the manufacturer's instructions. The positive clones were identified by agarose gel electrophoresis of EcoRI restriction enzyme (NEW ENGLAND BioLabs® Inc.) digested plasmid DNAs and sequencing the insert with the universal M13 reverse primer (Sigma Aldrich®): 5'– CAGGAAACAGCTATGACC – 3'. The sequencing was performed by IFOM Sequencing Facility according to Big Dye terminator method[360] using BigDye® Terminator v3.1 Cycle Sequencing Kit (Life Technologies) following the manufacturer's instructions and analysed on 3500xL Dx Genetic Analyzer (Life Technologies).

6.3.6 Microarray

The RNA quality control was assessed using Bioanalyzer 2100 (Agilent Technologies). Biotin-labelled cDNA targets were synthesised starting from 150 ng of total RNA using Ambion® WT Expression Kit (Life Technologies) following the manufacturer's instructions. cDNAs were fragmented and labelled with Affymetrix GeneChip® WT Terminal Labelling Kit (Affymetrix) according to the manufacturer's instructions. Targets cDNAs were hybridised on Human Gene 2.1 ST Array Strip (Affimetrix) in which 19607 human genes are spotted. Hybridization was performed using the GeneAtlas® Hybridization, Wash and Stain Kit (Affimetrix) following the manufacturer's instructions at 48 °C for 20 h in the GeneAtlas® Hybridization Station (Affimetrix). The Array Strips were washed and stained in the GeneAtlas® Personal Fluidics Station (Affimetrix) according to the manufacturer's instructions and the array strips were imaged using the GeneAtlas® Imaging Station (Affimetrix). The data were analysed using Partek® Genomics Suite® v6.4 (Partek®) and normalised according to Robust Multi-array Average (RMA) algorithm[361,362,363]. The genes significantly differential expressed are identified employed as cut off values adjusted p value (Benjamini-Hochberg method[364]) < 0.05 and fold change negative control versus miR-340 mimic ≥ 1.4.

6.4 BIOCHEMESTRY

6.4.1 Protein lysates and supernatants

IFOM Cell Biology Unit provided NCI-60 protein lysates for uPAR immunoassay in RIPA lysis buffer [RIPA buffer 1X (50mM Tris-HCl pH 8, 150 mM NaCl, 1% Tritox-X-100, 0.5 sodium deoxycholate, 0.1% SDS), 1:500 cocktail of protease inhibitors (Calbiochem), 1:200 Na_3VO_4, 1:200 NaF]. The protein lysates for immunoblot analysis were obtained plating 10^6 cells in 10-cm dish. After 48 h cells were washed with 1X PBS and 1 ml of RIPA lysis buffer was added and incubated for 10' on ice. The cells were then scraped, the

protein lysates collected and stored at -20 °C. The NCI-60 supernatants were obtained plating $4.3*10^6$ cells in a FN (Sigma Aldrich®)-coated 10-cm dish in 10 ml of Opti-MEM® (Life Technologies). After 48 h, the cell-conditioned media were centrifuged at 1200 rpm for 5' and the supernatants collected, filtered and stored at -80 °C.

6.4.2 Protein quantification

Protein lysates were quantified by DC™ Protein Assay (Bio-Rad) using a bovine serum albumin (BSA) standard curve as reference and following the manufacturer's instructions. Absorbance at 595 nm was measured using Wallac VICTOR^3™ 1420 Multilabel Counter (PerkinElmer®). The standard curve was fitted to the experimental data and the sample concentrations were interpolated by linear regression using Microsoft Excel.

6.4.3 Immunoassay

6.4.3.1 suPAR

suPAR quantification was performed by suPARnostic® Standard ELISA Assay (ViroGates) following the manufacturer's instructions. This kit is based on a double monoclonal antibody sandwich enzyme-linked immunosorbent assay (ELISA) whereby samples and peroxidase-conjugated α-suPAR are first mixed together and then incubated in α-suPAR pre-coated 96-well plates. Absorbance at 450 nm was measured using Wallac VICTOR^3™ 1420 Multilabel Counter (PerkinElmer®). The standard curve was fitted to the experimental data and the sample concentrations were interpolated by non-linear regression using GraphPad Prism v5.0b.

The immunoassays for protein quantification of uPAR, uPA and PAI-1 were performed by an ELISA-based technique called dissociation-enhanced lanthanide fluorescent immunoassay (DELFIA®). DELFIA® utilises the unique chemical properties of

lanthanide chelates in concert with time-resolved fluorescence (TRF) detection providing a high sensitivity, wide dynamic range, superior stability and excellent flexibility assay compared to the standard ELISA.

6.4.3.2 uPAR

Black 96-well plates (MAXI-SORP, NUNC Corp.) were coated with 1 µg/ml of α-uPAR monoclonal antibody $R2^{365}$ in coating buffer (50 mM Na_2CO_3, pH 9.6) at 4 °C o/n. After plates washing with the washing buffer, consisting of 1X PBS and 0.1% Tween-20 (PBS-T), wells were blocked with 150 µl of blocking solution (2% of BSA diluted in 1X PBS) at rt for 1 h shaking. After 1 h, wells were washed and incubated with 100 µl of 1:10, 1:20 or 1:50 NCI-60 protein lysates and $suPAR^{79}$ standard curve (2-fold dilution, 8 points starting from 16 pM), diluted in 1% BSA in 1X PBS (dilution buffer) at rt for 2 h shaking. Subsequently, wells were washed and bound uPAR was detected incubating with 100 µl of 1 µg/ml biotin-conjugated α-uPAR polyclonal antibody SI369 in dilution buffer at rt for 1 h shaking. The wells were further washed and incubated with 100 µl of 1:10000 of Eu^{3+}-labelled streptavidin (PerkinElmer®) in dilution buffer at rt for 1 h shaking. After an extensive plate washing, 100 µl of DELFIA® enhancement solution (PerkinElmer®) was added. The Eu^{3+}-label was detected after 5' by measuring TRF intensity using an Envision Xcite plate reader (PerkinElmer®) employing the DELFIA® label protocol. The standard curve was fitted to the experimental data and the sample concentrations were interpolated by non-linear regression using GraphPad Prism v5.0b.

6.4.3.3 uPA

Black 96-well plates (MAXI-SORP, NUNC Corp.) were coated with 1 µg/ml α-uPA polyclonal antibody SI367 in coating buffer at 4 °C o/n. After plate washing with PBS-T, wells were blocked in blocking solution at rt for 1 h shaking. After 1 h, wells were washed and incubated with 100 µl of 1:20 NCI-60 supernatants and uPA standard curve (3-fold

dilution, 8 points starting from 16 pM), diluted in dilution buffer at rt for 2 h shaking. Subsequently, wells were washed and bound uPA was detected incubating with 100 µl of 1 µg/ml biotin-conjugated α-uPA polyclonal antibody SI367 in dilution buffer at rt for 1 h shaking. The wells were further washed and incubated with 100 µl of 1:10000 Eu^{3+}-labelled streptavidin (PerkinElmer®) in dilution buffer at rt for 1 h shaking. After an extensive plate washing, 100 µl of DELFIA® enhancement solution (PerkinElmer®) was added. The Eu^{3+}-label was detected after 5' by measuring TRF intensity using an Envision Xcite plate reader (PerkinElmer®) employing the DELFIA® label protocol. The standard curve was fitted to the experimental data and the sample concentrations were interpolated by non-linear regression using GraphPad Prism v5.0b.

6.4.3.4 PAI-1

Black 96-well plates (MAXI-SORP, NUNC Corp.) were coated with 2 µg/ml of α-PAI polyclonal antibody in coating buffer at 4 °C o/n. After plate washing with PBS-T, wells were blocked with 150 µl of blocking solution at rt 1 h shaking. After 1 h, wells were washed and incubated with 100 µl of 1:10 or 1:100 NCI-60 supernatants and PAI-1 standard curve (3-fold dilution, 8 points starting from 500 pM), diluted in dilution buffer at rt 2 h shaking. Subsequently, wells were washed and bound PAI-1 was detected incubating with 100 µl of 1 µg/ml of α-PAI polyclonal antibody in dilution buffer at rt for 1 h shaking. The wells were further washed and incubated with 100 µl of 1:2500 Eu^{3+}-labelled α-mouse antibody (PerkinElmer®) in dilution buffer at rt for 1 h shaking. After an extensive plate washing, 100 µl of DELFIA® enhancement solution (PerkinElmer®) was added. The Eu^{3+}-label was detected after 5' by measuring TRF intensity using an Envision Xcite plate reader (PerkinElmer®) employing the DELFIA® label protocol. The standard curve was fitted to the experimental data and the sample concentrations were interpolated by non-linear regression using GraphPad Prism v5.0b.

6.4.4 Immunoblot

Protein lysates were normalised for the lowest sample protein concentration in Laemmli loading buffer (62.5 mM Tris-HCl pH 6.8, 2% SDS, 10% glycerol and 0.001% bromophenol blue) with or without 0.1 M DTT. The protein lysates were sonicated in 3 cycles of 10'' each using Bioruptor™ Next Gen (Diagenode) and solved by sodium dodecyl sulphate-polyacrylamide gel electrophoresis (SDS-PAGE)[366]. 20 µl of protein lysate and 10 µl of NOVEX® Sharp Pre Stained protein standard (Life Technologies) were run onto 10% polyacrylamide gel electrophoresis and transferred by dry iBlot® Dry Blotting System (Life Technologies) to nitrocellulose membranes (iBlot® Gel Transfer Stack, Life Technologies) in 10'. The proper transfer onto nitrocellulose membrane was checked by Ponceau S staining solution (0.1 % Ponceau S and 5% acetic acid). Membranes were destained in tris-buffered saline-tween (TBS-T) (20 mM Tris-HCl pH 7.4, 500 mM NaCl, 0,1% Tween-20) and incubated in blocking solution (5% powder milk dissolved in TBS-T) at rt 1 h shaking. The membranes were incubated with the primary antibody at rt for 1 h or at 4 °C o/n shaking. After three 5' washes in TBS-T, the membrane was incubated with the proper secondary antibody horseradish peroxidase (HRP)-conjugated in blocking solution at rt for 1 h shaking. The bound secondary antibody was detected incubating with SuperSignal™ West Pico Chemiluminescent Substrate (ThermoFisher Scientific) or SuperSignal® West Dura Extended Duration Substrate (ThermoFisher Scientific) according to the manufacturer's instructions and detected by different exposures using Molecular Imager® ChemiDoc™ XRS+ Imaging System (Bio-Rad). The stripping of membranes was performed incubating the membranes with Restore™ PLUS Western Blot Stripping Buffer (ThermoFisher Scientific) at rt for 15' shaking. The protein level was determined by Image Lab™ software (Bio-Rad).

Table 1 summarises the proper conditions for each employed antibody.

	Primary Abs	Condition	Dilution	Secondary Abs	Detection
uPAR	polyclonal rabbit SI369 o/n	Non reducing	1:1000 blocking solution	α-rabbit-HRP (Cell Signaling) 1:2000 blocking solution	Dura
uPA	polyclonal rabbit SI367 o/n	Non reducing	1:1000 blocking solution	α-rabbit-HRP (Cell Signaling) 1:2000 blocking solution	Dura
YAP1	monoclonal rabbit α-YAP1 (Cell Signaling) o/n	Reducing (DTT)	1:500 5% BSA in TBS-T	α-mouse-HRP (Cell Signaling) 1:2000 blocking solution	Dura
Vinculin	monoclonal mouse α-vinculin 1h (Sigma Aldrich®)	Reducing (DTT)	1:10000 blocking solution	α-mouse-HRP (Cell Signaling) 1:2000 blocking solution	Pico
Tubulin	monoclonal mouse α-tubulin 1h (Sigma Aldrich®)	Reducing (DTT)	1:10000 blocking solution	α-mouse-HRP (Cell Signaling) 1:2000 blocking solution	Pico

Table 1: antibodies employed for the immunoblot.

The table summarises the characteristics and the experimental conditions followed for the antibodies employed in the immunoblot assay.

6.5 IMAGING

6.5.1 Time-lapse microscopy

$3*10^5$ MDA-MB-231 cells reverse transfected with miR-340 mimic and negative control were recorded 16 h post transfection by time-lapse live cell imaging at 37 °C, 5% CO_2, for 24 h with an inverted microscope (IX80, Olympus) equipped with an incubation chamber (OKOlab). The frames were visualised and adjusted for brightness/contrast using ImageJ v1.47. The adjustments were applied to the entire image.

6.5.2 Fluorescence-activated cell sorting (FACS)

6.5.2.1 GFP positive cells

10^6 MDA-MB-231 cells infected with miR-340 precursor construct pMIRNA1 (SBI) or scramble lentiviral vector (SBI) were fixed in 1 ml of 4% paraformaldehyde (PFA) for 10'. The cells were then centrifuged at 1200 rpm for 5' and resuspended in 500 µl of 1X PBS. The green fluorescence protein (GFP) positive cells were acquired analysing 10^4 events/sample on a FACSCalibur (BD Bioscience) and the data were analysed using FlowJo software v9.3.2.

6.5.2.2 Cell cycle

10^6 MDA-MB-231 cells reverse transfected with miR-340 mimic and negative control for 48 h were pulsed with 33 μM thymidine analogy 5-bromo-2'-deoxyuridine (BrdU) (Sigma Aldrich®) for 1 h. The cells were collected centrifuging at 1200 rpm for 10', resuspended in 1X PBS and fixed, adding drop wise cold ethanol on vortexing cells, for 30' on ice. The fixed cells were stained for cell cycle analysis according to the following protocol. The cells were washed in cold 1% BSA in 1X PBS, resuspended in cold 2 N HCl and incubated at rt for 25'. The cells were then incubated with 3 ml of cold 0.1 M $Na_2B_4O_7$ at rt for 2', collected centrifuging at 1200 rpm for 10' and washed twice with cold 1% BSA in 1X PBS. The cells were incubated with 100 μl of 1:5 mouse α-BrdU primary antibody (BD Bioscience) diluted in cold 1% BSA in 1X PBS at rt for 1 h in the dark. Subsequently, the cells were washed twice with cold 1% BSA in 1X PBS and incubated with 100 μl of 1:100 α-mouse Alexa647-conjugated secondary antibody (Life Technologies) diluted in cold 1% BSA in 1X PBS at rt for 1 h in the dark. After the incubation, the cells were washed twice with cold 1% BSA in 1X PBS and resuspended in 1 ml of 2.5 μg/ml propidium iodide (PI) (Sigma Aldrich®) and 250 μg/ml RNase (QIAGEN) in cold 1% BSA in 1X PBS at 4 °C o/n. The samples were acquired the day after by FACSCalibur (BD Bioscience) and analysed using FlowJo software v9.3.2.

6.6 LABEL-FREE REAL-TIME CELL-BASED ASSAY (RTCA)

The RTCA technology is a label-free system that allows for real-time monitoring of cellular events through measurements of electrical impedance by microelectrodes located at the bottom of each well[367]. The adhesion of the cells to the well plate induces an increase of electrode impedance. As a consequence, cellular processes, which cause changes in the quantity and/or quality of the cell-matrix interactions (e.g. cell proliferation and cell spreading), can be quantitative analysed with this technique. Impedance measurements are

reported as a dimensionless parameter called cell index (CI) that is defined as the relative change in measured impedance at a given time-point respect to the background measurement.

MDA-MB-231 cells (10^4 cells/well), mixed with the transfection mix diluted in Opti-MEM®, were plated in 96-well E-plates (Roche). Subsequently, the plate was transferred to the real time cell analyser instrument (RTCA, xCELLigence SP, Roche) located in a humidified cell culture incubator (Sanyo) at 37 ˚C and 5% CO_2 and the impedance was measured every 30' for 48 h.

6.7 *IN VIVO*

6.7.1 Xenograft procedure

6 weeks-old CD-1® nude mice (Charles River Laboratories) were anesthetised through intraperitoneal injection (IP) of 2.5% avertin 15 µl/body weight gram. $5*10^6$ MDA-MB-231 cells infected with miR-340 precursor construct pMIRNA1 (SBI) or scramble lentiviral vector diluted 1:1 with Matrigel (Sigma-Aldrich®) were inoculated into the left inguinal mammary fat pad. Tumour formation was monitored every day and tumour growth was measured by caliper once a week. The tumour volume was calculated according to the following formula: $V = (length*width^2)/2$. Mice were sacrificed when tumour volume reached 1200 mm^3. Mice were maintained in high-efficiency particulate arrestance (HEPA)-filtered individually ventilated cages (IVC) system and the experiment was performed according to the guidelines for animal care. The employed procedures were approved by the institutional ethical animal care committee.

6.7.2 Mir340 deficient mouse model

6.7.2.1 Generation of Mir340 deficient mouse model

10 FVB/NCrl and 10 C57BL/6 female mice (Charles River Laboratories) were stimulated with hormones to synchronise the oestrous cycle to induce a massive oocytes production. To this purpose, hormones were administrated through IP injection: first 100 µl of pregnant mare serum gonadotropin (PMSG) (MSD Animal Health) (5 UI/female) and after 46-48 h 100 µl of the human chorionic gonodotropin (hCG) (5 UI/female) (MSD Animal Health). Subsequently, each hormone-stimulated female was bred with a wild-type male mouse (Charles River Laboratories) of the corresponding background. The day after, the females were sacrificed, the oviducts collected and the fertilised oocytes picked up. 20 ng/µl of RNAs encoding the zinc fingers (ZNFs) (Sigma Aldrich®) and 2 ng/µl of the replacement template oligonucleotide (Sigma Aldrich®) diluted in injection buffer (10 mM Tris-HCl pH 7.4 and 0.25 mM EDTA) were microinjected into the male pronuclei of fertilised oocytes using inverted microscope Aziovert 200 M (Zeiss) equipped with microinjector FemtoJet® (Eppendorf) and micromanipulator TransferMan NK 2 (Eppendorf). The manipulated embryos were incubated in humidified cell culture incubator (CB53 Binder) at 37 °C, 5% CO_2 for 16 h and the day after were implanted in a pseudo pregnant CD-1® female mice (Charles River Laboratories). The pseudo pregnant females are the positive plug females derived from breeding with a vasectomised male. During the embryo transfer the females were anesthetised through IP injection of 1.25% avertin 0.02 ml/body weight gram and subsequently treated with analgesic Rimadyl® (Carprofen) 5 mg/kg. Mice were maintained in HEPA-filtered IVC system; the procedure was performed according to the guidelines for animal care and approved by the institutional ethical animal care committee.

ZNFs pair (Sigma Aldrich®):

5’ – AATCAACTGCGCGGGTAAA – 3’

3’ – TCGGTTAAGGAAATTACTG – 5’

Replacement template (Sigma Aldrich®):

5’ –

TTCTTTCCCAAACAGCTTCCTGTTGAGATTAGTTGACGCGCCCATTTAGTCATA

CCTGGTATCTTAACACCACAGATCATGCCTGTTGATCAACATTGTA – 3’

6.7.2.2 Screening of targeted animals

The PCR products (see genotyping section) were digested, on the one hand with BamHI restriction enzyme (NEW ENGLAND BioLabs® Inc.) at 37 °C 2 h in Thermomixer compact (Eppendorf); on the other hand the PCR products were denaturated at 95 °C for 4’, reannealed gradually reaching 25 °C and digested with T7E1 restriction enzyme (NEW ENGLAND BioLabs® Inc.) at 37 °C for 15’ in Thermomixer compact (Eppendorf). The PCR products and the two different digestions were run onto agarose gel in TAE 1X buffer by electrophoresis. The sequencing of PCR products was performed using the primers employed for the genotyping PCR by the IFOM Sequencing Facility according to Big Dye terminator method[360] using BigDye® Terminator v3.1 Cycle Sequencing Kit (Life Technologies) following the manufacturer’s instructions and analysed on 3500xL Dx Genetic Analyzer (Life Technologies).

6.8 TISSUE ANALYSIS

6.8.1 Immunohistochemistry (IHC)

Mice tumours were collected and fixed in 4% formaldehyde at rt for 6 h and then stored in 70% ethanol at rt. In the IFOM Tissue Unit, the samples were processed using tissue processor ASP300 S (Leica) according to the manufacturer’s instructions. 4 μm tissue slides were obtained using the microtome RM2125 RTS (Leica).

6.8.1.1 Ki-67

Tissue slides were deparaffinised by two 10' incubation with xilene and hydrated dipping the slides in a descending scale of ethanol (100-90-90-70%) and distilled H_2O (dH_2O) at rt for 5' each. The antigen (Ag) unmasking was performed in buffer citrate 10 mM pH 6 Ready-to-Use (Thermo Fisher Scientific) in microwave by one 5' step and two 90'' steps at max power refilling the buffer citrate after each step. The slides were gradually cooled at rt 30' under chemical hood and then rinsed three times with 1X PBS without ions Ca^{2+} and Mg^{2+} (PBS -/-). The endogenous peroxidase was inactivated with 0.3% of peroxidase blocking solution (Sigma Aldrich®) in 1X PBS containing 0.05% Tween-20 at rt 20' and then rinsed three times with PBS -/-. The slides were incubated with the primary antibody rabbit α-Ki-67 (Cell Signaling) 1:400 in PBS -/- at rt for 30' and then rinsed three times with PBS -/-. As secondary antibody MACH 1 Universal HRP-Polymer Detection (Biocare Medical) was employed and incubated at rt for 30'. The slides were rinsed three times with PBS -/- and incubated with the peroxidase substrate using DAB Peroxidase (HRP) Substrate Kit (Vector Laboratories) according to the manufacturer's instructions. The peroxidase reaction was blocked incubating with dH_2O at rt for 5' and counterstained with haematoxylin (VWR®) at rt for 1'. The slides were rinsed with running H_2O, dehydrated in an ascending scale of ethanol (70-90-100-100%) at rt 5' each and incubated three times at rt 5' each in xilene. The slides were mounted with one drop of Eukitt (O. KINDLER) and cover slip. The images were acquired using Slide scanner VS120 dot slide (Olimpus Life Science), magnification 20X, and scale bar 1mm. The protein level was determined using ImageJ v1.47.

6.8.1.2 Cleaved CASP3

Tissue slides were deparaffinised by three 10' incubations with histolemon (CARLO ERBA) and hydrated dipping the slides in a descending scale of ethanol (100-95-80%) and dH_2O at rt 5' each. The Ag unmasking was performed in buffer citrate 10 mM pH 6

supplemented with 0.05% Tween-20 at 95 °C for 50' in a water bath. The slides were gradually cooled at rt 20' under chemical hood and then washed with dH_2O for 5'. The endogenous peroxidase was inactivated with 0.3% of peroxidase blocking solution (Sigma Aldrich®) in dH_2O at rt for 5' and then rinsed in 1X PBS. The aspecific Ag sites were blocked incubating the slides in blocking solution (2% BSA, 2% FBS SA (Biowest), 0.05% Tween-20 in 1X PBS) for 20' in a wet chamber. The slides were then incubated with the monoclonal primary antibody rabbit α-cleaved CASP3 (Cell Signaling) 1:300 in blocking solution at rt for 90' in wet chamber and then washed twice with 1X PBS 5' each. As secondary antibody biotinylated α-rabbit (Dako) was employed diluted 1:200 in blocking solution and incubated at rt for 1 h in wet chamber. The slides were washed twice with 1X PBS 5' each and incubated with avidin-HRP conjugated using VECTASTAIN ABC Kit (Standard) (Vector Laboratories) according to the manufacturer's instructions at rt for 45' in wet chamber. The slides were washed twice with 1X PBS 5' each and incubated with the peroxidase substrate using DAB Peroxidase (HRP) Substrate Kit (Vector Laboratories) according to the manufacturer's instructions. The peroxidase reaction was blocked incubating with dH_2O at rt for 5' and counterstained with haematoxylin (VWR®) at rt for 1'. The slides were rinsed with running H_2O and dehydrated incubating with dH_2O, an ascending scale of ethanol (70-95-100%) and histolemon (CARLO ERBA) at rt 2' each. The slides were mounted with one drop of Eukitt (O. KINDLER) and cover slip. The images were acquired using Slide scanner VS120 dot slide (Olimpus Life Science), magnification 20X, and scale bar 1mm. The protein level was determined using ImageJ v1.47.

6.8.2 In situ hybridization (ISH)

miR-340 chromogenic *in situ* hybridization (ISH) on human normal and tumour breast tissues was carried out by Bioneer ISH Service (DK-2970, Hørsholm). An automated

locked nucleic acid (LNA)-based ISH was performed according the sketched protocol reported in table 2[368,369]:

miRCURY LNA™ probe (Exiqon):

miR-340: AATCAGTCTCATTGCTTTATAA

scramble: TGTAACACGTCTATACGCCCA

Step	Cycles	Time (min)	Volume (µl)	Reagent	T (°C)
1	2	2	300	1X PBS	25
2	1	3	200	PK buffer	37
3	2	4	200	PK in PK buffer	37
4	3	2	300	1X PBS	37
5	1	15	100	Prehybridization	37
6	1	30	200	Probe addition	55
7	1	30	200	Probe addition	55
8	1	5	300	5X Saline Sodium Citrate (SSC)	55
9	1	5	300	1X SSC	55
10	2	5	300	0.2X SSC	55
11	1	5	300	0.2X SSC	30
12	2	2	300	1X PBS	30
13	1	5	200	Blocking reagent	30
14	2	15	200	α-FAM-alkaline phosphatase, 1:800	30
15	2	2	300	1X PBS	30
16	3	30	200	NBT/BCIP substrate incubation	30
17	2	3	300	KTBT buffer (Tris-HCl 50 mM, NaCl 150 mM, KCl 10 mM)	30
18	2	1	300	H_2O	RT
19	1	1	100	Nuclear Fast Red staining 1:2	RT
20	6	0.1	200	H_2O	RT

Table 2: ISH protocol.

The table summarises the protocol steps performed for the ISH analysis on normal and tumour breast tissues.

6.9 BIOINFORMATIC TOOLS AND PROGRAMS

Correlation and statistical analyses were performed using GraphPad Prism v5.0b. Microarray datasets from breast cancer patients and human cancer cell lines were mined from Oncomine®[370] and CellMiner™ [371] databases. The list of predictive microRNAs for the uPA-system components was downloaded from microrna.org[372] (http://www.microrna.org/microrna) based on miRanda algorithm[373]. The list of predictive miR-340 target genes was downloaded from both microrna.org and Targetscan[374]

(http://www.targetscan.org/). The 3'UTR sequences necessary for *in silico* analyses were downloaded from UCSC Genome Browser[375] (https://genome.ucsc.edu/). The genes spotted on the microarray were annotated according to their association with breast cancer prognosis using BreastMark database[376] (http://glados.ucd.ie/BreastMark/). The gene ontology analysis for the pathway enrichment in miR-340-dependent breast cancer signature was performed using Enrichr[377] (http://amp.pharm.mssm.edu/Enrichr/).

6.10 STATISTICAL ANALYSES

6.10.1 Student's t test

Statistical analysis of normally distributed values was performed by two-tailed unpaired Student's t-test. Differences were considered statistically significant at p value < 0.05. In case of multiple comparisons a multiple comparison correction, using the Benjamini-Hochberg method[364], was applied.

6.10.2 χ^2 test

Statistical analysis to test independence in contingency tables was performed using χ^2 test. Differences were considered statistically significant at p value < 0.05 with Yates correction[378].

6.10.3 Cox regression and logrank test

The hazard ratio is calculated using Cox regression and logrank test. The association with breast cancer prognosis was considered statistically significant at p value < 0.05. Multiple comparison correction was applied according to Bonferroni method[379].

7. RESULTS

7.1 GENE EXPRESSION ANALYSES IN A CROSS-SECTION OF DUTCH BREAST CANCER PATIENTS

7.1.1 ERBB2 and PLAUR are neither co-amplified nor co-expressed in the cohort of breast cancer patients

In order to shed light on the role of the uPA-system in breast cancer, we started investigating the proposed co-amplification between *ERBB2* and *PLAUR*[184,185,380] in a cross-section of unselected Dutch breast cancer patients (N = 133). To test this hypothesis, *ERBB2* and *PLAUR* copy number variation analysis was performed by qPCR. The *ERBB2* copy number highlighted a group of patients with *ERBB2* amplification that likely represents the subset of the ERBB2$^+$ breast cancers (fig. 10A). However this subset did not show *PLAUR* amplification. *PLAUR* copy number was indeed normal in almost all breast cancer patients (fig. 10B). These data point out that *ERBB2* and *PLAUR* are not co-amplified in the cohort of breast cancer patients here analysed.

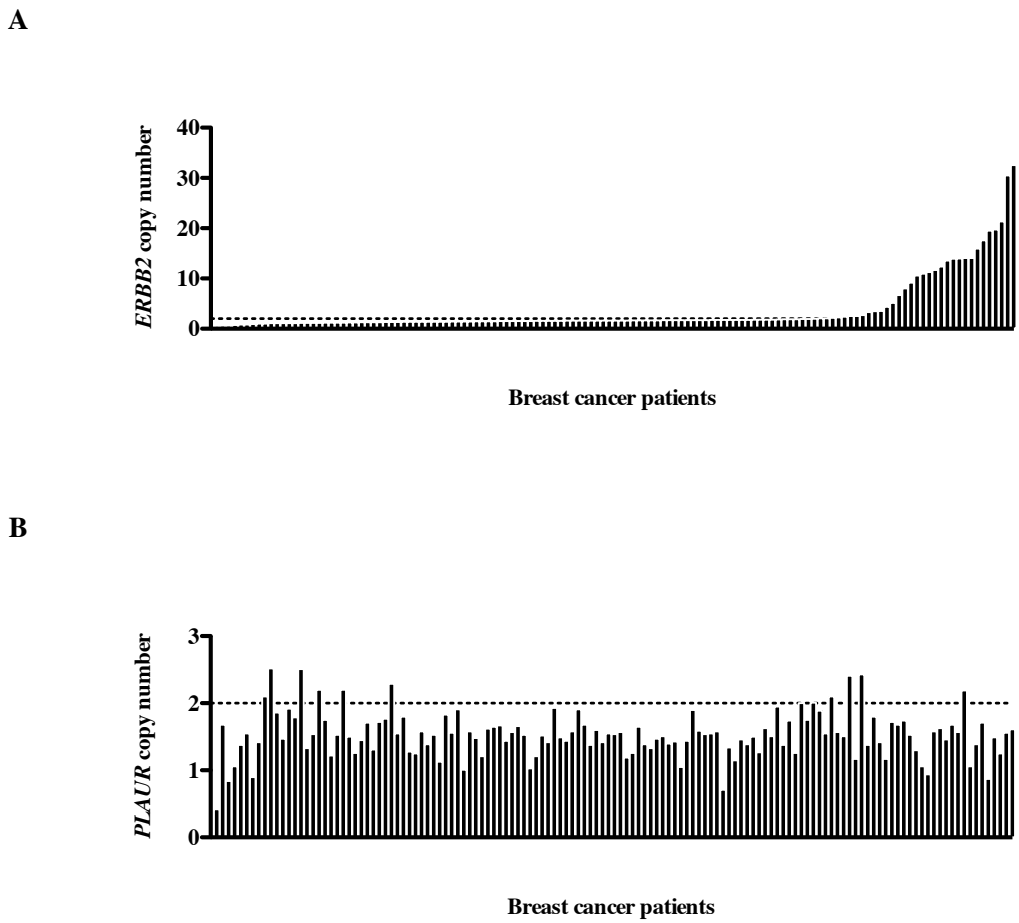

Figure 10: *ERBB2* and *PLAUR* copy number in the cohort of breast cancer patients.

(A-B) *ERBB2* (A) and *PLAUR* (B) copy number was measured in a cross-section of unselected Dutch breast cancer patients (N = 133) by qPCR. The copy number was calculated by relative quantification (RQ = $2^{-\Delta\Delta Ct}$). ΔCts were determined normalising *ERBB2* and *PLAUR* mean Ct values against the mean Ct values of the endogenous copy number reference, the telomerase reverse transcriptase (TERT). The ΔΔCt values were calculated subtracting the mean ΔCt values of two calibrator samples, the normal copy number cell lines: MCF10A (normal breast cell line) and MDA-MB-231 (triple negative breast cancer cell line) to the ΔCt value of each sample. The data were sorted for *ERBB2* copy number and the dotted line indicates the normal copy number.

To test whether these two genes may be co-expressed in breast cancer, as already shown in literature[380,185,184], *ERBB2* and *PLAUR* expression levels were measured by RT-qPCR in the same cohort of patients. *ERBB2* expression pattern showed a subset of patients characterised by *ERBB2* over expression (fig. 11A), which corresponds to the patients with *ERBB2* amplification. This correspondence supports the well known finding that in the

ERBB2^{+} breast cancers *ERBB2* over expression is mainly due to gene amplification[381]. On the contrary, no trend in *PLAUR* expression level was detected (fig. 11B).

A

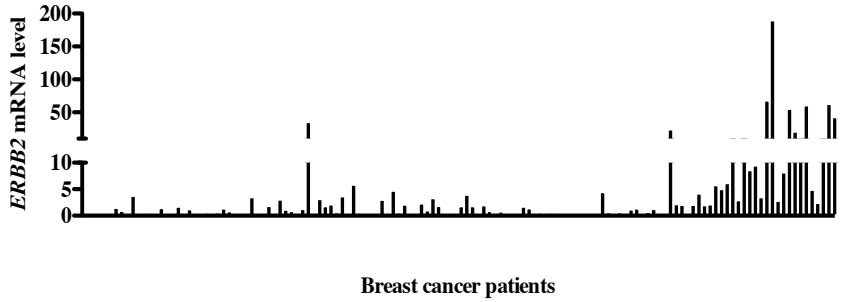

B

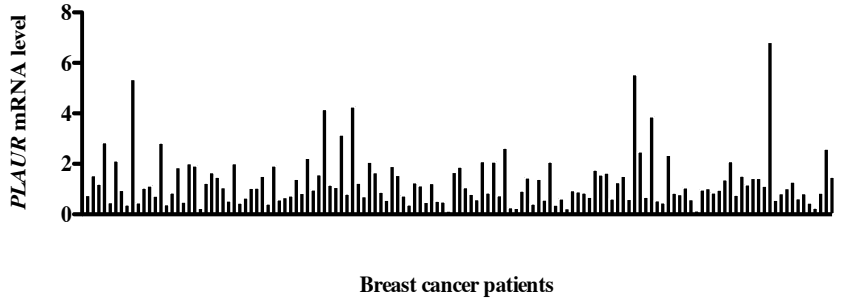

Figure 11: *ERBB2* and *PLAUR* expression level in the cohort of breast cancer patients.

(A-B) *ERBB2* (A) and *PLAUR* (B) expression levels were measured in the cross-section of unselected Dutch breast cancer patients (N = 133) by RT-qPCR. The mRNA levels were calculated normalising *ERBB2* and *PLAUR* mean Ct values against the mean Ct values of two housekeeping genes (*GAPDH* and *HPRT1*). The ΔΔCt values were calculated subtracting the Ct global mean to the ΔCt value of each sample[382]. The data were sorted for *ERBB2* copy number.

To further stress the absence of co-expression, the correlation between *ERBB2* and *PLAUR* expression level was evaluated. In this analysis no correlation between *ERBB2* and *PLAUR* mRNA level was observed ($r = 0.03$; $p = 0.77$) (fig. 12). These results highlight that in our subset of breast cancer patients *ERBB2* and *PLAUR* are not co-expressed.

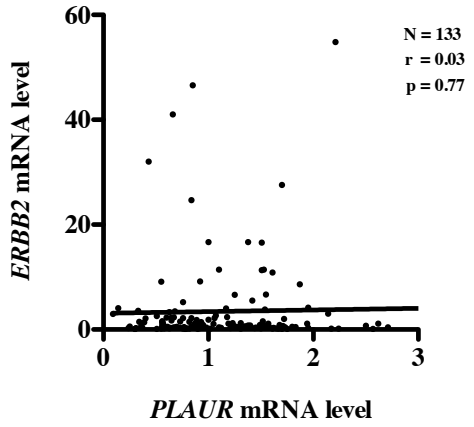

Figure 12: *ERBB2* and *PLAUR* expression level are not correlated in the cohort of breast cancer patients.

Scatter plot shows the correlation between *ERBB2* and *PLAUR* mRNA levels. The sample size (N), the Pearson correlation coefficient (r) and the p value (p) are reported.

In summary, the copy number and gene expression analyses show that *ERBB2* and *PLAUR* are neither co-amplified nor co-expressed in the investigated cohort of breast cancer patients.

7.1.2 PLAUR and PLAU expression levels are strongly correlated

Contextually the qPCR analyses of *ERBB2* and *PLAUR*, we also measured the expression of some putative breast cancer-driver genes (data not shown). Table 3 shows the correlations between *PLAUR* expression level and the expression levels of the other genes measured in the patient cohort.

Genes	r	p
PLAU	0.74	< 0.0001
LOX	0.64	< 0.0001
FN1	0.58	< 0.0001
SERPINE1	0.56	< 0.0001
SNAI1	0.45	< 0.0001
ACTA2	0.42	< 0.0001
CAV1	0.41	< 0.0001
COL1A1	0.33	< 0.0001
CXCL12	0.32	< 0.0001
HGF	0.19	0.03
MKI67	0.06	0.46
CDK12	0.02	0.83
TAZ	-0.05	0.53

Table 3: correlation analyses between *PLAUR* and the breast cancer-driver genes measured in the cohort of breast cancer patients.

The table summarises the correlation analyses between the mRNA levels of each gene analysed in the breast cancer cohort with *PLAUR* expression level. For each correlation the Pearson correlation coefficient (r) and the p value (p) are reported.

We found that the strongest correlation is between *PLAUR* and *PLAU* expression level (r = 0.74, p < 0.001) (fig. 13).

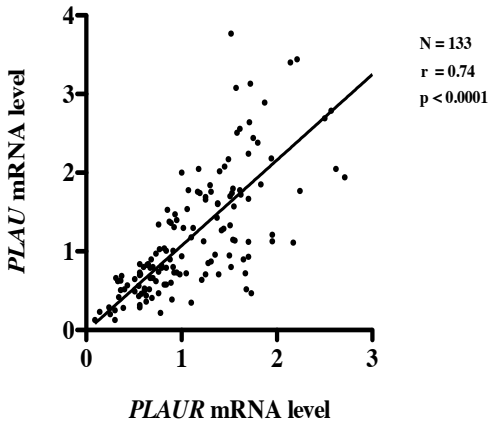

Figure 13: *PLAUR* and *PLAU* mRNA levels are strongly correlated.

Scatter plot shows the correlation between *PLAUR* and *PLAU* mRNA levels. The sample size (N), the Pearson correlation coefficient (r) and the p value (p) are reported.

In order to substantiate this finding in other sample collections, we performed correlation analyses between *PLAUR* and *PLAU* expression level mining expression data from microarrays of breast cancer patients and human cancer cell lines using Oncomine®[370] and CellMiner™ [371] databases. Out of more than 20,000 genes covered, *PLAU* was found to be one of the strongest correlated with *PLAUR* (table 4), corroborating the correlation observed in the cohort of breast cancer patients.

Sample Collection	N	r	*PLAU* rank	Source
Barretina cell lines	917	0.585	4 (19574)	Oncomine®
Wooster cell lines	318	0.478	13 (19574)	Oncomine®
NCI-60 cell lines	60	0.433	428 (26065)	CellMiner™
Bittner multi-cancer	1911	0.690	1 (19574)	Oncomine®
Sorlie breast	167	0.537	2 (6197)	Oncomine®
Minn breast	121	0.693	14 (12624)	Oncomine®
Perou breast	65	0.691	6 (6625)	Oncomine®

Table 4: validation of *PLAUR* and *PLAU* correlation in cancer databases.

Correlation between *PLAUR* and *PLAU* expression levels was analysed mining expression data from breast cancer patients and human cancer cell lines microarrays using Oncomine® and CellMiner™ databases. The table shows the name of the sample collection, the sample size (N), the Pearson correlation coefficient (r), the *PLAU* rank, the total number of genes analysed in the sample collection (in brackets) and the database used for the analysis (source).

These observations suggested the possibility that *PLAUR* and *PLAU* might be regulated by common transcriptional and/or post-transcriptional mechanisms.

7.2 IDENTIFICATION AND VALIDATION OF THE ROLE OF miR-340 AS MODULATOR OF THE EXPRESSION OF THE uPA-SYSTEM CORE COMPONENTS

7.2.1 Identification of miR-340 as modulator of the expression of the uPA-system core components

Although the strong correlation between *PLAUR* and *PLAU* expression might be due to multiple causes, we hypothesised that the regulation on the mRNA stability level by one or more microRNA (miRNA) is likely to contribute significantly to this co-expression. To identify candidate miRNAs, we inspected *PLAUR* and *PLAU* mRNAs for predicted miRNA target sites using miRanda algorithm[373] available in microrna.org website[372]. Using this prediction tool, we identified predicted target sites for six and 26 different conserved miRNAs in *PLAUR* and *PLAU* 3'UTR, respectively. The two miRNAs candidate lists contained three miRNAs in common: miR-193a-3p, miR-193b and miR-340 (table 5).

A

***PLAUR* miRNAs ordered by sum of mirSVR scores**
hsa-miR-335
hsa-miR-377
hsa-miR-340
hsa-miR-193a-3p
hsa-miR-193b
hsa-miR-876-5p

B

***PLAU* miRNAs ordered by sum of mirSVR scores**
hsa-miR-23a
hsa-miR-23b
hsa-miR-23a
hsa-miR-181d
hsa-miR-181a
hsa-miR-181b
hsa-miR-181c
hsa-miR-193a-3p
hsa-miR-193b
hsa-miR-342-3p
hsa-miR-340
hsa-miR-410
hsa-miR-874
hsa-miR-361-5p
hsa-miR-203
hsa-miR-192
hsa-miR-215
hsa-miR-19a
hsa-miR-19b
hsa-miR-143
hsa-miR-365
hsa-miR-27a
hsa-miR-27b
hsa-miR-149
hsa-miR-362-3p
hsa-miR-329

Table 5: putative miRNAs regulating *PLAUR* or *PLAU* expression.

(A-B) Tables show the lists of putative miRNAs able to target *PLAUR* (A) or *PLAU* (B) 3'UTR. The lists of putative miRNAs were downloaded from microrna.org website. The miRNAs binding sites are scored for likelihood of mRNA target gene down regulation using mirSVR[383] and ordered according to this score. In bold the miRNAs in common between *PLAUR* and *PLAU*.

We mined expression data of the NCI-60 panel (table 6), available in CellMiner™ web tool[371], to investigate if these miRNAs were likely to regulate *PLAUR* and *PLAU* expression.

Cancer type	Cell line
Breast	MCF-7
Breast	MDA-MB-231
Breast	HS 578T
Breast	BT549
Breast	T-47D
Central nervous system	SF268
Central nervous system	SF295
Central nervous system	SF539
Central nervous system	SNB-19
Central nervous system	SNB-75
Central nervous system	U251
Colon	Colo205
Colon	HCC 2998
Colon	HCT-116
Colon	HCT-15
Colon	HT29
Colon	KM12
Colon	SW620
Leukemia	CCRF-CEM
Leukemia	HL-60
Leukemia	K562
Leukemia	MOLT-4
Leukemia	RPMI-8226
Leukemia	SR
Melanoma	LOX IMVI
Melanoma	MALME-3M
Melanoma	M14
Melanoma	SK-MEL-2
Melanoma	SK-MEL-28
Melanoma	SK-MEL-5
Melanoma	UACC-257
Melanoma	UACC-62
Melanoma	MDA-MB-435
Lung	A549
Lung	EKVX
Lung	HOP-62
Lung	HOP-92
Lung	NCI-H226
Lung	NCI-H23
Lung	NCI-H322M
Lung	NCI-H460
Lung	NCI-H522
Ovary	IGROV1
Ovary	OVCAR-3
Ovary	OVCAR-4
Ovary	OVCAR-5
Ovary	OVCAR-8
Ovary	SK-OV-3
Ovary	NCI-ADR-RES
Prostate	PC-3
Prostate	DU145
Kidney	786-O
Kidney	A498
Kidney	ACHN
Kidney	CAKI
Kidney	RXF 393
Kidney	SN12C
Kidney	TK-10
Kidney	UO-31

Table 6: NCI-60 panel cell lines.

The NCI-60 panel consists of 59 human cancer cell lines belonging to different cancer types: five breast cancer, six central nervous system cancer, seven colon cancer, six leukemia, nine melanoma, nine lung cancer, seven ovary cancer, two prostate cancer and eight kidney cancer cell lines.

In this analysis, both *PLAUR* and *PLAU* mRNA levels were significantly negatively correlated with the expression level of both forms of miR-340 (miR-340 and miR-340*, also known as miR-340-5p and miR-340-3p, respectively), but not with miR-193a-3p or miR-193b expression levels (table 7A-B). The expression level of miR-340 and mir-340*

are both negatively correlated also with *SERPINE1* expression (table 7C), even if miRanda algorithm[373] does not predict a miR-340 binding site in *SERPINE1* mRNA.

A

PLAUR

miRNAs	r
hsa-miR-340	**-0.429**
hsa-miR-340*	**-0.547**
hsa-miR-193a-3p	0.291
hsa-miR-193b	0.058

B

PLAU

miRNAs	r
hsa-miR-340	**-0.462**
hsa-miR-340*	**-0.449**
hsa-miR-193a-3p	0.083
hsa-miR-193b	0.17

C

SERPINE1

miRNAs	r
hsa-miR-340	**-0.379**
hsa-miR-340*	**-0.475**
hsa-miR-193a-3p	0.299
hsa-miR-193b	0.137

Table 7: miR-340/miR-340* level is inversely correlated with the expression of the core components of the uPA-system.

(A-C) The tables show the correlation analyses between the mRNA levels of *PLAUR* (A), *PLAU* (B) and *SERPINE1* (C) and the level of the three candidate miRNAs across the NCI-60 panel. The expression levels were mined from CellMiner™ database. The Pearson correlation coefficient (r) is reported for each correlation. CellMiner™ database identifies significant correlations at $r > 0.334$ or < -0.334 on a minimum of 35 informative cell lines, yielding $p < 0.05$ in the absence of multiple comparisons correction. Significant correlations based on these criteria are presented in bold.

All the correlation analyses between the three uPA-system components with miR-340 and miR-340* are statistically significant and are plotted in fig. 14.

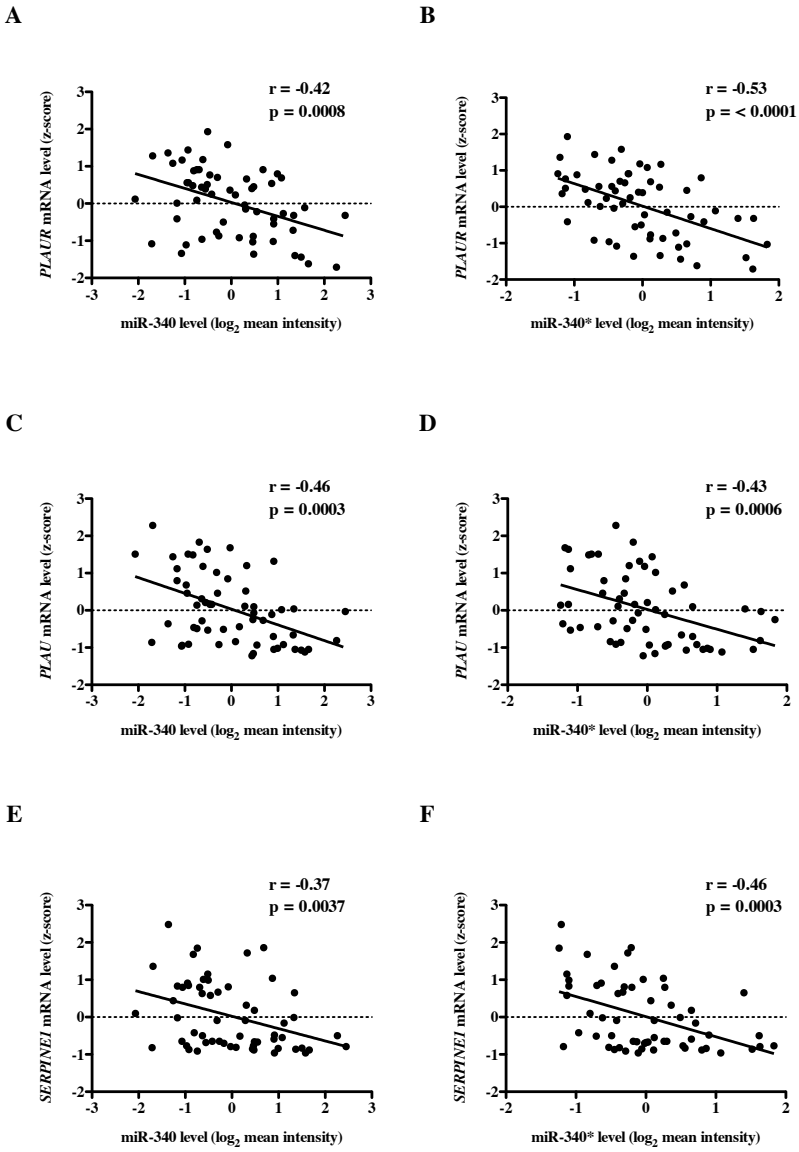

Figure 14: correlation analyses between the mRNA levels of core components of the uPA-system and miR-340/miR-340* levels.

(A-F) Scatter plots show the significant correlations described in table 4. The expression levels of *PLAUR* (A-B), *PLAU* (C-D) and *SERPINE1* (E-F) and miR-340/miR340* were mined from CellMiner™ database as z score and log_2 mean intensity, respectively. The Pearson correlation coefficient (r) and the p value (p) are reported for each correlation.

In addition, based on expression data in CellMiner™ web tool[371], we chose three different NCI-60 cell lines, which displayed high (MDA-MB-231 and SF-539) or low (MCF-7) *PLAUR* expression to perform RT-qPCR for *PLAUR* and miR-340. We focused the attention specifically on miR-340, since it is considered the predominant form compared to

miR-340*[322]. RT-qPCR analysis confirmed that MDA-MB-231 and SF-539 showed high while MCF-7 low *PLAUR* expression compared to the calibrator sample HEK 293 (fig. 15A). The level of miR-340 behaved in the opposite trend: MDA-MB-231 and SF-539 showed lower miR-340 level compared to MCF-7 (fig. 15B). Thus, the negative correlation between *PLAUR* and miR-340 was further confirmed.

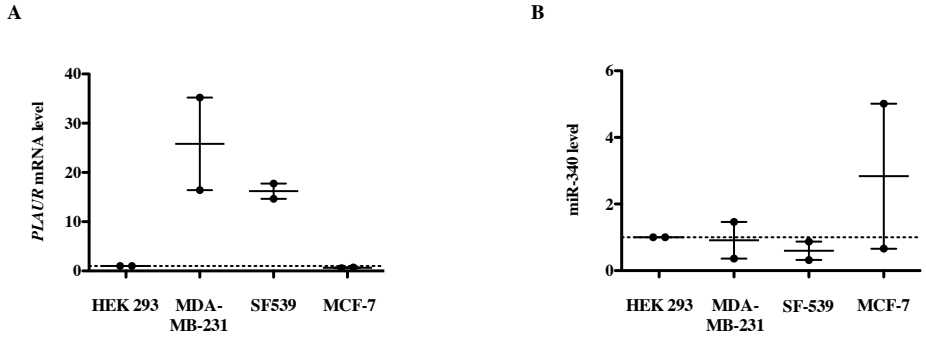

Figure 15: *PLAUR* and miR-340 expression level in three NCI-60 cell lines.

(A-B) The expression levels of *PLAUR* (A) and miR-340 (B) were measured by RT-qPCR. The RQ was calculated normalising *PLAUR* and miR-340 mean Ct values against the mean Ct values of the housekeeping genes *GAPDH* and rnu6b, respectively (ΔCt). The ΔΔCt values were obtained subtracting the ΔCt values of the calibrator sample HEK 293 cell line (normal human embryonic kidney cell line) to the ΔCt value of each sample. The dotted line indicates the expression level of the calibrator sample. Dots are data from two independent experiments, means ± standard error of the mean (SEM) are shown.

To test whether the inverse correlation is true also at protein level, we measured the protein levels of the main uPA-system components (uPAR and its soluble form suPAR, uPA and PAI-1) across the NCI-60 panel by immunoassay. We analysed protein lysates for uPAR quantification and conditioned media for the other uPA-system components. In line with the correlation observed at mRNA level, both miR-340 and miR-340* levels were significantly negatively correlated with the protein levels of all the uPA-system components except miR-340 with suPAR (fig. 16A-H).

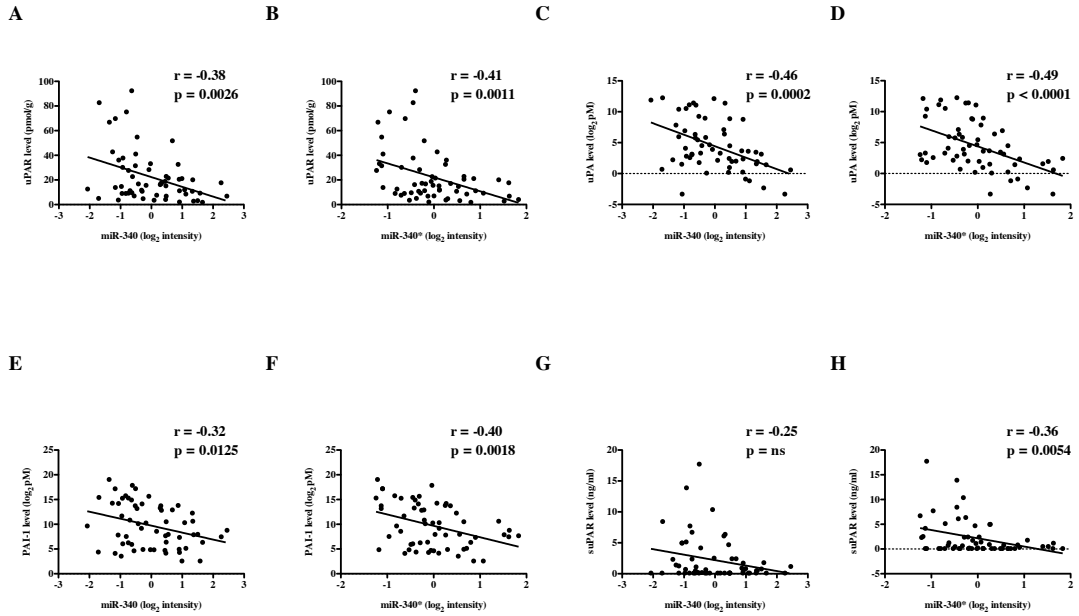

Figure 16: correlation analyses between the protein levels of the uPA-system components and miR-340/miR-340* levels.

(A-H) Scatter plots show the correlation analyses between the protein levels of the uPA-system components with miR-340/miR-340* levels. The protein levels of uPAR (A-B), uPA (C-D), PAI-1 (E-F) and suPAR (G-H) were quantified by immunoassay. uPAR and the other uPA-system components quantification was analysed in the protein lysates and in the conditioned media, respectively. The measured concentrations were used to perform correlation analysis with miR-340/miR-340* levels, mined from CellMiner™ database as $\log_2$ intensity. Pearson correlations coefficient (r) and p values (p) are reported for each correlation.

Taken together these data demonstrate that the expression of miR-340 is negatively correlated with the expression of the core components of the uPA-system both at mRNA and protein level.

7.2.2 Exogenous administration of miR-340 negatively regulates the expression of the core components of the uPA-system in the human triple negative breast cancer cell line MDA-MB-231

To test experimentally whether the predominant form of miR-340 may negatively regulate the expression of the uPA-system components, we administrated miR-340 in MDA-MB-231 cells, which showed low miR-340 level (fig. 15B) according to CellMiner™ [371]

expression data, transfecting them with a synthetic miR-340 (miR-340 mimic) and a non-targeting negative control miRNA (negative control). We first verified by RT-qPCR whether the miR-340 mimic was efficiently transfected so as to increase miR-340 level. We found that miR-340 expression resulted 20,000-fold increased compared to the negative control (fig. 17A). Secondly, we tested whether the increase of miR-340 level down regulated the mRNA levels of the core components of the uPA-system (*PLAUR*, *PLAU* and *SERPINE1*) together with other components of the plasminogen activation system (PA-system) (*SERPINB2* and *PLAT*). We uncovered that miR-340 negatively regulates the expression of the core components of the uPA-system and *PLAT* (tPA) (subsequently validated by Yamashita *et al*.[384]), whereas it seems to up regulate *SERPINB2* (PAI-2) expression, even if the difference with the negative control is not statistically significant (fig. 17B-F).

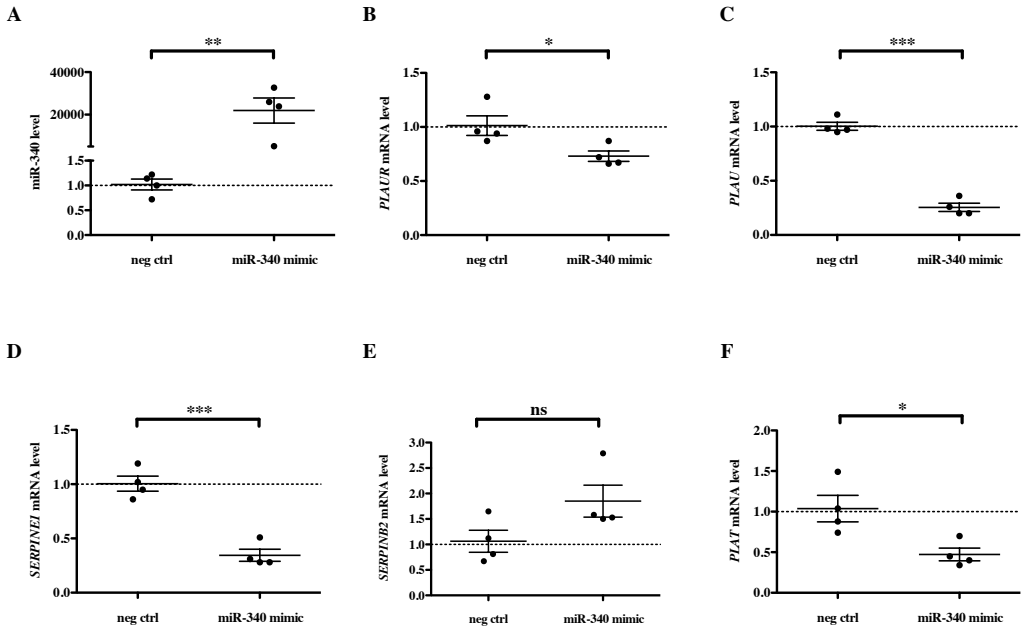

Figure 17: exogenous administration of miR-340 down regulates the mRNA levels of the uPA-system components.

(A-F) MDA-MB-231 cells, transfected with miR-340 mimic and the negative control (neg ctrl), were analysed by RT-qPCR to verify miR-340 level (A) and the effect of miR-340 administration on the expression of the uPA-system components (B-F). The RQ was calculated normalising the miR-340 and uPA-system components mean Ct values against the mean Ct values of rnu19 and two housekeeping genes (*HMBS* and *HPRT1*), respectively (ΔCt). The ΔΔCt values were calculated subtracting the ΔCt values of the calibrator sample, the negative control, to the ΔCt values of miR-340 transfected cells. The dotted line indicates the expression level of the calibrator sample. The graphs represent four independent experiments, means ± SEM are shown. Statistical significance was probed using Student's t-test (* = $p < 0.05$, ** = $p < 0.01$, *** = $p < 0.001$ and ns = not significant).

These data show that the exogenous administration of miR-340 negatively modulates the expression of *PLAUR*, *PLAU* and *SERPINE1*.

In order to test whether the negative regulation was mirrored by the protein level as well, we performed an immunoblot analysis for uPAR and uPA in protein lysates collected from MDA-MB-231 cells transfected with the miR-340 mimic and the negative control (fig 18A). We found that miR-340 strongly down regulates uPA protein level while the effect on uPAR is minor and not statistically significant (fig 18B-C).

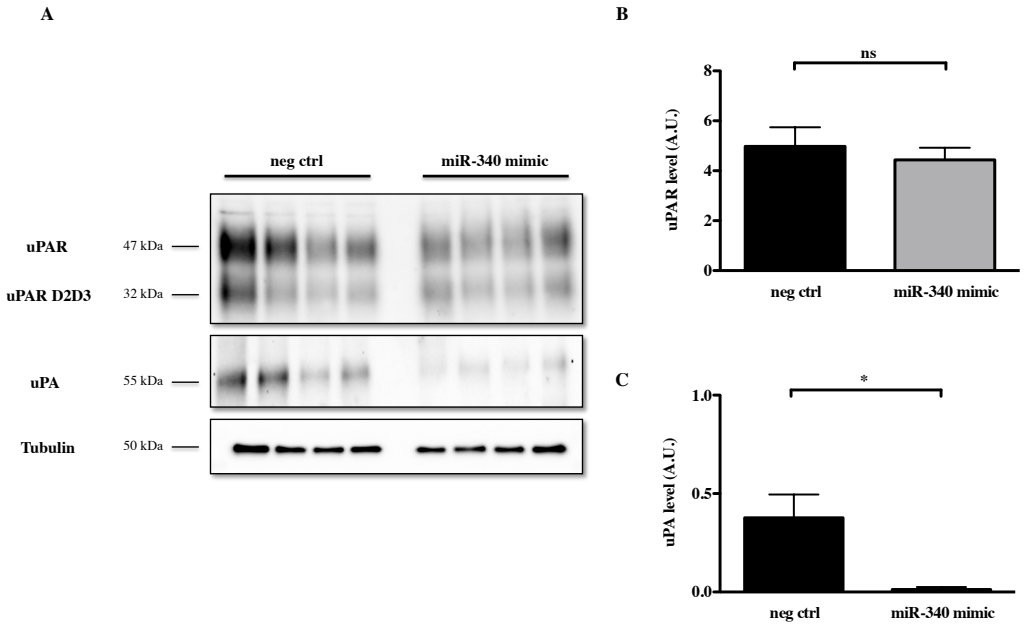

Figure 18: exogenous administration of miR-340 down regulates uPAR and uPA protein level.

(A) Protein lysates collected from MDA-MB-231 cells, transfected with miR-340 mimic and the negative control (neg ctrl), were solved by SDS-PAGE and analysed by immunoblot. uPAR and uPA protein levels were assayed by polyclonal antibodies. (B-C) The protein levels were quantified in arbitrary unit (A.U.) with ImageLab™ software (Bio-Rad) and normalised according to tubulin protein level. The graphs represent four independent experiments, means ± SEM are shown. Statistical significance was probed using Student's t-test (* = $p < 0.05$, ** = $p < 0.01$, *** = $p < 0.001$ and ns = not significant).

7.2.3 In silico analysis uncovers miR-340 may affect the mRNA stability of the uPA-system components

The transcriptional and post-transcriptional regulation of the core components of the uPA-system has been extensively studied (reviewed in[189]). Concerning the post-transcriptional regulation, mRNA instability elements, called AU-rich elements (AREs), were experimentally identified and mapped in the 3'UTRs of both *PLAUR*[306] and *PLAU*[295].

The seed region of a miRNA is a 2–8 nucleotide sequence, located at the 5' end, essential for the miRNA binding to generally the 3'UTR of its target genes[323]. The 3'UTRs of *PLAUR* and *PLAU* contain one and two miR-340 target sites, predicted by miRanda algorithm[373], respectively. We found that the miR-340 seed region binding sites coincide with the previously identified AREs for both *PLAUR*[306] and *PLAU*[295] (fig. 19). In addition,

even if not predicted, a miR-340 seed region binding site is located also in the *SERPINE1* 3'UTR, inside an AU-rich sequence (fig. 19), corroborating the role of miR-340 in modulating also *SERPINE1* mRNA instability.

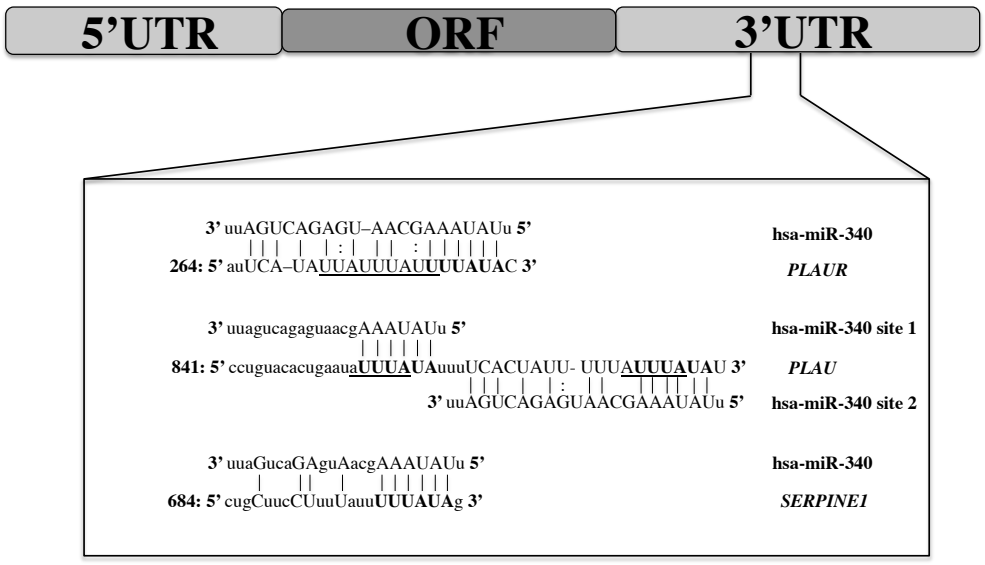

Figure 19: miR-340 may affect the mRNA instability of the core components of the uPA-system.

PLAUR and *PLAU* 3'UTRs display one and two predicted miR-340 binding sites, respectively. The miR-340 seed region binding sites (in bold) are located within the AREs (underlined), key regulators of *PLAUR* and *PLAU* mRNA instability. Although *SERPINE1* is not a predicted miR-340 target by miRanda algorithm, one miR-340 seed region binding site is located in the *SERPINE1* 3'UTR. The sequences were downloaded from UCSC genome browser[375] (https://genome.ucsc.edu/) and microrna.org website (http://www.microrna.org).

Overall these observations suggest that the binding of miR-340 to the previously identified mRNA instability elements, located within *PLAUR* and *PLAU* 3'UTRs, may enhance the degradation of the mRNAs.

7.3 CHARACTERISATION OF THE ROLE OF miR-340 IN MDA-MB-231 CELL LINE TRANSCRITOME

7.3.1 Identification of miR-340 target genes in the transcriptome of the human triple negative breast cancer cell line MDA-MB-231

To get a more complete picture of the genes regulated by miR-340, we repeated the MDA-MB-231 transfection with miR-340 mimic and the negative control to evaluate the global transcriptome changes by microarray analysis using Affimetrix Human Gene 2.1 ST Array Strip technology. The genes spotted on the microarray are 19607 and we used the following cut off values: adjusted (Benjamini-Hochberg correction[364]) p value (p) < 0.05 and fold change (fc) negative control vs. miR-340 mimic ≥ 1.4, to discriminate the genes significantly regulated by miR-340. We identified a high number of genes (1987/19607, 10.1%) significantly regulated by miR-340 among which the majority were down regulated (down regulated: 1255/1987, 63.2% vs. up regulated: 732/1987, 36.8%) (table 8).

N = 19607; fc ≥ 1.4; p < 0.05

	n	%
miR-340 targets	1987	10.1%
miR-340 down regulated targets	1255	63.2%
miR-340 up regulated targets	732	36.8%

Table 8: miR-340 regulates the 10% of MDA-MB-231 cells transcriptome.

The table summarises the microarray results derived from MDA-MB-231 cells transfected with miR-340 mimic and the negative control in four independent experiments. The total number of genes spotted on Affimetrix Human Gene 2.1 ST Array Strip is 19607 (N). The number of genes regulated by miR-340 (n) and the corresponding percentage (%) are shown. Statistical significance was probed using Student's t-test (* = $p < 0.05$, ** = $p < 0.01$, *** = $p < 0.001$ and ns = not significant). The multiple comparison correction was applied according to Benjamini-Hochberg method. The adjusted p value (p) < 0.05 and fold change (fc) negative control versus (vs.) miR-340 mimic ≥1.4 were chosen as cut off values.

The changes in gene expression were consistent with miRNA-induced mRNA instability as 1.7-fold more genes were down regulated than up regulated (63.2%/36.8%; 1255/1987 vs.

732/1987; $p < 0.001$). Among the genes significantly regulated by miR-340, the core components of the uPA-system are affected by miR-340 administration, further confirming the role of miR-340 as negative modulator of the three main uPA-system components (table 9).

N = 19607; fc ≥ 1.4; p < 0.05

	fc	p
PLAUR	1.39	0.0001
PLAU	2.93	0
SERPINE1	2.47	0

Table 9: microarray analysis confirms that miR-340 down regulates the expression of the core components of the uPA-system.

The table shows the fold change (fc) (negative control vs. miR-340 mimic) and the p value (p) of the core components of the uPA-system.

To address whether the experimentally determined miR-340 target genes were enriched in predicted ones, we generated a list of miR-340 putative target genes, predicted by both Targetscan[374] and miRanda algorithms[373], which contains 21.5% (4208/19607) of the genes recorded on the microarray. This list was intersected with the miR-340 target genes, determined by microarray, and 782 genes were found to be in common (fig. 20). Consistent with miR-340 contributing to the changes in gene expression, the predicted target genes were 1.8-fold over represented among the experimentally regulated genes (39.4%/21.5%; 782/1987 vs. 4208/19607; $p < 0.001$). The enrichment was 2.3-fold for genes repressed by miR-340 (48.5%/21.5%, 609/1255 vs. 4208/19607; $p < 0.001$) and not significant for genes induced by miR-340 (23.6%/21.5%; 173/732 vs. 4208/19607; $p = 0.16$).

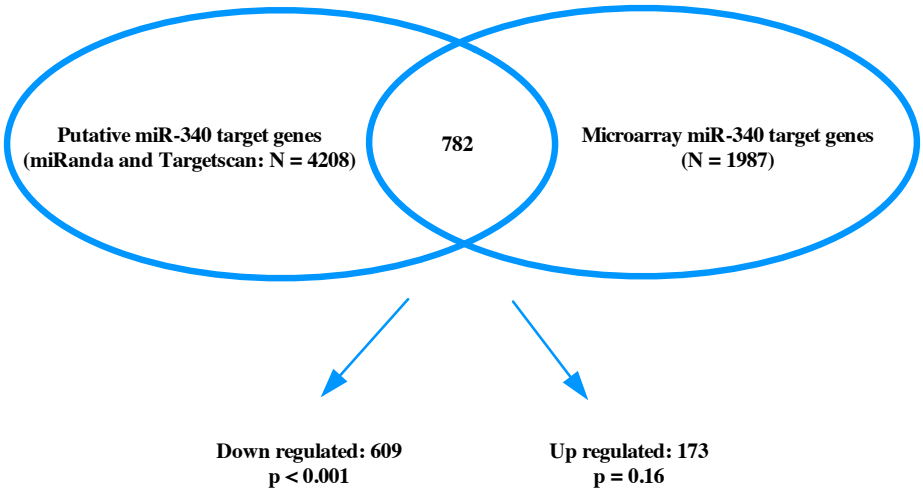

Figure 20: the experimentally determined miR-340 target list is enriched in predicted ones.

The list of putative miR-340 target genes was generated from miRanda (http://www.microrna.org) and TargetScan (http://www.targetscan.org/) algorithms and intersected with the microarray miR-340 targets. The two lists have 782 targets in common: 609 down regulated and 173 up regulated by miR-340. Statistical significance of the miR-340 putative target genes enrichment was probed using χ^2 test with Yates correction at the p value (p) < 0.05. The p concerning the enrichment analysis is reported.

Taken together, these data show that miR-340 regulates about 10% of MDA-MB-231 transcriptome mainly in a negative fashion.

7.3.2 miR-340 modulates desmoplastic reaction-related genes

The relevance of miR-340 in gene regulation has recently emerged. Several studies reported and validated miR-340 target genes involved in the tumourigenesis of different cancer types or in other disorders[385,386]. In cancer, it mainly affects the expression of tumour promoting genes such as *MET* in breast[387] and colorectal cancer[388], *ROCK1* in osteosarcoma[389,390] and glioblastoma[391] and *SOX2* in neuroblastoma[392]. In colorectal cancer miR-340 has been shown to be also involved in tumour-related processes as the Warburg effect[393] and therapy resistance[394]. Likewise miR-340 modulates cell proliferation targeting *PUM1*, *PUM2* and *SKP2*[395], *CDK6* and *CCND2*[396], *CCND1*[391,396], *EZH2*, *AKT*, *EGFR* and

BMI1[391], invasion and migration through the negative regulation of *VEGF*, *MMP-1*, *MMP-2* and *MMP-9*[391] and autophagy-related genes such as *LL3-II*, p62 and *XIAP*[391].

The microarray data revealed the ability of miR-340 to significantly down regulate the expression of the connective tissue growth factor (*CTGF*), the Rho-associated, coiled-coil containing protein kinase 1 (*ROCK1*) and the Yes-associated protein 1 (*YAP1*), which are genes involved in the desmoplastic reaction[397-399] (table 10).

N = 19607; fc ≥ 1.4; p < 0.05

	fc	p
CTGF	2.16	0
ROCK1	2.90	0
YAP1	2.38	0

Table 10: microarray analysis shows that miR-340 down regulates the expression of desmoplastic reaction-related genes.

The table shows the fold change (fc) (negative control vs. miR-340 mimic) and the p value (p) of the cluster of genes involved in desmoplasia reaction.

This phenomenon consists of an abnormal growth of fibrous or connective tissue in response to a tumour[400,401]. MDA-MB-231 cells were transfected with miR-340 mimic and the negative control and RT-qPCR analysis was performed to validate the ability of miR-340 to regulate this cluster of genes. In this analysis we also included *LOX*, which is another important player of the desmoplastic reaction[402], even if it is not significantly regulated in the microarray analysis (data not shown). We found that miR-340 significantly down regulates the expression of *CTGF*, *ROCK1* and *YAP1*, while up regulates the expression of *LOX* (fig. 21A-D).

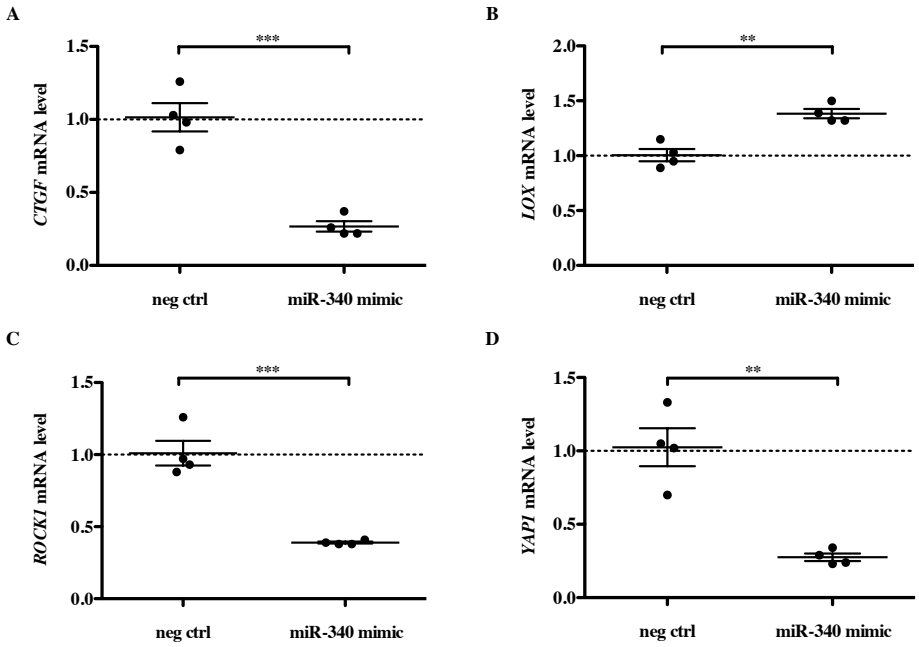

Figure 21: validation of miR-340 desmoplastic reaction-related target genes.

(A-D) The experiment was performed as in figure 17. The mRNA levels of *CTGF* (A), *LOX* (B), *ROCK1* (C) and *YAP1* (D) are shown. The graphs represent four independent experiments, means ± SEM are shown. Statistical significance was probed using Student's t-test (* = $p < 0.05$, ** = $p < 0.01$, *** = $p < 0.001$ and ns = not significant).

Although the miR-340 regulation of core genes of the desmoplastic response is not coordinated in the same fashion, we can conclude that miR-340 might have an impact in the regulation of the desmoplastic reaction.

YAP1 is a nuclear effector of the Hippo signalling pathway, which is involved in a plethora of biological functions such as development, growth, repair and homeostasis. Moreover, this gene is known to play a role in the development and progression of multiple cancers as transcriptional regulator of tumour-related pathways (reviewed in[403]). Taken into account the distinctive role of *YAP1* in tumour biology, we also evaluated the capability of miR-340 to regulate *YAP1* expression at protein level. Immunoblot analysis of protein lysates, collected from MDA-MB-231 cell line transfected with miR-340 mimic and the negative control, showed that miR-340 is able to significantly negatively regulate *YAP1* protein level (fig. 22A-B).

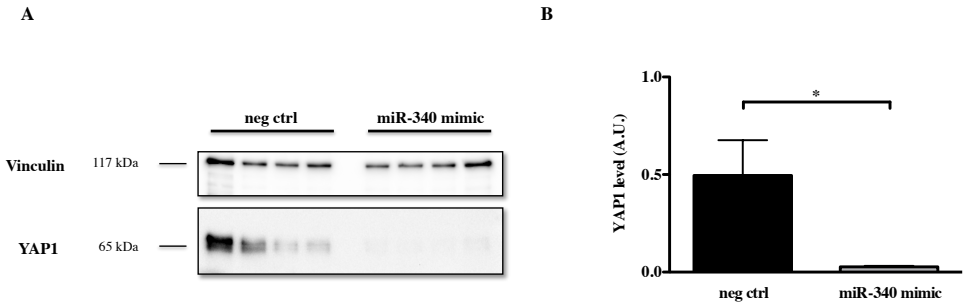

Figure 22: miR-340 down regulates YAP1 protein level.

(A-B) The experiment was performed as in figure 18. (A) YAP1 protein level was assayed by a monoclonal antibody. (B) YAP1 protein level was quantified in arbitrary unit (A.U.) using ImageLab™ software (Bio-Rad) and normalised according to vinculin protein level. The graph represents four independent experiments, means ± SEM are shown. Statistical significance was probed using Student's t-test (* = $p < 0.05$, ** = $p < 0.01$, *** = $p < 0.001$ and ns = not significant).

We conclude that miR-340 might have an important role in breast cancer tumourigenesis not only acting as modulator of the core components of the uPA-system, but possibly also modulating the desmoplastic reaction.

7.3.3 The miR-340 target list is enriched in genes significantly associated with breast cancer prognosis

The ability of miR-340 in regulating genes involved in breast cancer, including the uPA-system and the desmoplastic reaction-related genes, led us to investigate the potential clinical relevance of the experimentally determined miR-340 target genes in breast cancer. We annotated all the genes analysed in the microarray according to their association with OS performing meta-analyses of published microarray data sets using BreastMark database[376] (http://glados.ucd.ie/BreastMark/). In this procedure a p value is assigned to each gene, reflecting the statistical strength of the association with patient OS, and a hazard ratio (HR), indicating the sign and the magnitude of the effect of this association. A summary of the findings is shown in table 11.

	All genes			p < 0.05			Bonferroni correction		
	All	**HR > 1**	**HR < 1**	**All**	**HR > 1**	**HR < 1**	**All**	**HR > 1**	**HR < 1**
All genes	**19607**	9743	9864	**5326**	2901	2425	**403**	306	97
miR-340 targets	**1987**	1159	828	**726**	497	226	**141**	134	7
miR-340 down regulated targets	**1255**	814	441	**517**	413	104	**136**	129	7
miR-340 up regulated targets	**732**	345	387	**209**	84	125	**5**	5	0

Table 11: miR-340 regulates genes associated with breast cancer prognosis.

All genes spotted on Affimetrix Human Gene 2.1 ST Array Strip were annotated according to their association with breast cancer prognosis by meta-analyses of published microarray data sets using BreastMark database (http://glados.ucd.ie/BreastMark/). The association with prognosis is expressed as Hazard Ratio (HR > 1, poor; HR < 1, good). The statistical significance of miR-340 target enrichment in genes associated with breast cancer prognosis was probed using χ^2 test with Yates correction at the p value (p) < 0.05. The multiple comparison correction was applied according to Bonferroni method.

Among all the genes on the microarray (19607), 27.2% (5326/19607) are associated with significant prognostic value and 2.1% (403/19607) with a highly significant prognostic value (i.e. significant after Bonferroni multiple comparisons correction[379]). Among the miR-340 target genes, 36.5% (726/1987) are associated with a significant prognostic value and 7.1% (141/1987) with highly significant prognostic value. The experimental miR-340 target list is thus 1.3-fold enriched in genes associated with a significant prognostic value (27.2%/36.5%, 5326/19607 vs. 726/1987; $p < 0.001$) and 3.4-fold enriched in genes associated with a very significant prognostic value (2.1%/7.1%, 403/19607 vs. 141/1987; $p < 0.001$). Overall, miR-340 preferentially regulates genes associated with breast cancer prognosis.

In the whole dataset roughly half of the genes (49.7%, 9743/19607) are associated with a poor prognosis (i.e. HR > 1). For the miR-340 target list this fraction is increased 1.2-fold (58.3%/49.7%, 1159/1987 vs. 9743/19607; $p < 0.001$). When the same comparison is restricted to genes significantly associated with prognostic value, 54.4% of these have HR > 1 in the whole dataset (2901/5326), while this fraction is increased 1.3-fold for the miR-

340 targets (68.5%/54.5%, 497/726 vs. 2901/5326; $p < 0.001$). For genes that are highly significantly associated with prognosis 75.9% have HR > 1 (306/403) in the whole dataset and this fraction is increased 1.3-fold in the miR-340 target list (95.0%/75.9%, 134/141 vs. 306/403; $p < 0.001$). Thus, miR-340 preferentially regulates the mRNA levels of genes associated with a poor clinical outcome in breast cancer.

When considering the potential benefit of using miR-340 as a drug, it is desirable that genes associated with a poor prognosis (HR > 1) are down regulated and genes associated with a good prognosis (HR < 1) up regulated. To address if miR-340 has such selectivity, we analysed if the genes down regulated by miR-340 are enriched in genes associated with poor prognosis. In this analysis genes with HR > 1 were 1.3-fold over represented among genes down regulated by miR-340 when considering the whole dataset (64.9%/49.7%, 814/1255 vs. 9743/19607; $p < 0.001$), 1.5-fold when considering only the subset of genes significantly associated with prognosis (79.9%/54.5%, 413/517 vs. 2901/5326; $p < 0.001$) and 1.3-fold when considering only the highly significant genes (94.9%/75.9%, 129/136 vs. 306/403; $p < 0.001$). Importantly, the enrichment for genes with HR > 1 was not observed among genes up regulated by miR-340, in fact genes with HR > 1 were under represented: 1.1-fold considering the whole dataset (47.1%/49.7%, 345/732 vs. 9743/19607; $p = 0.09$) and 1.4-fold considering the gene significantly associated with prognosis (40.2%/54.5%, 84/209 vs. 2901/5326; $p = 0.02$). For genes highly significantly associated with prognosis only 5 are up regulated by miR-340 and no significant association was detected (100%/75.9%, 5/5 vs. 306/403; $p = 0.34$). This finding highlights the presence of a putative miR-340-dependent breast cancer signature (N = 129), which might be informative for both the prognosis and diagnosis of breast cancer patients.

In order to define the functional role of miR-340-dependent breast cancer signature, we performed a gene ontology analysis for functional categories. We found that the 129 genes are mainly involved in pathways associated with cell proliferation (fig. 23).

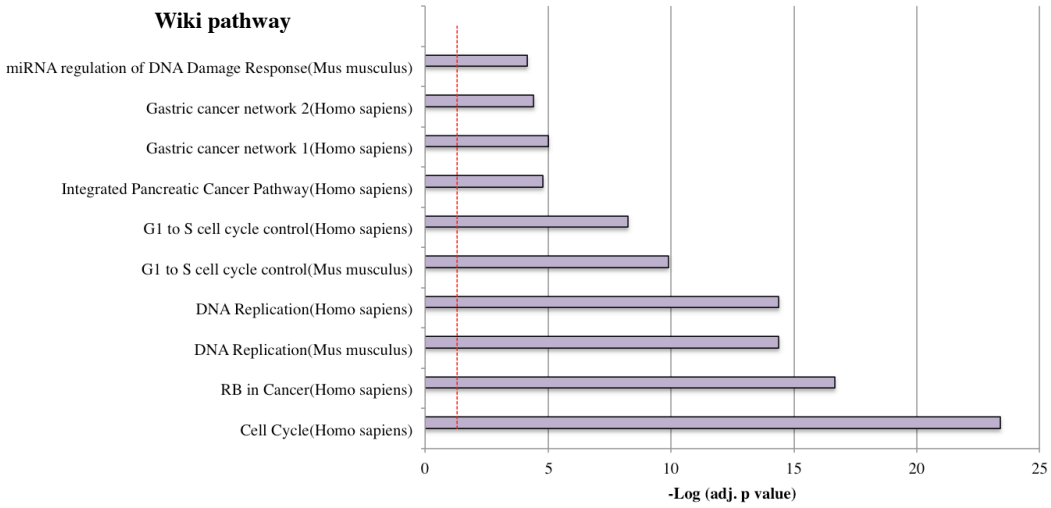

Figure 23: functional categories of miR-340-dependent breast cancer signature.

Wiki pathway of the top ten categories of miR-340-dependent breast cancer signature was performed using Enrichr software tool. The threshold of the p value ($p = 0.05$) was reported as red dotted line.

Moreover, the miR-340-dependent breast cancer signature is enriched in predictive miR-340 targets ($p < 0.0001$). Yet, the majority of these genes are not negatively correlated with miR-340 level in the NCI-60 panel (data not shown).

In summary, these data demonstrate that miR-340 targets a fraction of the MDA-MB-231 transcriptome highly enriched in genes associated with poor prognosis in breast cancer. The genes belonging to miR-340-dependent breast cancer signature are mainly involved in proliferation-related pathways. These observations suggest that the delivery of exogenous miR-340 to breast cancer tissue might ameliorate breast cancer prognosis through a biased down regulation of a large number of tumour promoting genes.

7.4 FUNCTIONAL CHARACTERISATION OF THE ROLE OF miR-340 IN BREAST CANCER

7.4.1 miR-340 expression is spread in different cell population in human breast cancer tissues

Microarray analysis unveiled that the 35% of miR-340 regulated MDA-MB-231 transcriptome consists of genes associated with poor clinical outcomes in breast cancer. In order to understand how miR-340 might influence breast cancer tumourigenesis, we firstly verified whether miR-340 is expressed in human breast cancer tissue and where it is localised. For this purpose, an *in situ* hybridization analysis (ISH) was conducted in normal, benign and malignant human breast tissues hybridising the tissue slides with a miR-340 or scramble LNA-probe. We observed that the miR-340 staining is complex with signal present in different cell population (in particular in epithelial cells and lymphocytes) both in normal and tumour tissues (fig. 24A-D).

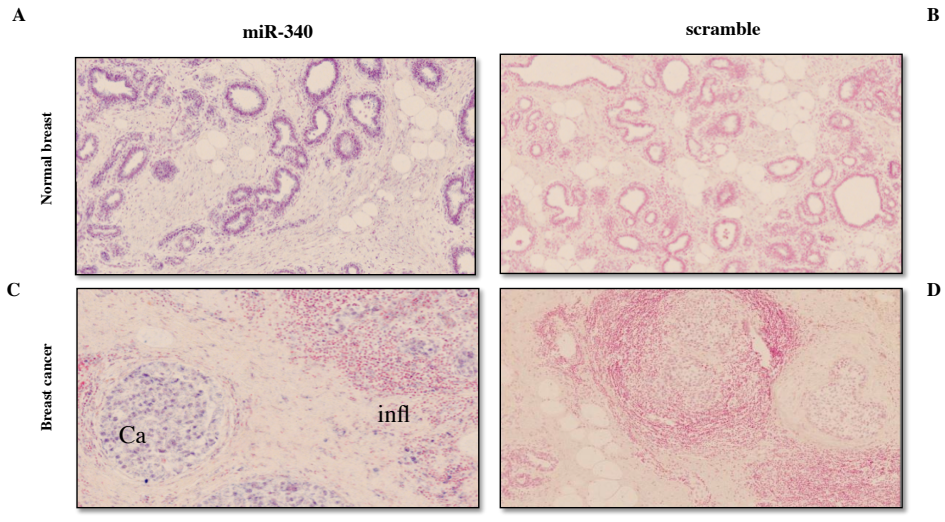

Figure 24: miR-340 is expressed in human breast epithelium.

(A-D) Tissue sections including normal and tumour breast were tested for miR-340 expression by *in situ* hybridization analysis using miR-340 (A-C) and scramble (B-D) LNA-probes. miR-340 signal is present in different cell populations, in particular in the breast cancer tissue is expressed in the tumour compartment (Ca) and in the inflammatory cells (infl). Representative images are shown. Magnification 20X.

Although this experiment does not indicate if cancer epithelium shows lower or higher miR-340 staining intensity than the normal counterpart, it is nevertheless clear that miR-340 is expressed in human breast epithelium.

7.4.2 Exogenous administration of miR-340 affects cell number and cell morphology of MDA-MB-231 cell line

To understand the effect of miR-340 in breast cancer cells, we recorded the MDA-MB-231 cells, transfected with miR-340 mimic and the negative control, by time-lapse microscopy. 16 h after transfection no difference between MDA-MB-231 cells transfected with miR-340 mimic and the negative control could be appreciated (fig 25A, D); in contrast, at later time-points a reduction of cell number and an increased cell-rounding was observed in miR-340 mimic transfected cells (fig. 25B, E and C, F).

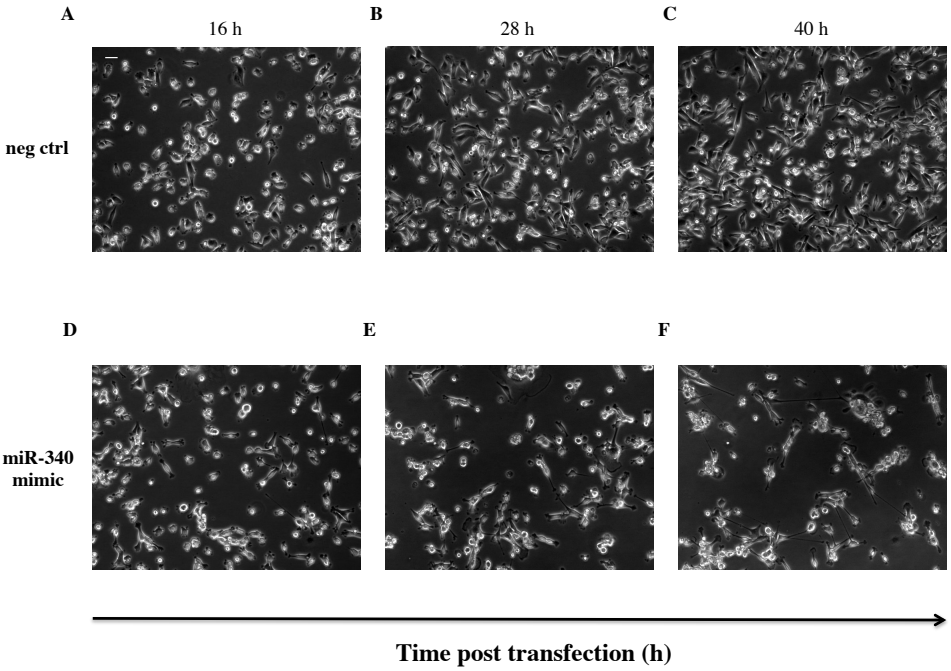

Figure 25: miR-340 administration induces a decreased cell number and increased cell-rounding in MDA-MB-231 cell line.

(A-F) MDA-MB-231 cells were transfected with miR-340 mimic and the negative control (neg ctrl) and 16 h post-transfection were recorded by time-lapse microscopy. Three different frames are shown: 16 h (A, D), 28 h (B, E) and 40 h (C, F) post transfection. The complete time-lapse recording can be found as Movie 1(miR-340 mimic) and 2 (neg ctrl). Magnification 10X. Scale bar 20 μm.

This effect suggests that miR-340 might modulate genes involved in cell cycle and cell morphology. To substantiate this result, we took advantage of the Real Time Cell-based Assay (RTCA, xCELLigence) technology, which allows for real-time monitoring of cellular events by continuous and non-invasive evaluation of impedance measurements (see materials and methods section). In line with the time-lapse observations, miR-340 transfected cells showed a different behaviour compared to the negative control. We found indeed that the miR-340 mimic curve displayed a cell index much lower compared to the negative control (fig. 26), again consistent with a growth inhibitory effect.

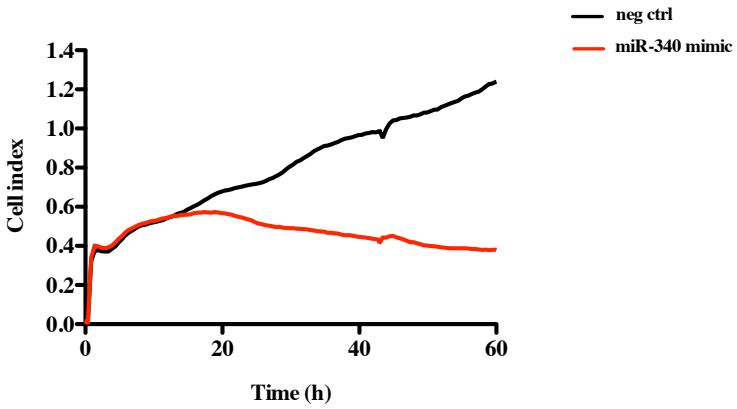

Figure 26: miR-340 administration causes a reduced cell index in MDA-MB-231 cell line.

RTCA experiments were performed on MDA-MB-231 cells transfected with miR-340 mimic and the negative control (neg ctrl). Each condition was recorded in quadruplicates and the curves represent the average cell index as a function of time. A representative experiment is shown.

To understand which miR-340 target genes is responsible for the behaviour observed in fig. 25 and 26, we knocked down the main validated miR-340 targets and compared the knock-down effect with the mimic treatment. Among the main miR-340 target genes, only *SERPINE1* and *YAP1* knockdowns seem to partially recapitulate the effect of miR-340 administration (fig. 27).

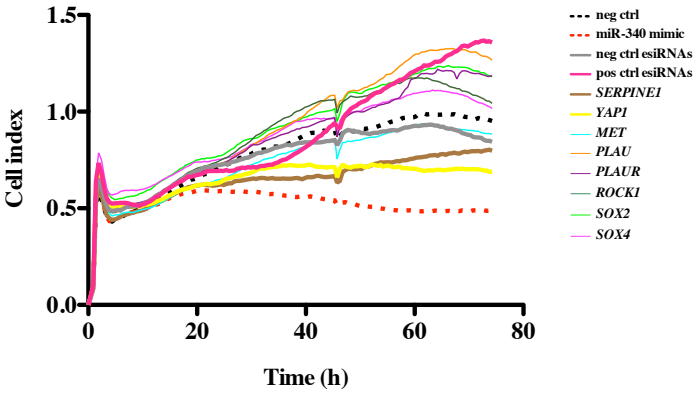

Figure 27: *SERPINE1* and *YAP1* knockdowns partially recapitulate the effect of miR-340 administration in MDA-MB-231 cell line.

RTCA experiments were performed in MDA-MB-231 cells transfected with miR-340 mimic and the negative control (neg ctrl) or esiRNAs, related to the main validated miR-340 target genes, together with the corresponding negative (neg ctrl esiRNAs) and positive control (pos ctrl esiRNAs). Each condition was recorded in quadruplicates and the curves represent the average cell index as a function of time. The curves concerning the effect of miR-340 mimic/negative control are dotted; *SERPINE1* and *YAP1* knockdowns and esiRNA positive/negative control curves are thick while the curves germane to the other knockdowns are thin. A representative experiment is shown.

This suggests that these two target genes might be the mediators of phenotypic effect of miR-340 in MDA-MB-231 cells. Since we did not knock down all the validated miR-340 target genes, the involvement of other miR-340 target genes can not be excluded.

7.4.3 miR-340 modulates the cell cycle distribution of the MDA-MB-231 cell line

To better understand whether miR-340 might have a role in cell cycle distribution, we performed a cell cycle analysis. MDA-MB-231 cells transfected with miR-340 mimic and the negative control were pulsed with BrdU for 1 h and analysed by flow cytometry. MDA-MB-231 transfected with miR-340 mimic showed a reduction in the BrdU positive cells compared to the negative control (fig. 28A-B). The quantification of the cell cycle distribution highlighted that the mimic transfected MDA-MB-231 cells exhibited a

significant reduction in the number of cells in S phase compared to the control. This effect may be due to a G1 phase arrest, even if not statistically significant (p = 0.10) (fig. 28C).

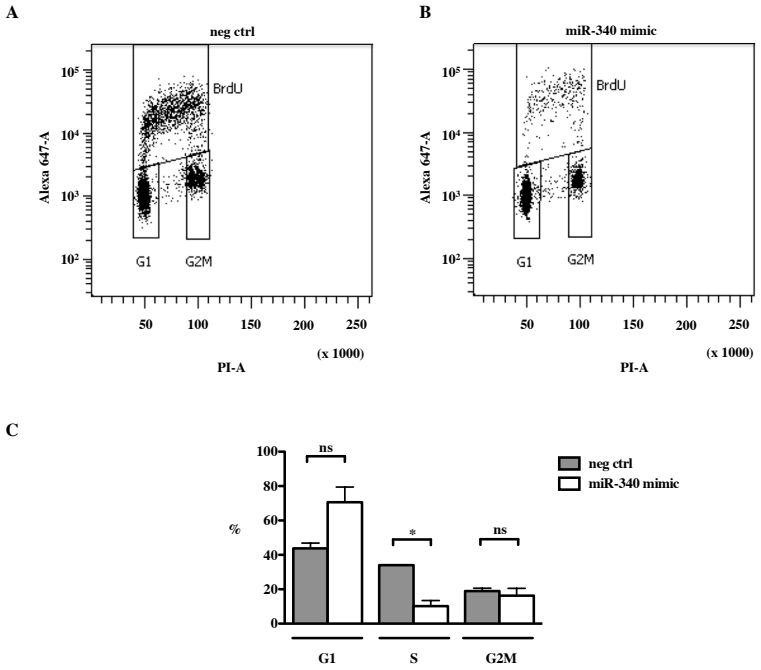

Figure 28: miR-340 affects cell cycle distribution in MDA-MB-231 cell line.

(A-B) MDA-MB-231 cells transfected with the negative control (neg ctrl) (A) and miR-340 mimic (B) were pulsed with BrdU for 1 h. The BrdU positive cells were assayed with a α-BrdU primary antibody and detected with a α-mouse Alexa 647-conjugated secondary antibody. A representative flow cytometry analysis of cell cycle distribution is reported. (C) The graph represents two independent experiments, means ± SEM are shown. Statistical significance was probed using Student's t-test (* = $p < 0.05$, ** = $p < 0.01$, *** = $p < 0.001$ and ns = not significant).

Overall, the miR-340 shows a role in the regulation of cell cycle distribution since the administration of miR-340 may determine a G1 arrest with a consequent reduction of the number of cells in S phase. This finding might justify the effect observed in time-lapse microscopy and RTCA experiments. As a consequence, the miR-340 target genes *SERPINE1* and *YAP1* might partially act as driver of these cellular changes.

7.5 IN VIVO VALIDATION OF THE ROLE OF miR-340 IN BREAST CANCER TUMOURIGENESIS

7.5.1 miR-340 over expression does not influence breast cancer growth and apoptosis rate

To test whether the effect of miR-340 in cell cycle distribution and breast cancer prognosis may have an impact on tumour growth *in vivo*, we generated stable miR-340 over expressing MDA-MB-231 cells infecting them with miR-340 or scramble control GFP-lentiviral vector (see materials and methods section). Before starting with the *in vivo* experiments, we tested viral insertion of the infected MDA-MB-231 cells measuring the number of GFP positive cells by FACS analysis. We found that MDA-MB-231 cells infected with both miR-340 and scramble lentiviral vector were viable and showed high viral insertion (fig 29).

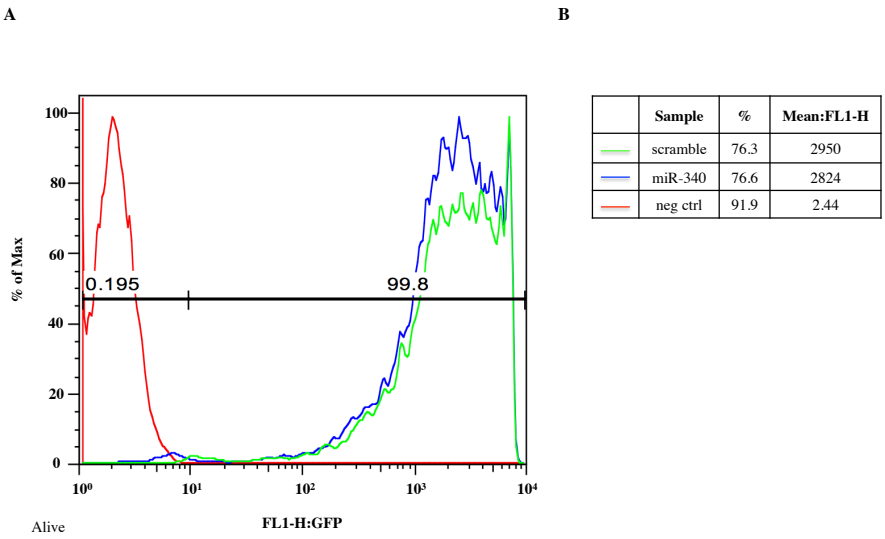

Figure 29: miR-340 and scramble infected MDA-MB-231 cells show high viral insertion.

(A-B) The viral insertion was tested measuring the GFP positive cells by FACS analysis. (A) The histograms show the GFP positive cells within the gate of alive cells. (B) The table reports the mean fluorescence intensity of each sample. The negative control (neg ctrl) represents MDA-MB-231 cells treated with H_2O.

In addition, we also quantified miR-340 levels in MDA-MB-231 cells upon infection by RT-qPCR and we observed that miR-340 expression was 100-fold increased compared to scramble (fig. 30).

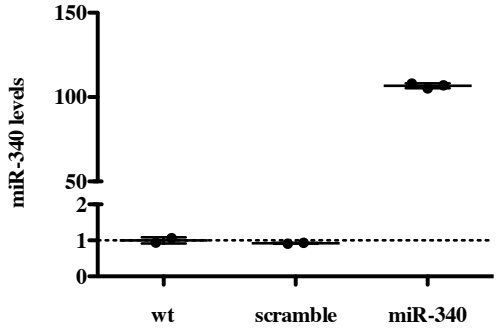

Figure 30: MDA-MB-231 cell line infected with miR-340 lentiviral vector displays a 100-fold increase of miR-340 expression.

MDA-MB-231 cells infected with miR-340 or scramble lentiviral vector were tested by RT-qPCR for miR-340 expression. The RQ was calculated normalising miR-340 Ct values against the Ct values of the housekeeping gene rnu19 (ΔCt). The ΔΔCt values were obtained subtracting the ΔCt values of the calibrator sample, wild-type (wt) MDA-MB-231 cells, to the ΔCt values of each sample. The dotted line indicates the expression level of the calibrator sample. Dots represent technical triplicates, means ± standard deviation (SD) are shown.

We injected MDA-MB-231 cells, infected with miR-340 or scramble lentiviral vector, into the mammary fat pad of CD-1 nude mice. The animals were monitored every day and, when the tumours onset, they were measured once a week by caliper. miR-340 over expression does not negatively influence the tumour volume, as a matter of fact miR-340 over expression seems to induce a slight increase in tumour growth in late tumour progression compared to scramble (fig. 31).

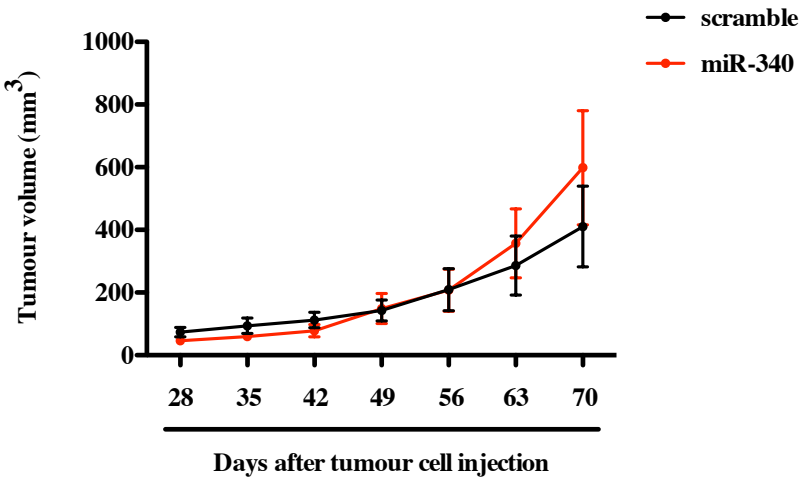

Figure 31: miR-340 does not influence breast cancer growth in CD-1 nude mice.

$5*10^6$ MDA-MB-231 cells infected with miR-340 or scramble lentiviral vector were injected into the mammary fat pad of CD-1 nude mice (N = 10/group). Tumours were measured every week by caliper until a volume of 1200 mm^3. The tumour growth curves show a merge of two independent experiments, means ± SEM are shown.

Mice were sacrificed when tumours reached 1200 mm^3 and the tumours collected and fixed in formalin. In order to better elucidate the tumour growth data, we evaluated by immunohistochemistry (IHC) analysis the expression of the proliferation marker Ki-67 and the apoptosis marker cleaved CASP3 in four mice for each experimental group. We found that miR-340 over expression does not affect the expression of Ki-67 (fig. 32 A, C-E) and the cleavage of CASP3 (fig. 32 B, F-H). The IHC analysis substantiates the data of tumour growth, since it confirm that *in vivo* miR-340 over expression does not influence both the proliferation and the apoptosis rate of breast cancer.

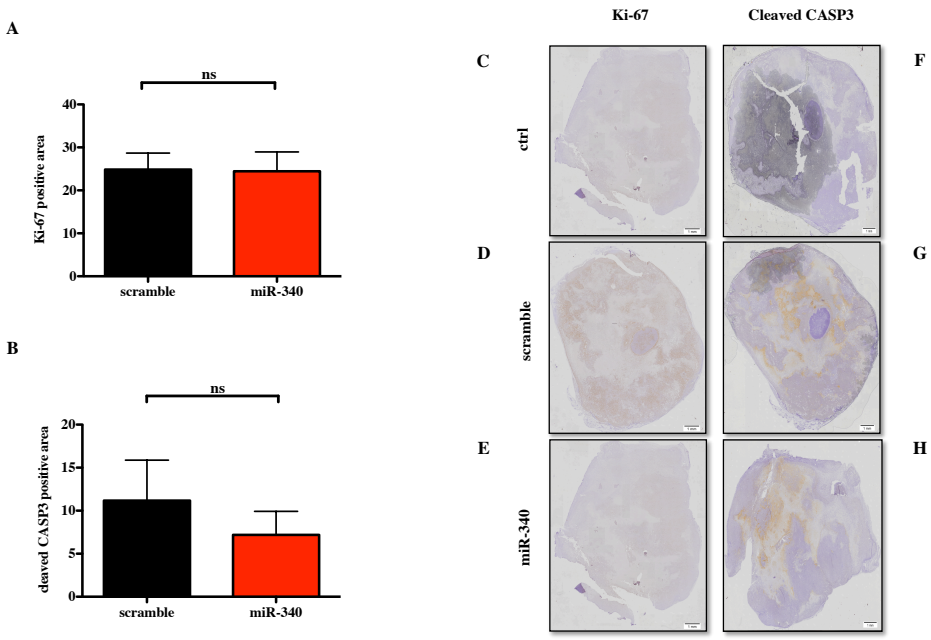

Figure 32: miR-340 over expression does not influence the expression of Ki-67 and the cleavage of CASP3 in mice tumour samples.

(A-H) Mouse tumours, described in the legend to fig. 31, were assayed for the proliferation marker Ki-67 and the apoptosis marker cleaved CASP3 by immunohistochemistry analysis in four mice/group. (A-B) The quantification of the Ki-67 and cleaved CASP3 signal was performed using ImageJ and measured as percentage of positive area. Statistical significance was probed using t-test (* = $p < 0.05$, ** = $p < 0.01$, *** = $p < 0.001$ and ns = not significant). (C-H) Representative images were shown. The control (ctrl) represents the sample without the primary antibody. Magnification 20X. Scale bar 1 mm.

Overall, miR-340 over expression does not affect breast cancer tumour growth *in vivo*. The discordance between *in vitro* and the *in vivo* data might be due to the different employed miR-340 gain-of-function systems. The lentiviral vector and the mimic increase miR-340 level 100- and 20,000-fold, respectively (fig. 17A and 30). Since the validation of miR-340 target genes was not performed in infected MDA-MB-231, likely the 200-fold less miR-340 level is not sufficient to affect the expression of miR-340 breast cancer-driver target genes.

7.5.2 Generation and characterisation of FVB/NCrl Mir340 deficient mouse model

As a consequence of the absence of concordance between the results obtained from the two different miR-340 gain-of-function systems, we decided to characterise the role of miR-340 by a more reliable loss-of-function model thus to minimise all the possible off-target effects. We first tried to transient inhibit miR-340 using a miR-340 antisense oligonucleotide but the inhibitory effect was too slight to appreciate an outcome on target genes (data not shown). Taken into account the difficulties in the transient inhibition of miR-340, we attempted to generate a stable miR-340 knock out cell line using transcription activator-like effector nuclease (TALEN) technology. Regrettably, no miR-340 knock out clone was obtained, even if the TALENs were found to target the desired locus (data not shown). Subsequently, we chose to generate a straight knock out mouse model taken advantage of the zinc fingers (ZNFs) technology[404], which are specific genomic scissors for the targeted editing of the genome.

ZNFs are engineered proteins composed of two functional domains: a DNA-binding domain, which recognises a specific hexamer on the interested DNA region, and a DNA-cleaving domain comprised of the nuclease domain of the restriction endonuclease Fok I. When these two domains are fused together the ZNFs cut in the specific DNA region causing a double-strand break. This DNA damage can be repaired by homologous or non-homologous end joining recombination obtaining a site-specific mutagenesis or a complete knock out, respectively.

The ZNFs were designed to bind a region located 130 bp upstream the Mir340 locus. The ZNFs-directed double strand break was repaired by homologous recombination, providing a specific replacement template, which mediates a 188 bp deletion, aimed to the complete disruption of Mir340 locus (fig. 33).

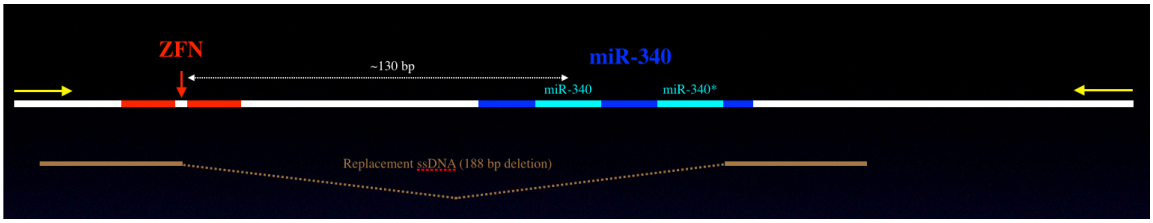

Figure 33: ZNFs strategy for the deletion of Mir340 locus.

The zinc fingers (ZNFs) were designed to bind a DNA region (red) 130 bp upstream the miR-340 locus (blue and light blue). The replacement template, which mediates the complete deletion (188 bp) of miR-340 locus, was depicted in brown. The yellow arrows indicate the primer pair employed for the genotyping and sequencing.

Starting from three rounds of ZNFs and replacement template pronuclear microinjection, two in FVB/NCrl and one in C57BL/6 background (see material and method section), the new born-targeted animals were screened for the Mir340 deletion. The DNAs extracted from mouse tail were amplified using the primer pair depicted in figure 33 and digested with two different restriction enzymes: BamHI and T7E1. BamHI digestion was assayed because the replacement template-mediated deletion causes the lost of a BamHI site; the T7E1 restriction enzyme was employed after the denaturation and reannealing of the PCR product since it cuts only in the presence of heteroduplex, which indicates the presence of mismatches.

In the first round 19 FVB/NCrl pups were screened and no suspected founder animals were found (fig. 34).

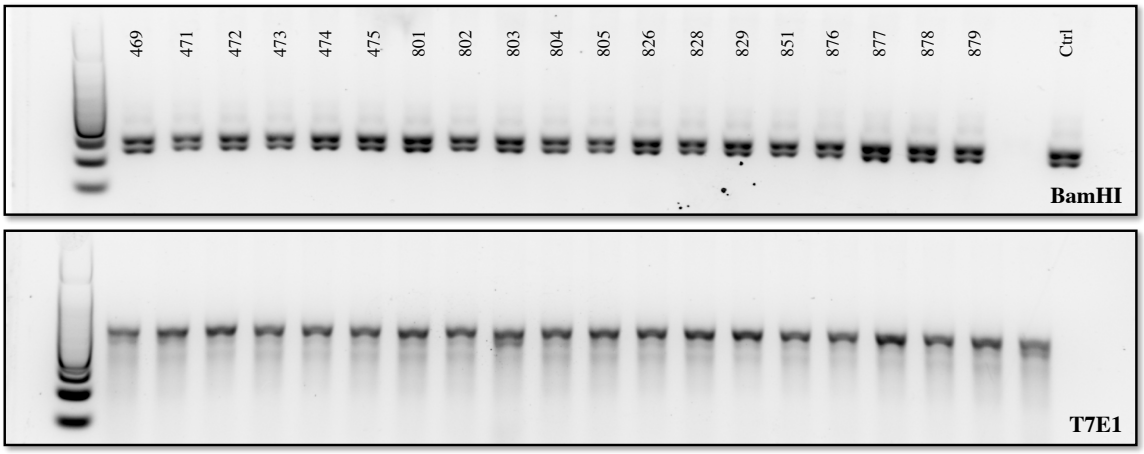

Figure 34: screening of pups derived from the first round of pronuclear microinjection.

The Mir340 locus was amplified using the primer pair depicted in fig. 33 and subsequently digested by two different restriction enzymes: BamHI and T7E1.

The sequencing confirmed that the 19 mice did not show the deletion of Mir340 locus (table 12).

Strain	ID	Sex	Allele
FVB miR-340	469	M	wild-type
FVB miR-340	471	F	wild-type
FVB miR-340	472	F	wild-type
FVB miR-340	473	F	wild-type
FVB miR-340	474	M	wild-type
FVB miR-340	475	F	wild-type
FVB miR-340	801	F	wild-type
FVB miR-340	802	F	wild-type
FVB miR-340	803	M	wild-type
FVB miR-340	804	M	wild-type
FVB miR-340	805	M	wild-type
FVB miR-340	826	M	wild-type
FVB miR-340	828	F	wild-type
FVB miR-340	829	F	wild-type
FVB miR-340	851	F	wild-type
FVB miR-340	876	M	2 bp deletion in ZNFs binding site (homozygote)
FVB miR-340	877	F	wild-type
FVB miR-340	878	F	wild-type
FVB miR-340	879	F	wild-type
C57BL/6 miR-340	809	M	wild-type
FVB miR-340	810	M	deletion miR-340 locus (heterozygote)
C57BL/6 miR-340	818	M	wild-type
FVB miR-340	821	F	rearrangement ZNFs binding site (heterozygote)
FVB miR-340	822	F	wild-type
FVB miR-340	827	F	rearrangement in ZNFs binding site (heterozygote)
FVB miR-340	830	F	deletion miR-340 locus (heterozygote)
FVB miR-340	853	F	wild-type
FVB miR-340	854	M	wild-type
FVB miR-340	882	M	wild-type
FVB miR-340	883	M	wild-type
FVB miR-340	884	M	wild-type
FVB miR-340	885	F	wild-type

Table 12: sequencing of the targeted animals.

The Mir340 locus of the mice generated by the three rounds of pronuclear microinjection was sequenced by Big Dye chemistry using the primer pair depicted in fig. 33. The strain, mouse ID, sex and sequencing result (allele) were reported.

The second and the third rounds of microinjection gave rise to two C57BL/6 and 11 FVB/NCrl pups, respectively. According to the same restriction enzyme-based assays, we identified two suspected founder mice (#810 and #830) in FVB background, one male and one female (fig. 35).

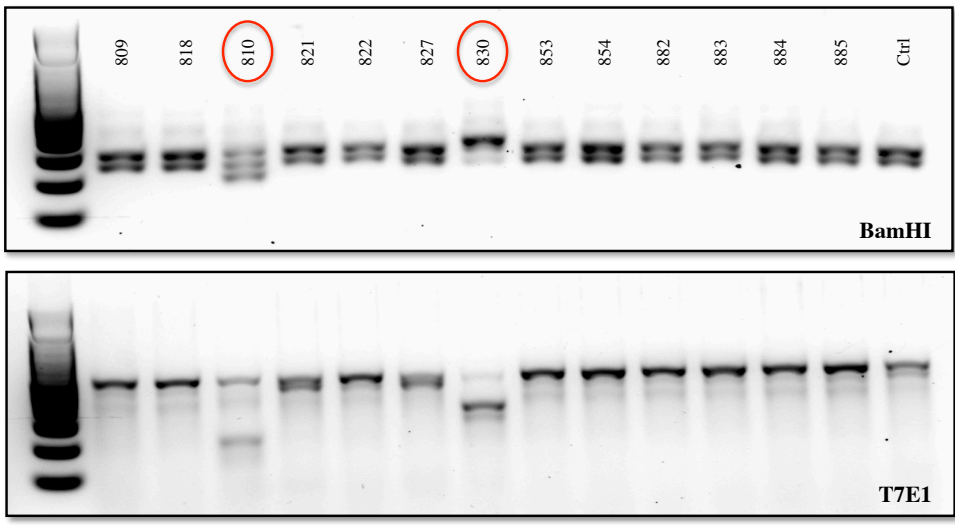

Figure 35: screening of pups derived from the second and third rounds of pronuclear microinjection.

The editing of Mir340 locus was assayed as in figure 34. The founder animals are highlighted with a red circle.

Nevertheless, also in this case, we sequenced the Mir340 locus of all pups. The results of the sequencing are summarised in table 12. The mice #810 and #830 had the complete deletion of miR-340 locus on one allele (fig. 36), whereas #821 and #827 displayed ambiguous rearrangements.

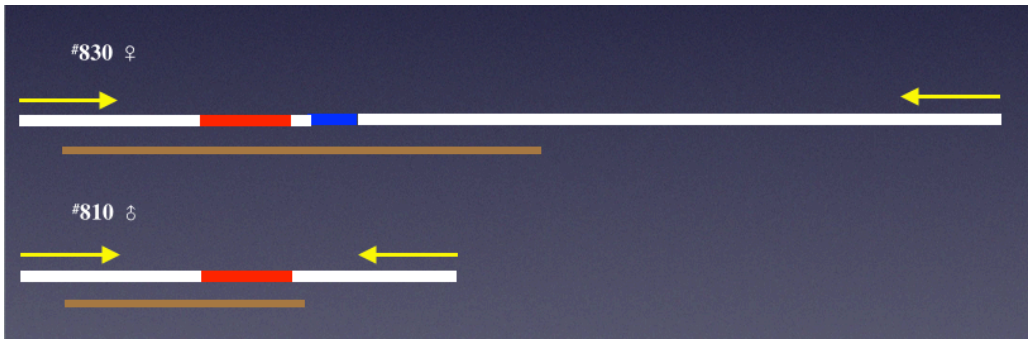

Figure 36: #810 and #830 Mir340 allele.

The two founder mice show the complete deletion of Mir340 locus. The colour legend is the same of fig. 33.

In order to better understand the kind of rearrangements in #821 and #827 mice, we cloned their miR-340 locus in one shot® TOP10 chemically competent *E.Coli* using pCR™4-TOPO® vector. The sequencing of the Mir340 positive colonies revealed that #821 and #827 presented only deletions upstream the Mir340 locus.

To confirm the germ line transmission of the Mir340 deleted allele in F1 offspring the founders #810 and #830 were crossed. Since the germ line transmission was confirmed, FVB Mir340 colony was generated crossing heterozygous F1 animals, carrying mother deleted allele. The breeding pairs were replaced every six months with new heterozygous breeders.

A new genetically modified mouse strain has to be subjected to phenotypic studies in order to verify whether the genome editing affects mouse health. According to European guidelines for the generation of a genetically modified mouse strain (implementation of Directive 2010/63/EU), the phenotypic analysis has to be conducted, from the weaning until the sexual maturity, in seven wild type and seven genetically modified animals, derived from more than one litter and belonging to F2 onwards generation. This analysis revealed that FVB Mir340 knock out mice showed a normal phenotype. The criteria followed and the results obtained in the phenotypic analysis are summarised in table 13.

	Wild types	Knockouts
Overall appearance		
Morphologically normal	YES	YES
Malformations	NO	NO
Size, conformation and growth		
Deviation from expected size	NO	NO
Deviation from expected growth curve	NO	NO
Behaviour		
Social interaction	YES	YES
Grooming	YES	YES
Walking	YES	YES
Running	YES	YES
Digging	YES	YES
Climbing	YES	YES
Movements	NORMAL	NORMAL
Orientation	NORMAL	NORMAL
Rigidity and tremors	NO	NO
Iper- or ipo- activity	NO	NO
Clinical signs		
Nasal or ocular discharge	NO	NO
Swollen or closed eyes	NO	NO
Respiratory rate	NORMAL	NORMAL
Seizure/twitched/tremors	NO	NO
Vocalization	NORMAL	NORMAL
Teeth	NORMAL	NORMAL
Tumours	NO	NO
Neurological or muscukoskeletal abnormalities	NO	NO
Metabolism	NORMAL	NORMAL
Coat/whiskers/skin	NORMAL	NORMAL
Numbers		
Death pre- or post- weaning	NO	NO
Post mortem examination	NORMAL	NORMAL
Fertility	YES	YES

Table 13: phenotypic analysis of FVB Mir340 strain.

The phenotypic analysis was conducted in seven FVB Mir340 knock out and seven FVB Mir340 wild type mice from weaning to sexual maturity, derived from more than one litter and belonging to F2 onwards generation. The table summarises the criteria followed and the results obtained.

Subsequently, we verified whether the Mir340 allele followed the Mendelian distribution in 167 mice born from heterozygous breeders. The expected ratio of Mir340 allele distribution is 25% wild type, 50% heterozygous and 25% knock out. We found 23.4% of wild type (39/167), 51.5% of heterozygous (86/167) and 25.1% of knock out (42/167) mice (table 14). Considering the expected proportion, the distribution of the genetically modified allele is completely consistent with Mendel's rules.

N = 167

	wt	het	ko
Male	21	46	22
Female	18	40	20
All	**39**	**86**	**42**

Table 14: Mir340 allele follows Mendelian distribution.

The table shows the distribution of the Mir340 allele in 167 FVB Mir340 mice derived from heterozygous breeders. The absolute numbers of wild type (wt), heterozygous (het) and knock out (ko) mice are shown.

We also checked if the Mir340 knock out mice were fertile. To this purpose, we crossed one male and one female FVB Mir340 knock out mice and followed the fertility for two oestrus cycles. We obtained new generations for each oestrus, the new-borns were healthy and the number of pups/litter was comparable to the expected. Thus, the fertility of knock out mice is as good as the wild type and heterozygous mice.

8. DISCUSSION

The emerging importance of the microenvironment during tumourigenesis has raised attention to identify determinants, which orchestrate microenvironment plasticity during cancer onset and progression. The uPA-system is well established to be involved in microenvironment homeostasis both in normal and pathological conditions. In the context of cancer, the uPA-system is able, on the one hand to sustain tumour formation enhancing proliferative signalling; on the other hand it supports tumour invasion and metastases through the activation of pericellular proteolysis and migratory intracellular signalling pathways. In breast cancer, the components of the uPA-system are frequently co-over expressed and mainly localised in the stromal compartment. Clinical studies unveiled that high levels of uPA, uPAR and PAI-1 are associated with poor clinical outcome in breast cancer[169]. Specifically uPA and PAI-1 are among the strongest breast cancer prognostic markers with the highest level of evidence[167]. In spite of the relevant role of the uPA-system components in breast cancer and the extended characterisation of their transcriptional and post-transcriptional regulation, the molecular mechanisms underling the co-over expression of *PLAU*, *PLAUR* and *SERPINE1* are still to uncover. In this study we propose that a miRNA, the miR-340, contributes to the coordinated expression of the three uPA-system components in the context of breast cancer. In addition, miR-340 is able to negatively regulate the expression of desmoplastic reaction and poor breast cancer prognosis-related genes, thus representing a new potential drug for breast cancer patients.

8.1 ERBB2 AND *PLAUR* ARE NEITHER CO-AMPLIFIED NOR CO-EXPRESSED

The role of uPAR in breast cancer has not been fully elucidated yet. Unlike uPA and PAI-1, uPAR is considered a less strong breast cancer prognostic marker[169], even if it has been reported to be associated with poor clinical outcomes[170,171]. Several studies have proposed the synergistic effect of uPAR and ERBB2 in the aggressiveness of $ERBB2^{+}$ breast cancer

subtype; co-amplification and co-expression of *ERBB2* and *PLAUR* were indeed observed in advanced breast CTSs, TPs of frozen primary breast carcinoma[183,184] and in bone marrow micro metastatic cells[185]. The possibility of a functional cross talk between uPAR and the ERBB2 has been also supported by *in vitro* experiments using different breast cancer cell lines. Namely, Li *et al*.[188] showed the synergistic effect of uPAR and ERBB2 in supporting proliferation via the ERK signalling and in inhibiting apoptosis in ERBB2 and uPAR over expressing breast cancer cells. In addition, Tan *et al*.[186] reported, in breast cancer cell lines and patients, that the over expression of uPAR relies on an ERBB2-mediated induction of the Src/PKCα signalling axis. Several studies also investigated the cross talk between uPAR and EGFR. Jo *et al*.[187] demonstrated that the proliferative signalling triggered by EGF is supported by uPAR; indeed they proposed that EGFR and uPAR may enhance proliferative signalling pathway through Src-mediated STAT5 activation. A different mechanism was suggested by Liu *et al*.[89] in which EGFR mediated the growth of HEp3 human carcinoma and MDA-MB-231 cells via uPAR/integrin/FN/FAK/ERK signalling cascade in uPAR-rich environment.

In order to test the proposed *ERBB2* and *PLAUR* co-amplification and co-over expression, we performed a copy number variation and expression analysis in a cohort of 133 unselected Dutch breast cancer patients. In our cohort, we identified a subset of patients characterised by *ERBB2* amplification and over expression (fig. 10A and 11A), which confirmed the well known finding that in *ERBB2*$^+$ breast cancer *ERBB2* over expression is mainly due to *ERBB2* locus amplification[381]. The cluster of patients with *ERBB2* amplification did not show the concomitant *PLAUR* amplification (fig. 10B). *PLAUR* expression data indeed did not display a specific trend (fig. 11B). The correlation analysis between *ERBB2* and *PLAUR* expression levels clearly showed the absence of a correlation between the two genes ($r = 0.03$; $p = 0.77$) in our cohort of patients (fig. 12).

The discordance between our data and those shown in the previous studies may have several explanations. First, we carried out the study in a cohort of unselected breast cancer

patients, while in the above-mentioned studies the analyses were conducted mainly in advanced breast carcinoma patients. Second, the sample types are different: our samples derive from standard tumour biopsies, which represent a mixture of different epithelial and stromal cells while, in the previous studies, the *ERBB2* and *PLAUR* gene status was analysed in CTCs, TPs and isolated micro metastatic cells. Taken into account that tumour is a dynamic and heterogeneous disease, which continuously arranges itself during cancer progression and different mutations/alterations may be acquired only by a specific subset of cells, it can not be excluded that distinct cell types, analysed at different tumour stages, might show different rearrangements. This observation is supported by Markiewicz *et al*.[184], which also reported the absence of correlation between *ERBB2* status in primary tumours and CTCs. Furthermore, the studies on the localisation of uPAR in human breast cancer tissues mainly support a stromal localisation of the uPA-system components[155-157]; on the contrary ERBB2 is a well-known epithelial marker. Likely *ERBB2* and *PLAUR* co-amplification and co-expression is a very late step of tumourigenesis and only a small portion of cells shows this kind of rearrangement. A third aspect to be considered is the kind of assay employed. We analysed gene amplification and gene expression using qPCR while, in the previous works, at least one of the two genes was assessed by immunofluorescence (IF), IHC or fluorescence *in situ* hybridization (FISH), which are less sensitive than qPCR.

8.2 PLAUR AND *PLAU* EXPRESSION IS HIGHLY CORRELATED IN BREAST CANCER

In the same cohort of patients, we measured the expression of putative breast cancer-related genes. Correlation analysis between *PLAUR* expression level and the expression of the other genes measured highlighted that the strongest correlation is between *PLAUR* and *PLAU* ($r = 0.74$, $p < 0.001$) (table 3 and fig. 13). To corroborate this observation, correlation analyses mining expression data from microarrays of breast cancer patients and

human cancer cell lines were performed. Out of more than 20,000 genes covered, *PLAU* was always one of the strongest correlated with *PLAUR* (table 4).

The existence of common mechanisms of transcriptional and post-transcriptional regulation of *PLAU* and *PLAUR* has already been documented. At transcriptional level, they share SP1 transcription factor and several enhancers, which are mainly recognised by FOS transcription factor family and NF-κB (reviewed in[189]). *PLAU* and *PLAUR* may be subjected to the same post-transcriptional mechanisms for the regulation of mRNA half-life. Indeed, the mRNA instability mainly depends on modules of AU-rich sequences, called AREs, located within the 3'UTR of both *PLAU*[295] and *PLAUR*[306], and the binding of specific RNA-binding proteins. This mechanism might be impaired in cancer as demonstrated for *PLAU* up regulation in MDA-MB-231 cells[299]. On the contrary, a direct evidence of *PLAUR* up regulation in cancer due to an impairment of AREs-mediated mRNA instability has not been reported yet, but a different mechanism of mRNA stabilisation has been proposed. Interestingly, a uPA-dependent binding of an unknown RNA-binding protein to *PLAUR* mRNA coding region seems to stabilise the transcript in *PLAUR* transfected kidney cells and in non-small cell lung cancer primary cells[307,308]. In addition, p38α MAPK signalling pathway is important for the maintenance of breast cancer invasive phenotype since it promotes the stability of both *PLAU* and *PLAUR* mRNA[405]. In contrast, studies on the aberrant transcription of *PLAU* and *PLAUR* in cancer have not reported shared mechanisms of transcriptional regulation, even if they can not be excluded. Indeed, *PLAU* over expression was shown to mainly depend on NF-κB- and β-catenin-mediated transcription in pancreatic adenocarcinomas[222] and colorectal cancer[223], respectively. In addition, epigenetic modifications in the methylation status of the promoter may also influence *PLAU* expression in breast cancer cell lines[224,225]. On the other hand, *PLAUR* over expression in tumours has been shown to mainly depend on tumour-specific transcription factors binding the AP2/SP1 sites in gastrointestinal tumours[243]. Furthermore, it has been observed that the over expression of B-cell lymphoma 2 (BCL-2) in breast

cancer cells, in hypoxic conditions, induces SP1-mediated *PLAUR* expression through ERK1/2 signalling[406].

The studies on *PLAUR* and *PLAU* post-transcriptional regulation suggested us the possibility that post-transcriptional regulation mechanisms, in addition to those involved in the regulation of transcription, might contribute significantly to the co-expression. In the context of post-transcriptional regulation, miRNAs have emerged as important players. Several microRNAs have been identified to regulate the expression of individual uPA-system components and a single microRNA, miR-146a, has been reported to indirectly target both *PLAUR* and *PLAU* in mouse brain metastases[349].

8.3 IDENTIFICATION OF miR-340 AS MODULATOR OF THE EXPRESSION OF THE uPA-SYSTEM COMPONENTS

Starting from the findings concerning *PLAUR* and *PLAU* post-transcriptional regulation, we hypothesised that one or more microRNAs might be the determinants of the *PLAUR* and *PLAU* co-expression. To test this hypothesis, we inspected *PLAUR* and *PLAU* mRNAs for predicted miRNA target sites using miRanda database[373] and we found three candidates microRNAs in common: miR-193a-3p, miR-193b and miR-340 (table 5). Using the CellMiner™ web tool[371], we found that only miR-340 level is negatively correlated with the expression of *PLAUR* and *PLAU* and remarkably also with *SERPINE1* (table 7 and fig. 14). The inverse correlation was also observed at protein level, except miR-340 level with suPAR (fig. 16).

suPAR is mainly generated by post-translational processing of the protein through uPAR shedding and cleavage[77,78]. As a consequence, the level of suPAR is mainly dependent on the *PLAUR* transcription. Likely the effect of miR-340-mediated *PLAUR* down regulation was not so strong to induce a down regulation also on suPAR protein level. In addition, a *PLAUR* transcript variant encoding for a soluble form of uPAR has been identified[227,229];

this variant shows a completely different 3'UTR compared to the most abundant isoform, therefore it might be not regulated by miR-340.

To test whether miR-340 down regulates the expression of the uPA-system components, we exogenously administrated miR-340 in MDA-MB-231 cells, which show high *PLAUR* and low miR-340 expression, using miR-340 mimic oligonucleotides and measured the expression levels of the three main uPA-system components together with other components of the PA-system: *SERPINB2* (PAI-2) and *PLAT* (tPA). In line with the data of correlation analyses, miR-340 administration elicited the down regulation of the core components of the uPA-system and *PLAT* (fig. 17B-D, F); on the contrary a trend of *SERPINB2* up regulation was observed (fig. 17E). Immunoblot analysis of miR-340 mimic transfected MDA-MB-231 cells confirmed the negative regulation of uPA also at the protein level while the effect on uPAR was minor and not statistically significant (fig. 18). The identification of *PLAT* as miR-340 target is in line with the prediction of miRanda algorithm available in microRNA.org and has been recently documented by Yamashita *et al*.[384] in glioblastoma samples. The opposite trend observed in *SERPINB2* expression level is unexpected since two miR-340 binding sites are predicted by miRanda algorithm. The mirSVR score suggests a miR-340-mediated negative regulation of *SERPINB2*. PAI-1 and PAI-2 participate to the same biological functions, such as the inhibition of uPA and tPA, but are also involved in different cellular mechanisms (reviewed in[127]). Furthermore, the PAI-2-mediated functions are not fully clarified yet (reviewed in[407]). In breast cancer, for example, PAI-1 levels are mainly associated with poor prognosis; on the contrary, PAI-2 levels are associated with good prognosis, especially in patients with high uPA level[408]. This observation suggests that likely miR-340 might act, on the one hand as negative regulator of tumour-promoter genes, on the other hand as positive regulator of oncosuppressor-like genes as *SERPINB2*.

8.4 miR-340 MAY AFFECT THE mRNA STABILITY OF THE uPA-SYSTEM COMPONENTS

The binding of a miRNA to its target mRNA may elicit either inhibition of mRNA translation or mRNA degradation, interfering with the translational machinery[324-326] or sustaining the destabilisation of the mRNA through miRNA-mediated mRNA deadenylation and decay[327-329], respectively. The previously published observations suggest that miR-340 acts on the degradation of the mRNA. The presence of the AREs sequences within the 3'UTR of both *PLAU* and *PLAUR* prompted us to investigate whether the binding of miR-340 to the AREs sequences might enhance the destabilisation of the mRNA. We mapped *in silico* the miR-340 seed region binding site/s in the 3'UTR of *PLAUR*, *PLAU* and *SERPINE1*. We found that miR-340 is predicted to bind the 3'UTR of both *PLAUR* and *PLAU* within the AREs (fig 19). In addition, even if not predicted, a miR-340 seed region binding site is located also in the *SERPINE1* 3'UTR inside an AU-rich sequence (fig 19), corroborating the role of miR-340 in regulating also *SERPINE1* expression. The weaker miR-340-mediated *PLAUR* down regulation on mRNA and protein levels, compared to the other components of the uPA-system, might be due to partial overlap between miR-340 binding site and the ARE sequence (fig 19). On the other side, Tran *et al*.[302] demonstrated the importance of AREs sequences in *PLAU* mRNA instability proposing a mechanism of mRNA instability regulation, which involves different AREs binding proteins; in addition Jing *et al*.[409] showed the involvement of miR-16 in AREs-mediated mRNA instability. This mechanism might act also on *SERPINE1* mRNA since, even if miR-340 seed region does not coincide with AREs, the binding of miR-340 occurs within AU-rich sequence; on the contrary it does not fit with *PLAT* and *SERPINB2* miR-340-mediated regulation. The miR-340 binding site in the *PLAT* transcript does not map neither within AREs nor AU-rich sequences. Yet AU-rich sequences, present within the *PLAT* 3'UTR, are associated with mRNA adenylation/deadenylation rather than decay

(reviewed in[189]). Studies on *PLAT* post-transcriptional regulation underlined that it is mainly dependent on the 5'UTR sequence through the control of the translational process rather than mRNA instability (reviewed in[189]). *SERPINB2* shows two miR-340 binding sites located neither in the identified ARE sequence nor in AU-rich sequences (reviewed[189]). These observations suggest that miR-340 might act as negative modulator, through ARE-mediated enhancement of mRNA instability, only of the three main uPA-system components: *PLAUR*, *PLAU* and *SERPINE1*.

8.5 CHARACTERISATION OF THE miR-340 TARGETOME IN MDA-MB-231 CELL LINE

To get a complete picture of the miR-340 target genes, we performed a microarray analysis in MDA-MB-231 cells transfected with miR-340 mimic and negative control. This analysis unveiled that miR-340 is able to regulate the expression of 10% (1987/19607) of MDA-MB-231 transcriptome mainly in a negative fashion (1.7-fold more genes were down regulated than up regulated), consistent with miRNA-induced mRNA instability. The negative regulation of the uPA-system components was further confirmed (table 9). Actually, the regulation of 10% of the transcriptome is sizeable. This might be due to off-target effects, since miR-340 level in transfected cells largely exceeds the physiological level[410], or to indirect miR-340-mediated gene regulation. In the latter case, miR-340 might modulate the expression of transcription factors that in turn might regulate the expression of a consistent number of genes. On the opposite side, the effect on the MDA-MB-231 transcriptome might also depend on a toxic effect of miR-340 mimic. To partially exclude these hypotheses, we verified whether the experimentally determined miR-340 target list was enriched in putative miR-340 targets and we found that the predicted target genes were 1.8-fold over represented among the experimentally regulated genes.

The involvement of miR-340 in regulating gene expression has emerged in the last decade. Several papers showed the capability of miR-340 to modulate the expression of cancer-

related genes such as *MET* in breast and colorectal cancer[387,388], *ROCK1* in osteosarcoma[389,390] and glioblastoma[391] and *SOX2* in neuroblastoma[392]. Moreover, miR-340 has been shown to regulate also the expression of genes involved in cancer-related processes such as the Warburg effect[393], therapy resistance[394], proliferation[391,395,396], invasion/migration[391] and autophagy[391]. The microarray analysis showed that miR-340 is able to negatively regulate genes involved in the desmoplastic reaction[397-399]: *CTGF*, *ROCK1* and *YAP1*. We validated the microarray data by qPCR including also *LOX*, another important determinant of the desmoplasia, even if it was not significantly regulated in the microarray analysis. We found that miR-340 significantly down regulates the expression of *CTGF*, *ROCK1* and *YAP1*, while up regulates the expression of *LOX* (fig. 21A-D). This observation suggests that miR-340 might negatively regulate the expression of a cluster of genes involved in the desmoplastic reaction. The up regulation of *LOX* is in contrast with the previous conclusion since *LOX* is a strong promoter of desmoplasia-related metastasis formation[402,411]. Nevertheless, it is not obvious that a single miRNA should have the same effect on all the genes related to a specific biological process. Furthermore, it is also important to stress that miRNAs are an additional layer of gene regulation, which follow stronger mechanisms of regulation (i.e. transcriptional regulation). The effect on *ROCK1* is in line with previous studies in osteosarcoma[389,390] and glioblastoma[391]. On the contrary, the identification of *CTGF* and *YAP1* as miR-340 target genes, to our knowledge, has never been reported before. *YAP1* is involved in a plethora of biological functions and in the development and progression of multiple cancers as a transcriptional regulator of the Hippo pathway[403]. For this reason, we also validated the miR-340 negative regulation of *YAP1* protein level by immunoblot and the effect of down regulation was very robust (fig. 22).

Overall, we conclude that miR-340 might have an anti-tumour effect in breast cancer since it is able to negatively regulate not only the uPA-system components but also a cluster of desmoplastic reaction-related genes. Specifically, the effect on *YAP1* expression might

open new scenarios on the miR-340 potentiality in gene regulation of cancer-related pathways.

The miR-340-mediated down regulation of target genes involved in breast cancer tumourigenesis led us to investigate the potential clinical relevance of the experimentally determined miR-340 target genes in breast cancer. To this purpose, all the genes analysed in the microarray were annotated according to their association with OS performing meta-analysis of published microarray data sets using BreastMark database[376]. We found that the experimental miR-340 target list is 1.3-fold ($p < 0.001$) enriched in genes associated with a significant prognostic value and 3.4-fold enriched ($p < 0.001$) in genes associated with a very significant prognostic value. Specifically, miR-340 target genes were 1.3-fold enriched ($p < 0.001$) in genes significantly and highly significantly associated with poor prognosis. Importantly, miR-340 down regulated target genes are 1.5-fold ($p < 0.001$) and 1.3-fold ($p < 0.001$) enriched in genes significantly and highly significant associated with poor prognosis, respectively. The miR-340 down regulated target genes, highly significant associated with poor prognosis in breast cancer ($N = 129$), may act as a miR-340-dependent breast cancer signature. In order to understand which kind of pathways are related to this signature, we performed a gene ontology analysis, which highlighted enrichment in proliferation-related pathways (fig. 23). Moreover, the miR-340-dependent breast cancer signature is enriched in putative miR-340 targets ($p < 0.0001$) but the negative correlation of each gene with miR-340 levels was not observed in the NCI-60 panel. These latest observations point out that miR-340 may down regulate cell proliferation-dependent genes thus to influence the outcome of breast cancer. This hypothesis is partially substantiated by the enrichment in putative miR-340 targets, while the absence of an inverse correlation with miR-340 level in the NCI-60 panel might be due to the fact that we analysed expression data concerning different human cancer cell lines. Likely, the role of miR-340 in cancer prognosis is linked only to a specific type of tumour

(i.e. breast cancer), which in the NCI-60 panel represents only five out 59 cancer cell lines (table 6).

In summary miR-340 targets a fraction of the MDA-MB-231 transcriptome highly enriched in genes associated with poor prognosis in breast cancer and related to cell proliferation pathways. Remarkably, 92% of the highly significant prognostic genes are tumour promoters and are repressed by miR-340. On the other side, miR-340 also down regulates seven tumour suppressors and up regulates five tumour promoters. However, overall, miR-340 acts mainly as an oncosuppressor suggesting the possibility that in the future it might represent a good candidate for breast cancer therapy. pre-miR-340 administration has already been tested in pre-established HCT116 tumours in animal models; indeed it has been shown that systemic administration of pre-miR-340 suppresses tumour growth *in vivo*[388].

8.6 FUNCTIONAL CHARACTERISATION OF THE ROLE OF miR-340 IN BREAST CANCER

The miR-340-mediated down regulation of genes associated with poor prognosis in breast cancer, prompted us to investigate how miR-340 might influence breast cancer tumourigenesis. We firstly verified whether miR-340 is expressed in human breast cancer tissue and in which compartment it is localised. ISH analyses on normal and tumour breast tissues unveiled a complex staining for miR-340. Both normal and tumour tissues expressed miR-340 specifically in the epithelial compartment and in lymphocytes but not into the bulk of inflammatory infiltrate surrounding tumour cells (fig. 24). Furthermore, the magnification of tumour samples highlighted that the localisation of miR-340 seems predominantly nuclear (appreciable in fig. 24C). A nuclear localisation of a miRNA means that it is mainly expressed as primary or precursor form rather than the mature one, which is localised in the cytoplasm[317,319,322]. In cancer, the components of the microprocessor complex are often mutated, as a consequence the functional mature form of miRNAs is not

generated and the tumour-related miRNAs target genes are not fully regulated anymore[332,412,413]. This deregulation might concern also miR-340. Although this experiment does not indicate if cancer epithelium shows lower or higher miR-340 expression than the normal counterpart, it is nevertheless clear that miR-340 is expressed in human breast epithelium.

In order to evaluate whether miR-340 administration might induce a cell proliferation-dependent phenotypic changes in MDA-MB-231 cells, as the gene ontology analysis suggested, we recorded miR-340 mimic transfected MDA-MB-231 cells by time-lapse. It is evident that miR-340 mimic transfected cells showed a reduction of cell number and an increased cell rounding compared to the negative control (fig. 25). These observations corroborated the possibility that miR-340 might influence genes involved in cell proliferation and morphology. This hypothesis was further supported by RTCA experiments conducted in MDA-MB-231 cells reverse transfected with miR-340 mimic and negative control (fig. 26). RTCA experiments were also performed to understand which miR-340 target genes might be responsible for the observed phenotype knocking down some validated miR-340 targets. We found that *SERPINE1* and *YAP1* knockdowns partially recapitulate the effect of miR-340 administration (fig. 27). This piece of information is not fully conclusive since we did not knock down all the validated miR-340 target genes. To test unambiguously whether miR-340 might have a role in proliferation, a cell cycle distribution analysis was performed. miR-340 elicited a significant reduction in the number of cells in S phase compared to the control. This effect might be due to a G1 phase arrest (fig. 28C). The role of miR-340 in cell cycle regulation has been previously described. Fernandez *et al*.[395] showed the involvement of miR-340 as negative regulator of *PUM1*, *PUM2* and *SKP2* in non-small cell lung cancer; Li *et al*.[396] demonstrated the role of miR-340 in inhibiting glioblastoma cell proliferation suppressing *CDK6*, *CCND1* and *CCND2*. Huang *et al*.[391] also reported the miR-340-mediated negative regulation of *CCND1* together with *EZH2*, *AKT*, *EGFR* and *BMI1* in multiform glioblastoma. In our

experiments, among the few tested candidates, the main proliferation-drivers seem to be *SERPINE1* and *YAP1*. This hypothesis is corroborated by the finding that *SERPINE1* and *YAP1* are both involved in cell cycle regulation. Indeed, *YAP1* may promote breast cell proliferation and survival[414] and metastasis formation[415], even if it could act also as tumour suppressor (reviewed in[403]). Also *SERPINE1* may sustain proliferation; indeed the expression of *SERPINE1* is under the control of E2F transcription factor family, which inhibits the expression of *SERPINE1* and *PLAU* as well[214,416], for the proper regulation of the cell cycle. The fact that *SERPINE1* and *YAP1* recapitulate only partially the effect of miR-340 administration might be due to the fact that their role on cell cycle might be less strong compared to the previously mentioned cell-cycle target genes and/or to the knock down efficiency that has not been tested yet. Additionally, *SERPINE1* and *YAP1* belong to the list of miR-340 down regulated target genes significantly associated with breast cancer prognosis. Specifically, *SERPINE1* (HR = 1.22) and *YAP1* (HR = 0.84) are poor and good prognosis-related genes, respectively. Therefore, on our hands, *YAP1* is associated with a good outcome in breast cancer (HR < 1). This observation is in line with to the above-mentioned references concerning the bivalent role of *YAP1* in tumourigenesis processes, as a consequence further analyses are needed to better elucidate the role of *YAP1* in breast cancer prognosis.

The ability of miR-340 to regulate breast cancer poor prognosis-related genes and the possibility that it might negatively regulate proliferation-related genes should have an impact in breast cancer growth *in vivo*. To test this hypothesis, we generated stable over expressing miR-340 MDA-MB-231 cells infecting them with miR-340 precursor lentiviral vector. We tested cell viability and miR-340 over expression by FACS analysis of GFP positive cells (fig. 29) and qPCR, respectively (fig. 30). The qPCR analysis confirmed that miR-340 infected MDA-MB-231 cells showed a 100-fold increase of miR-340 expression compared to scramble and wild type MDA-MB-231 cells (fig. 30) but 200-fold less miR-340 level compared to the mimic transfected MDA-MB-231 cells (fig. 17A). We injected

MDA-MB-231 cells, infected with miR-340 or scramble lentiviral vector, into the mammary fat pad of CD-1 nude mice and we monitored tumour growth. The merge of two independent experiments showed that miR-340 over expression does not negatively influence the tumour growth (fig. 31). To quantify the cell proliferation, we evaluated by IHC analyses the proliferation marker Ki-67 together with the apoptosis marker cleaved CASP3 in four tumours/group. We found that miR-340 over expression did not affect the expression of Ki-67 (fig. 32 A, C-E) and the cleavage of CASP3 (fig. 32 B, F-H). The discrepancy with the *in vitro* data might be due to the different miR-340 gain-of-function systems employed since they induce a different miR-340 levels. We did not test whether lentiviral vector-induced miR-340 over expression is sufficient to down regulate the previously validated targets. At the same time, the miR-340 level in mimic transfected MDA-MB-231 cells might be not comparable with the physiological level of a miRNA[410] and off-target effects can not be excluded. A second explanation might concern the possibility of miR-340 silencing as a consequence of epigenetic mechanisms. Indeed, it has already been shown that miR-340 can be epigenetically regulated in neuroblastoma patients[392]. Furthermore, it was the first time we performed this xenograft procedure. Therefore, variability due to technical inexperience might have affected the results of the experiments.

As a consequence of the absence of concordance between the results obtained from the two different miR-340 gain-of-function systems, we decided to characterise the role of miR-340 by an *in vivo* loss-of-function model to minimise all the possible off-target effects. We generated a straight Mir340 knock out mouse model taken advantage of the ZNFs technology[404]. Mir340 knock out mice show a normal phenotype (table 13), are fertile and the edited allele segregation is consistent with Mendel's rules (table 14). The absence of a pathological phenotype in normal condition is in line with previous miRNA knock out mice, even if abnormalities has been also reported[417]. The contribution of the components of the uPA-system in breast cancer has been widely studied in *in vivo* breast cancer mouse

model. The straight knock out of each component of the uPA-system mainly affects the metastasis formation rather then the tumour growth or burden (reviewed in[418]). It will be interesting to evaluate whether the absence of Mir340 might have an effect in breast cancer pathogenesis since the concomitant down regulation of the uPA-system components together with the desmoplasia reaction- and poor prognosis related genes should be occurred.

8.7 FUTURE EXPERIMENTS AND PERSPECTIVES

According to the present state of experiments, the characterisation of the miR-340 targetome and its role in breast cancer tumourigenesis has to be still accomplished.

The identification of miR-340 as negative modulator of the expression of the uPA-system core components, including *PLAUR*, *PLAU* and *SERPINE1*, was first assayed using both prediction algorithms, based on the base pairing between mRNA and miRNAs, and performing correlation analyses between miR-340 level and the expression level of the uPA-system components mining expression data available in CellMiner™ web tool[371]. The correlation analyses showed a negative correlation between miR-340 and the three main uPA-system components both at mRNA and protein level. Secondly, the inverse correlation was experimentally validated by qPCR through exogenous administration of miR-340 mimic oligonucleotides. The same approach was also employed for the validation of desmoplasia-related miR-340 target genes: *CTGF*, *ROCK1* and *YAP1*. The miR-340 negative regulation at protein level was measured by immunoblot for uPAR, uPA and YAP1. To further support the role of miR-340 as negative modulator of the expression of the previous validated target genes, a complement over expression approach using an efficient inhibitor of miR-340 in miR-340 low expressing breast cancer cell line is necessary. Moreover, to demonstrate that these genes are direct miR-340 targets, we will perform a reporter assay, taken advantage to the luciferase chemistry. The wild type or miR-340 mutated seed region binding sites 3'UTR of the validated miR-340 target genes

will be cloned in an expression vector downstream the luciferase reporter gene. HEK 293 cell line will be transfected with the reporter vector, expressing the 3'UTR of a specific miR-340 target, with or without miR-340 mimic administration. The luciferase signal will be quantified after 48 h post transfection; a decrease in the luciferase signal will be the read out of a direct interaction between the 3'UTR of the target gene and the miR-340.

In order to understand how miR-340 affects the mRNA half-life of its target genes, a mRNA stability assay will be performed. miR-340 binding site is located within the AU-rich instability region of *PLAU*, *PLAUR* and *SERPINE1* 3'UTR thus to likely negatively affect mRNA half-life. Tran *et al*.[302] reported that the binding of specific ARE-binding proteins is essential for the regulation of *PLAU* mRNA decay. Specifically, the binding of the ARE-binding protein DHX36 to the *PLAU* AREs sequences displaces the mRNA stabiliser AREs binding proteins HuR and NFAR thus to enhance the degradation of the mRNA. In addition, a miRNA targeting AREs has been reported to be essential in ARE-mediated mRNA degradation[409]. Our hypothesis is that miR-340 may cooperate with DHX36 in order to promote the degradation of *PLAU*, *PLAUR* and *SERPINE1* mRNA. To test this hypothesis *in vitro* decay experiments, transfecting HEK 293 cells with miR-340, DHX36 and the 3'UTR of each component of the uPA-system, will be performed together with the identification of all the possible mRNA binding proteins involved in the mechanism of mRNA half-life regulation of the uPA-system components.

The microarray analysis unveiled that miR-340 significantly down regulates a cluster of genes involved in desmoplastic reaction: *CTGF*, *ROCK1* and *YAP1*. To experimentally define the role of miR-340 in this phenomenon, contractility assay using miR-340 mimic transfected fibroblast cell lines should be informative. Subsequently, qPCR and immunoblot might shed light on the regulation of desmoplastic reaction-related genes. Furthermore, to better clarify the miR-340 mediated *LOX* up regulation, a matrix stiffness assay might be performed. Fibroblasts cells transfected with miR-340 mimic and negative control will be plated in collagen matrices; the collagen deposition and the matrix stiffness

will be assayed by LOX-staining through SirCol Assay and shear rheology, respectively. The LOX expression at mRNA and protein level will be measured through qPCR and immunoblot, respectively.

The RTCA experiments showed that *SERPINE1* and *YAP1* knockdowns might partially recapitulate the effect of mimic administration. The behaviour observed in miR-340 mimic transfected MDA-MB-231 cells both in time-lapse and RTCA experiments seems to be due to a miR-340-mediated G1 phase arrest. A cell cycle distribution analysis on miR-340 mimic transfected MDA-MB-231 and also over expressing *SERPINE1* and/or *YAP1* will elucidate their involvement in the cell cycle regulation. If a rescue of the normal cell cycle distribution will be observed, a microarray analysis on *SERPINE1* and *YAP1* knocked down MDA-MB-231 cells should better explain the miR-340-mediated regulation of the proliferation pathway, considering that several cell proliferation-related genes are negatively affected by miR-340. The microarray analysis should also allow the discrimination between direct and indirect targets of miR-340 involved in the control of cell proliferation.

The discrepancy between the results obtained using transiently or stably miR-340 transfected MDA-MB-231 cells should be elucidated. The two employed gain-of-function systems actually elicit a different miR-340 level. The data concerning the xenograft breast cancer model do not confirm the miR-340 phenotype observed *in vitro*. A microarray analyses on miR-340 infected MDA-MB-231 cells will reveal whether the 100-fold increase in miR-340 expression is sufficient to recapitulate the miR-340 targetome identified using the miR-340 mimic. Furthermore, a cell cycle analysis on miR-340 infected MDA-MB-231 cells will show whether the miR-340 over expression affects the cell cycle distribution as observed for mimic transfected MDA-MB-231 cells. If these experiments will show that the lentiviral miR-340 over expression recapitulate the miR-340 mimic-mediated effects in MDA-MB-231 transcriptome and the cell cycle distribution, the xenograft experiment will be performed again.

The generation of a straight Mir340 knock out animal model will allow us to characterise the miR-340 *in vivo* target genes, bypassing the issue of the off-target effects. We would first generate the list of *in vivo* miR-340 target genes performing a microarray analysis starting from RNA isolated from whole mammary gland and epidermis of Mir340 knock out and wild-type mice. In this way, considering that the mammary gland is predominantly made up of epithelial cells, while the skin contains a large fraction of fibroblasts, we believe that we will be able to deconvolute, at least partially, the cellular origin of the differentially expressed genes. The target list generated in this way might be employed for gene enrichment analysis to evaluate its relevance in breast cancer and desmoplasia reaction. This analysis might identify an *in vivo* miR-340-dependent breast cancer signature useful for both diagnostic and prognostic purposes. This approach will allow a more direct evidence on what is the effect of miR-340 in a pathological condition rather than a stratification of patients according to the a microRNA/host gene expression level. The uPA-system components and the desmoplastic response are well accepted to be an important driver of breast cancer growth and invasion and miR-340 should act as negative regulator of both aspects together with its role in down regulating highly significant breast cancer poor prognosis-related genes. To unequivocally determine the role of miR-340 in breast cancer tumourigenesis and desmoplastic response, we will cross the Mir340 strain with the MMTV-PymT breast cancer model[419]. Animals will be monitored regularly and the appearance of palpable tumours recorded. Tissue biopsies will be collected at different stages of tumour development and the histology will be carried out. If these experiments will confirm the role of miR-340 in breast cancer, miR-340 precursor with carbonate apatite as vehicle will be intravenously administrated via tail vein injection when tumour volume reaches approximately 80 mm^3 as already tested by Takeyama *et al.*[388]. The miR-340 administration should down regulate the expression of tumour promoter genes and ameliorate breast cancer outcome. This might represent a new cue to improve breast cancer therapy.

9. REFERENCES

1 Yeo, B. An update on the medical management of breast cancer. *BMJ*. (2014).

2 Maller, O. Extracellular matrix composition reveals complex and dynamic stromal-epithelial interactions in the mammary gland. *J Mammary Gland Biol Neoplasia* **15(3)**, 301-318 (2010).

3 Sidenius, N. The urokinase plasminogen activator system in cancer: recent advances and implication for prognosis and therapy. *Cancer Metastasis Rev*. **22(2-3)**, 205-222 (2003).

4 Gudjonsson, T. Normal and tumor-derived myoepithelial cells differ in their ability to interact with luminal breast epithelial cells for polarity and basement membrane deposition. *J Cell Sci*. **115**, 39-50 (2002).

5 Tzu, J. Bridging structure with function: structural, regulatory, and developmental role of laminins. *Int J Biochem Cell Biol*. **40(2)**, 199-214 (2008).

6 Streuli, C. H. Control of mammary epithelial differentiation: basement membrane induces tissue-specific gene expression in the absence of cell-cell interaction and morphological polarity. *J Cell Biol*. **115(5)**, 1383-1395 (1991).

7 Slade, M. J. The human mammary gland basement membrane is integral to the polarity of luminal epithelial cells. *Exp Cell Res*. **247(1)**, 267-278 (1999).

8 Debnath, J. Morphogenesis and oncogenesis of MCF-10A mammary epithelial acini grown in three-dimensional basement membrane cultures. *Methods*. **30(3)**, 256-268 (2003).

9 Pöschl, E. Collagen IV is essential for basement membrane stability but dispensable for initiation of its assembly during early development. *Development*. **131(7)**, 1619-1628 (2004).

10 Yurchenco, P. D. Molecular architecture of basement membranes. *FASEB J*. **4(6)**, 1577-1590 (1990).

11 Wicha, M. S. Basement membrane collagen requirements for attachment and growth of mammary epithelium. *Exp Cell Res*. **124(1)**, 181-190 (1979).

12 Wicha, M. S. Effects of inhibition of basement membrane collagen deposition on rat mammary gland development. *Dev. Biol*. **80(2)**, 253-256 (1980).

13 Mundel, T. M. Type IV collagen-derived angiogenesis inhibitors. *Microvasc Res*. **74(2-3)**, 85-89 (2007).

14 Böse, K. Loss of nidogen-1 and -2 results in syndactyly and changes in limb development. *J Biol Chem*. **281(5)**, 39620-39629 (2006).

15 Nischt, R. Lack of nidogen-1 and -2 prevents basement membrane assembly in skin-organotypic coculture. *J Invest Dermatol*. **127(3)**, 545-554 (2007).

16 Fox, J. W. Recombinant nidogen consists of three globular domains and mediates binding of laminin to collagen type IV. *EMBO J*. **10(11)**, 3137-3146 (1991).

17 Costell, M. Perlecan maintains the integrity of cartilage and some basement membranes. *J Cell Biol* **147(5)**, 1109-1122 (1999).

18 Arikawa-Hirasawa, E. Perlecan is essential for cartilage and cephalic development. *Nat Genet*. **23(3)**, 354-358 (1999).

19 Smith, S. M. Heparan and chondroitin sulfate on growth plate perlecan mediate binding and delivery of FGF-2 to FGF receptors. *Matrix Biol*. **26(3)**, 175-184 (2007).

20 Bix, G. Endorepellin causes endothelial cell disassembly of actin cytoskeleton and focal adhesions through alpha2beta1 integrin. *J Cell Biol*. **166(1)**, 97-109 (2004).

21 Gelse, K. Collagens--structure, function, and biosynthesis. *Adv Drug Deliv Rev* **55(12)**, 1531-1546 (2003).

22 Vogel, W. F. Discoidin domain receptor 1 tyrosine kinase has an essential role in mammary gland development. *Mol Cell Biol*. **21(8)**, 2906-2917 (2001).

23 McDaniel, S. M. Remodeling of the mammary microenvironment after lactation promotes breast tumor cell metastasis. *Am J Pathol*. **168(2)**, 608-620 (2006).

24 O'Brien, J. Alternatively activated macrophages and collagen remodeling characterize the postpartum involuting mammary gland across species. *Am J Pathol*. **176(3)**, 1241-1255 (2010).

25 Schedin, P. Fibronectin fragments induce MMP activity in mouse mammary epithelial cells: evidence for a role in mammary tissue remodeling. *J Cell Sci*. **113**, 795-806 (2000).

26 Huang, W. Interference of tenascin-C with syndecan-4 binding to fibronectin blocks cell adhesion and stimulates tumor cell proliferation. *Cancer Res*. **61(23)**, 8586-8594 (2001).

27 Jones, P. L. Tenascin-C in development and disease: gene regulation and cell function. *Matrix Biol*. **19(7)**, 581-596 (2000).

28 Burch, G. H. Tenascin-X deficiency is associated with Ehlers-Danlos syndrome. *Nat Genet*. **17(1)**, 104-108 (1997).

29 Brekken, R. A. SPARC, a matricellular protein: at the crossroads of cell-matrix communication. *Matrix Biol*. **19(8)**, 816-827 (2001).

30 Sweetwyne, M. T. Functional analysis of the matricellular protein SPARC with novel monoclonal antibodies. *J Histochem Cytochem*. **52(6)**, 723-733 (2004).

31 Barker, T. H. SPARC regulates extracellular matrix organization through its modulation of integrin-linked kinase activity. *J Biol Chem*. **280(43)**, 36483-36493 (2005).

32 Schaefer, L. Biological functions of the small leucine-rich proteoglycans: from genetics to signal transduction. *J Biol Chem*. **283(31)**, 21305-21309 (2008).

33 Schedin, P. Microenvironment of the involuting mammary gland mediates mammary cancer progression. *J Mammary Gland Biol Neoplasia* **12(1)**, 71-82 (2007).

34 Wight, T. N. Proteoglycans structure and functions. *Cell Biology of Extracellular Matrix*., 45-78 (1991).

35 Danielson, K. G. Targeted disruption of decorin leads to abnormal collagen fibril morphology and skin fragility. *J Cell Biol*. **136(3)**, 729-743 (1997).

36 Zhu, J. X. Decorin evokes protracted internalization and degradation of the epidermal growth factor receptor via caveolar endocytosis. *J Biol Chem*. **280(37)**, 32468-32479 (2005).

37 Yamaguchi, Y. Negative regulation of transforming growth factor-beta by the proteoglycan decorin. *Nature*. **346(6281)**, 281-284 (1990).

38 Reed, C. C. Decorin prevents metastatic spreading of breast cancer. *Oncogene*. **24(6)**, 1104-1110 (2005).

39 Grant, D. S. Decorin suppresses tumor cell-mediated angiogenesis. *Oncogene*. **21(31)**, 4765-4777 (2002).

40 San Martin, S. Small leucine-rich proteoglycans (SLRPs) in uterine tissues during pregnancy in mice. *Reproduction*. **125(4)**, 585-595 (2003).

41 Salgado, R. M. The estrous cycle modulates small leucine-rich proteoglycans expression in mouse uterine tissues. *Anat Rec (Hoboken)*. **291(19**, 138-153 (2009).

42 Reinboth, B. Molecular interactions of biglycan and decorin with elastic fiber components: biglycan forms a ternary complex with tropoelastin and microfibril-associated glycoprotein 1. *J Biol Chem*. **277(6)**, 3950-3957 (2002).

43 Levental, K. R. Matrix crosslinking forces tumor progression by enhancing integrin signaling. *Cell*. **139(5)**, 891-906 (2009).

44 Varkey, M. Superficial dermal fibroblasts enhance basement membrane and epidermal barrier formation in tissue-engineered skin: implications for treatment of skin basement membrane disorders. *Tissue Eng Part A*. **20(3-4)**, 540-552 (2014).

45 Wiseman, B. S. Stromal effects on mammary gland development and breast cancer. *Science*. **296(5570)**, 1046-1049 (2002).

46 Bainbridge, P. Wound healing and the role of fibroblasts. *J Wound Care*. **2288)**, 410-412 (2013).

47 Kendall, R. T. Fibroblasts in fibrosis: novel roles and mediators. *Front Pharmacol*. **5:123** (2014).

48 Powell, D. W. Myofibroblasts. I. Paracrine cells important in health and disease. *Am J Physiol*. **277**, C1-9 (1999).

49 Clayton, A. Cellular activation through the ligation of intercellular adhesion molecule-1. *J Cell Sci*. **111**, 443-453 (1998).

50 Lindner, D. Differential Expression of Matrix Metalloproteases in Human Fibroblasts with Different Origins. *Biochem Res Int*. (2012).

51 Bhowmick, N. A. Stromal fibroblasts in cancer initiation and progression. *Nature*. **432(7015)**, 332-337 (2004).

52 Dagouassat, M. Monocyte chemoattractant protein-1 (MCP-1)/CCL2 secreted by hepatic myofibroblasts promotes migration and invasion of human hepatoma cells. *Int J Cancer*. **126(5)**, 1095-1108 (2010).

53 Dvorak, H. F. Tumors: wounds that do not heal. Similarities between tumor stroma generation and wound healing. *N Engl J Med*. **315(26)**, 1650-1659 (1986).

54 Hanahan, D. Hallmarks of cancer: the next generation. *Cell*. **144(5)**, 646-674 (2011).

55 Rønnov-Jessen, L. Cellular changes involved in conversion of normal to malignant breast: importance of the stromal reaction. *Physiol Rev*. **76(1)**, 69-125 (1996).

56 Hynes, R. O. Integrins: versatility, modulation, and signaling in cell adhesion. *Cell*. **69(1)**, 11-25 (1992).

57 Schedin, P. Multistep tumorigenesis and the microenvironment. *Breast Cancer Res*. **6(2)**, 93-101 (2004).

58 Shekhar, M. P. Host microenvironment in breast cancer development: extracellular matrix-stromal cell contribution to neoplastic phenotype of epithelial cells in the breast. *Breast Cancer Res*. **5(3)**, 130-135 (2003).

59 Xing, F. Cancer associated fibroblasts (CAFs) in tumor microenvironment. *Front Biosci* **15**, 166-179 (2010).

60 Yuan, J. Mutagenesis induced by the tumor microenvironment. *Mutat Res*. **400(1-2)**, 439-446 (1998).

61 Koukourakis, M. I. Comparison of metabolic pathways between cancer cells and stromal cells in colorectal carcinomas: a metabolic survival role for tumor-associated stroma. *Cancer Res*. **66(2)**, 632-637 (2006).

62 Swann, J. B. Immune surveillance of tumors. *J Clin Invest*. **117(5)**, 1137-1146 (2007).

63 Li, H. Tumor microenvironment: the role of the tumor stroma in cancer. *J Cell Biochem*. **101(4)**, 805-815 (2007).

64 Sneddon, J. B. Bone morphogenetic protein antagonist gremlin 1 is widely expressed by cancer-associated stromal cells and can promote tumor cell proliferation. *Proc Natl Acad Sci U S A*. **103(40)**, 14842-14847 (2006).

65 Blasi, F. a. S., N. The urokinase receptor: focused cell surface proteolysis, cell adhesion and signaling. *FEBS Lett*. **584(9)**, 1923-1930 (2010).

66 Puente, X. S. Human and mouse proteases: a comparative genomic approach. *Nat Rev Genet*. **4(7)**, 544-558 (2003).

67 Spraggon, G. The crystal structure of the catalytic domain of human urokinase-type plasminogen activator. *Structure*. **3(7)**, 681-691 (1995).

68 Andreasen, P. A. The plasminogen activation system in tumor growth, invasion, and metastasis. *Cell Mol Life Sci*. **57(1)**, 25-40 (2000).

69 Montuori, N. The cleavage of the urokinase receptor regulates its multiple functions. *J Biol Chem*. **277(49)**, 46932-46939 (2002).

70 List, K. Plasminogen-independent initiation of the pro-urokinase activation cascade in vivo. Activation of pro-urokinase by glandular kallikrein (mGK-6) in plasminogen-deficient mice. *Biochemestry*. **39(3)**, 508-515 (2000).

71 Steffens, G. J. The complete amino acid sequence of low molecular mass urokinase from human urine. *Hoppe Seylers Z Physiol Chem*. **363(9)**, 1043-1058 (1982).

72 Marcotte, P. A. The matrix metalloproteinase pump-1 catalyzes formation of low molecular weight (pro)urokinase in cultures of normal human kidney cells. *J Biol Chem*. **267(20)**, 13803-13806 (1992).

73 Ploug, M. Cellular receptor for urokinase plasminogen activator. Carboxyl-terminal processing and membrane anchoring by glycosyl-phosphatidylinositol. *J Biol Chem*. **266(3)**, 1926-1933 (1991).

74 Ploug, M. Structure-function relationships in the receptor for urokinase-type plasminogen activator. Comparison to other members of the Ly-6 family and snake venom alpha-neurotoxins. *FEBS Lett*. **349(2)**, 163-168 (1994).

75 Solberg, H. The murine receptor for urokinase-type plasminogen activator is primarily expressed in tissues actively undergoing remodeling. *J Histochem Cytochem*. **49(2)**, 237-246 (2001).

76 Blasi, F. a. C., P. uPAR: a versatile signalling orchestrator (review). *Nat Rev Mol Cell Biol*. **3(12)**, 932-943 (2002).

77 Beaufort, N. Plasmin cleaves the juxtamembrane domain and releases truncated species of the urokinase receptor (CD87) from human bronchial epithelial cells. *FEBS Lett*. **574(1-3)**, 89-94 (2004).

78 Beaufort, N. Interplay of human tissue kallikrein 4 (hK4) with the plasminogen activation system: hK4 regulates the structure and functions of the urokinase-type plasminogen activator receptor (uPAR). *Biol Chem*. **38782)**, 217-222 (2006).

79 Resnati, M. Proteolytic cleavage of the urokinase receptor substitutes for the agonist-induced chemotactic effect. *EMBO J*. **15(7)**, 1572-1582 (1996).

80 Høyer-Hansen, G. Urokinase plasminogen activator cleaves its cell surface receptor releasing the ligand-binding domain. *J Biol Chem*. **267(25)**, 18224-18229 (1992).

81 Andolfo, A. Metalloproteases cleave the urokinase-type plasminogen activator receptor in the D1-D2 linker region and expose epitopes not present in the intact soluble receptor. *Thromb Haemost*. **88(2)**, 298-306 (2002).

82 Sidenius, N. Domain 1 of the urokinase receptor (uPAR) is required for uPAR-mediated cell binding to vitronectin. *FEBS Lett*. **470(1)**, 40-46 (2000).

83 Sier, C. F. Metabolism of tumour-derived urokinase receptor and receptor fragments in cancer patients and xenografted mice. *Thromb Haemost*. **91(2)**, 403-411 (2004).

84 Cubellis, M. V. Receptor-mediated internalization and degradation of urokinase is caused by its specific inhibitor PAI-1. *EMBO J*. **9(4)**, 1079-1085 (1990).

85 Conese, M. Protease nexin-1-urokinase complexes are internalized and degraded through a mechanism that requires both urokinase receptor and alpha 2-macroglobulin receptor. *J Biol Chem*. **269(27)**, 17886-17892 (1994).

86 Nykjaer, A. Purified alpha 2-macroglobulin receptor/LDL receptor-related protein binds urokinase.plasminogen activator inhibitor type-1 complex. Evidence that the alpha 2-macroglobulin receptor mediates cellular degradation of urokinase receptor-bound complexes. *J Biol Chem*. **267(21)**, 14543-14546 (1992).

87 Madsen, C. D. The interaction between urokinase receptor and vitronectin in cell adhesion and signalling. *Eur J Cell Biol*. **87(8-9)**, 617-629 (2008).

88 Kugler, M. C. Urokinase Receptor and Integrin Interactions. *Curr Pharm Des*. **9(19)**, 1565-1574 (2003).

89 Liu, D. EGFR is a transducer of the urokinase receptor initiated signal that is required for in vivo growth of a human carcinoma. *Cancer Cell*. **1(5)**, 445-457 (2002).

90 Kiyan, J. Urokinase-induced signaling in human vascular smooth muscle cells is mediated by PDGFR-beta. *EMBO J*. **24(10)**, 1787-1797 (2005).

91 Wei, Y. A role for caveolin and the urokinase receptor in integrin-mediated adhesion and signaling. *J Cell Biol*. **144(6)**, 1285-1294 (1999).

92 Czekay, R. P. Direct binding of occupied urokinase receptor (uPAR) to LDL receptor-related protein is required for endocytosis of uPAR and regulation of cell surface urokinase activity. *Mol Biol Cell*. **12(5)**, 1467-1479 (2001).

93 Li, Y. Low density lipoprotein (LDL) receptor-related protein 1B impairs urokinase receptor regeneration on the cell surface and inhibits cell migration. *J Biol Chem*. **277(44)**, 42366-42371 (2002).

94 Resnati, M. The fibrinolytic receptor for urokinase activates the G protein-coupled chemotactic receptor FPRL1/LXA4R. *Proc Natl Acad Sci U S A*. **99(3)**, 1359-1364 (2002).

95 Nykjaer, A. Mannose 6-phosphate/insulin-like growth factor-II receptor targets the urokinase receptor to lysosomes via a novel binding interaction. *J Cell Biol*. **141(3)**, 815-828 (1998).

96 Ferraris, G. M. Urokinase plasminogen activator receptor: a functional integrator of extracellular proteolysis, cell adhesion, and signal transduction. *Semin Thromb Hemost*. **39(4)**, 347-355 (2013).

97 Appella, E. The growth factor module of urokinase is the binding sequence for its receptor. *Ann N Y Acad Sci*. **511**, 192-195 (1987).

98 Kjaergaard, M. Structure and ligand interactions of the urokinase receptor (uPAR). *Front Biosci*. **13**, 5441-5461 (2008).

99 Gårdsvoll, H. Characterization of the functional epitope on the urokinase receptor. Complete alanine scanning mutagenesis supplemented by chemical cross-linking. *J Biol Chem*. **281(28)**, 19260-19272 (2006).

100 Gårdsvoll, H. Characterization of low-glycosylated forms of soluble human urokinase receptor expressed in Drosophila Schneider 2 cells after deletion of glycosylation-sites. *Protein Expr Purif*. **34(2)**, 284-295 (2004).

101 Suzuki, S. Domain structure of vitronectin. Alignment of active sites. *J Biol Chem*. **259(24)**, 15307-15314 (1984).

102 Smith, J. W. The Arg-Gly-Asp binding domain of the vitronectin receptor. Photoaffinity cross-linking implicates amino acid residues 61-203 of the beta subunit. *J Biol Chem*. **263(35)**, 18726-18731 (1988).

103 Ishikawa-Sakurai, M. Two collagen-binding domains of vitronectin. *Cell Struct Funct*. **18(4)**, 253-259 (1993).

104 Madsen, C. D. uPAR-induced cell adhesion and migration: vitronectin provides the key. *J Cell Biol*. **177(5)**, 927-939 (2007).

105 Seiffert, D. Evidence that type 1 plasminogen activator inhibitor binds to the somatomedin B domain of vitronectin. *J Biol Chem*. **266(5)**, 2824-2830 (1991).

106 Moser, T. L. Specific binding of urinary- type plasminogen activator (u-PA) to vitronectin and its role in mediating u-PA- dependent adhesion of U937 cells. *Biochem J*. **307**, 867-873 (1995).

107 Preissner, K. T. Specific binding of plasminogen to vitronectin. Evidence for a modulatory role of vitronectin on fibrin(ogen)-induced plasmin formation by tissue plasminogen activator. *Biochem Biophys Res Commun*. **168(3)**, 966-971 (1990).

108 Liang, O. D. Identification of novel heparin-binding domains of vitronectin. *FEBS Lett*. **407(2)**, 169-172 (1997).

109 Wei, Y. Identification of the urokinase receptor as an adhesion receptor for vitronectin. *J Biol Chem*. **269(51)**, 32380-32388 (1994).

110 Høyer-Hansen, G. The intact urokinase receptor is required for efficient vitronectin binding: receptor cleavage prevents ligand interaction. *FEBS Lett*. **420(1)**, 79-85 (1997).

111 Gårdsvoll, H. Mapping of the vitronectin-binding site on the urokinase receptor: involvement of a coherent receptor interface consisting of residues from both domain I and the flanking interdomain linker region. *J Biol Chem*. **282(18)**, 13561-13572 (2007).

112 Huai, Q. Crystal structures of two human vitronectin, urokinase and urokinase receptor complexes. *Nat Struct Mol Biol*. **15(4)**, 422-423 (2008).

113 Barinka, C. *et al*. Structural basis of interaction between urokinase-type plasminogen activator and its receptor. *J Mol Biol* **363**, 482-495, doi:10.1016/j.jmb.2006.08.063 (2006).

114 Xu, X. Crystal structure of the urokinase receptor in a ligand-free form. *J Mol Biol*. **416(5)**, 629-641 (2012).

115 Sidenius, N. Urokinase regulates vitronectin binding by controlling urokinase receptor oligomerization. *J Biol Chem*. **277(31)**, 27982-27990 (2002).

116 Cunningham, O. Dimerization controls the lipid raft partitioning of uPAR/CD87 and regulates its biological functions. *EMBO J*. **22(22)**, 5994-6003 (2003).

117 Caiolfa, V. R. Monomer dimer dynamics and distribution of GPI-anchored uPAR are determined by cell surface protein assemblies. *J Cell Biol*. **179(5)**, 1067-1082 (2007).

118 Yebra, M. Requirement of receptor-bound urokinase-type plasminogen activator for integrin alphavbeta5-directed cell migration. *J Biol Chem*. **271(46)**, 29393-29399 (1996).

119 Degryse, B. Urokinase/urokinase receptor and vitronectin/alpha(v)beta(3) integrin induce chemotaxis and cytoskeleton reorganization through different signaling pathways. *Oncogene*. **20(16)**, 2032-2043 (2001).

120 Tarui, T. Critical role of integrin alpha 5 beta 1 in urokinase (uPA)/urokinase receptor (uPAR, CD87) signaling. *J Biol Chem*. **278(32)**, 29863-29872 (2003).

121 Degryse, B. Domain 2 of the urokinase receptor contains an integrin-interacting epitope with intrinsic signaling activity: generation of a new integrin inhibitor. *J Biol Chem*. **280(26)**, 24792-24803 (2005).

122 Gargiulo, L. Cross-talk between fMLP and vitronectin receptors triggered by urokinase receptor-derived SRSRY peptide. *J Biol Chem*. **280(26)**, 25225-25232 (2005).

123 Xue, W. Physical association of complement receptor type 3 and urokinase-type plasminogen activator receptor in neutrophil membranes. *J Immunol*. **152(9)**, 4630-4640 (1994).

124 Ferraris, G. M. The interaction between uPAR and vitronectin triggers ligand-independent adhesion signalling by integrins. *EMBO J*. **33(21)**, 2458-2472 (2014).

125 Carrell, R. W. The biostructural pathology of the serpins: critical function of sheet opening mechanism. *Biol Chem Hoppe Seyler*. **377(1)**, 1-17 (1996).

126 Gils, A. Structure-function relationships in serpins: current concepts and controversies. *Thromb Haemost*. **80(4)**, 531-541 (1998).

127 Sprengers, E. D. Plasminogen activator inhibitors. *Blood*. **69(2)**, 381-387 (1987).

128 Dupont, D. M. Biochemical properties of plasminogen activator inhibitor-1. *Front Biosci (Landmark Ed.)* **14**, 1337-1361 (2009).

129 Declerck, P. J. Purification and characterization of a plasminogen activator inhibitor 1 binding protein from human plasma. Identification as a multimeric form of S protein (vitronectin). *J Biol Chem*. **263(30)**, 15454-15461 (1988).

130 Herz, J. LDL receptor-related protein internalizes and degrades uPA/PAI-1 complexes and is essential for embryo implantation. *Cell*. **73(3)**, 411-421 (1992).

131 Nykjaer, A. Recycling of the urokinase receptor upon internalization of the uPA:serpin complexes. *EMBO J*. **16(10)**, 2610-2620 (1997).

132 Deng, G. Is plasminogen activator inhibitor-1 the molecular switch that governs urokinase receptor-mediated cell adhesion and release? *J Cell Biol*. **13486)**, 1563-1571 (1996).

133 Stefansson, S. The serpin PAI-1 inhibits cell migration by blocking integrin alpha V beta 3 binding to vitronectin. *Nature*. **383(6599)**, 441-443 (1996).

134 Kjøller, L. Plasminogen activator inhibitor-1 represses integrin- and vitronectin-mediated cell migration independently of its function as an inhibitor of plasminogen activation. *Exp Cell Res*. **232(2)**, 420-429 (1997).

135 Kwaan, H. C. Plasminogen activator inhibitor 1 may promote tumour growth through inhibition of apoptosis. *Br J Cancer*. **82(10)**, 1702-1708 (2000).

136 Rifkin, D. B. Plasminogen/plasminogen activator and growth factor activation. *Ciba Found Symp*. **212**, 105-115 (1997).

137 Webb, D. J. Plasminogen Activator Inhibitor 1 Functions as a Urokinase Response Modifier at the Level of Cell Signaling and Thereby Promotes MCF-7 Cell Growth. *J Cell Biol*. **152(4)**, 741-752 (2001).

138 Aguirre Ghiso, J. A. Tumor dormancy induced by downregulation of urokinase receptor in human carcinoma involves integrin and MAPK signaling. *J Cell Biol*. **147(1)**, 89-104 (1999).

139 Pirazzoli, V. Direct evidence of the importance of vitronectin and its interaction with the urokinase receptor in tumor growth. *Blood*. **121(12)**, 2316-2323 (2013).

140 Carmeliet, P. Angiogenesis in cancer and other diseases. *Nature*. **407(6801)**, 249-257 (2000).

141 Binder, B. R. uPAR-uPA-PAI-1 interactions and signaling: a vascular biologist's view. *Thromb Haemost*. **97(3)**, 336-342 (2007).

142 Gately, S. Human prostate carcinoma cells express enzymatic activity that converts human plasminogen to the angiogenesis inhibitor, angiostatin. *Cancer Res*. **56(21)**, 4887-4890 (1996).

143 Cao, R. Suppression of angiogenesis and tumor growth by the inhibitor K1-5 generated by plasmin-mediated proteolysis. *Proc Natl Acad Sci U S A*. **96(10)**, 5728-5733 (1999).

144 Devy, L. The pro- or antiangiogenic effect of plasminogen activator inhibitor 1 is dose dependent. *FASEB J*. **16(2)**, 147-154 (2002).

145 Duffy, M. J. The urokinase plasminogen activator system: role in malignancy. *Curr Pharm Des*. **10(1)**, 39-49 (2004).

146 Weeks, B. H. Inducible expression of transforming growth factor beta1 in papillomas causes rapid metastasis. *Cancer Res*. **61(20)**, 7435-7443 (2001).

147 Giannelli, G. Induction of cell migration by matrix metalloprotease-2 cleavage of laminin-5. *Science*. **277(5323)**, 225-228 (1997).

148 Bemis, L. T. Reproductive state of rat mammary gland stroma modulates human breast cancer cell migration and invasion. *Cancer Res*. **60(13)**, 3414-3418 (2000).

149 Ossowski, L. Invasion of connective tissue by human carcinoma cell lines: requirement for urokinase, urokinase receptor, and interstitial collagenase. *Cancer Res*. **52(24)**, 6754-6760 (1992).

150 Kim, J. Requirement for specific proteases in cancer cell intravasation as revealed by a novel semiquantitative PCR-based assay. *Cell*. **94(3)**, 353-362 (1998).

151 Bagheri-Yarmand, R. LIM kinase 1 increases tumor metastasis of human breast cancer cells via regulation of the urokinase-type plasminogen activator system. *Int J Cancer*. **118(11)**, 2703-2710 (2006).

152 McGuire, P. G. Inhibition of urokinase synthesis and cell surface binding alters the motile behavior of embryonic endocardial-derived mesenchymal cells in vitro. *Development*. **118(3)**, 931-939 (1993).

153 Lu, H. Blockage of urokinase receptor reduces in vitro the motility and the deformability of endothelial cells. *FEBS Lett*. **380(1-2)**, 21-24 (1996).

154 Zhang, H. Regulation of CD11b/CD18 (Mac-1) adhesion to fibrinogen by urokinase receptor (uPAR). *Inflamm Res*. **52(2)**, 86-93 (2003).

155 Visscher, D. W. Immunohistologic evaluation of invasion-associated proteases in breast carcinoma. *Mod Pathol*. **6(3)**, 302-306 (1993).

156 Visscher, D. W. Biologic and clinical significance of basic fibroblast growth factor immunostaining in breast carcinoma. *Mod Pathol*. **8(6)**, 665-670 (1995).

157 Kennedy, S. Semi-quantitation of urokinase plasminogen activator and its receptor in breast carcinomas by immunocytochemistry. *Br J Cancer*. **77(10)**, 1638-1641 (1998).

158 Nielsen, B. S. Urokinase plasminogen activator is localized in stromal cells in ductal breast cancer. *Lab Invest*. **81(11)**, 1485-1501 (2001).

159 Hewitt, R. Stromal cell expression of components of matrix-degrading protease systems in human cancer. *Enzyme Protein*. **49(1-3)**, 163-173 (1996).

160 Dublin, E. Immunohistochemical expression of uPA, uPAR, and PAI-1 in breast carcinoma. Fibroblastic expression has strong associations with tumor pathology. *Am J Pathol*. **157(4)**, 1219-1227 (2000).

161 Pyke, C. Receptor for urokinase is present in tumor-associated macrophages in ductal breast carcinoma. *Cancer Res*. **53(8)**, 1911-1915 (1993).

162 Pyke, C. Urokinase-type plasminogen activator is expressed in stromal cells and its receptor in cancer cells at invasive foci in human colon adenocarcinomas. *Am J Pathol*. **13885)**, 1959-1967 (1991).

163 Nielsen, B. S. Stromal cells associated with early invasive foci in human mammary ductal carcinoma in situ coexpress urokinase and urokinase receptor. *Int J Cancer*. **120(10)**, 2086-2095 (2007).

164 Offersen, B. V. The myofibroblast is the predominant plasminogen activator inhibitor-1-expressing cell type in human breast carcinomas. *Am J Pathol*. **163(5)**, 1887-1899 (2003).

165 Duffy, M. J. Urokinase-plasminogen activator, a marker for aggressive breast carcinomas. Preliminary report. *Cancer*. **62(3)**, 531-533 (1988).

166 Look, M. P. Pooled Analysis of Prognostic Impact of Urokinase-Type Plasminogen Activator and Its Inhibitor PAI-1 in 8377 Breast Cancer Patients. *J Natl Cancer Inst*. **94(2)**, 116-128 (2002).

167 Harbeck, N. Urokinase-type plasminogen activator (uPA) and its inhibitor PAI-I: novel tumor-derived factors with a high prognostic and predictive impact in breast cancer. *Thromb Haemost*. **91(3)**, 450-456 (2004).

168 Harbeck, N. Ten-year analysis of the prospective multicentre Chemo-N0 trial validates American Society of Clinical Oncology (ASCO)-recommended biomarkers uPA and PAI-1 for therapy decision making in node-negative breast cancer patients. *Eur J Cancer*. **49(8)**, 1825-1835 (2013).

169 Bouchet, C. Dissemination risk index based on plasminogen activator system components in primary breast cancer. *J Clin Oncol*. **17(10)**, 3048-3057 (1999).

170 Kotzsch, M. Prognostic relevance of uPAR-del4/5 and TIMP-3 mRNA expression levels in breast cancer. *Eur J Cancer* **41(17)**, 2760-2768 (2005).

171 Kotzsch, M. Urokinase receptor splice variant uPAR-del4/5-associated gene expression in breast cancer: identification of rab31 as an independent prognostic factor. *Breast Cancer Res Treat*. **111(2)**, 229-240 (2008).

172 Kotzsch, M. Prognostic relevance of tumour cell-associated uPAR expression in invasive ductal breast carcinoma. *Histopathology*. **57(3)**, 461-471 (2010).

173 Mangel, W. F. Plasminogen activators in human breast cancer cell lines: hormonal regulation and properties. *J Steroid Biochem*. **30(1-6)**, 79-88 (1988).

174 Long, B. J. Invasive capacity and regulation of urokinase-type plasminogen activator in estrogen receptor (ER)-negative MDA-MB-231 human breast cancer cells, and a transfectant (S30) stably expressing ER. *Cancer Lett*. **99(2)**, 209-215 (1996).

175 Levenson, A. S. Oestradiol regulation of the components of the plasminogen-plasmin system in MDA-MB-231 human breast cancer cells stably expressing the oestrogen receptor. *Br J Cancer*. **78(1)**, 88-95 (1998).

176 Lin, V. C. Effect of progesterone on the invasive properties and tumor growth of progesterone receptor-transfected breast cancer cells MDA-MB-231. *Clin Cancer Res*. **7(9)**, 2880-2886 (2001).

177 Fernö, M. Urokinase plasminogen activator, a strong independent prognostic factor in breast cancer, analysed in steroid receptor cytosols with a luminometric immunoassay. *Eur J Cancer*. **32A(5)**, 793-801 (1996).

178 Grøndahl-Hansen, J. High levels of urokinase-type plasminogen activator and its inhibitor PAI-1 in cytosolic extracts of breast carcinomas are associated with poor prognosis. *Cancer Res*. **53(11)**, 2513-2521 (1993).

179 Duggan, C. Urokinase plasminogen activator and urokinase plasminogen activator receptor in breast cancer. *Int J Cancer*. **61(5)**, 597-600 (1995).

180 Foekens, J. A. Urokinase-type plasminogen activator and its inhibitor PAI-1: predictors of poor response to tamoxifen therapy in recurrent breast cancer. *J Natl Cancer Inst*. **87(10)**, 751-756 (1995).

181 Meijer-van Gelder, M. E. Urokinase-type plasminogen activator system in breast cancer: association with tamoxifen therapy in recurrent disease. *Cancer Res*. **64(13)**, 4563-4568 (2004).

182 Zemzoum, I. Invasion factors uPA/PAI-1 and HER2 status provide independent and complementary information on patient outcome in node-negative breast cancer. *J Clin Oncol*. **21(6)**, 1022-1028 (2003).

183 Meng, S. uPAR and HER-2 gene status in individual breast cancer cells from blood and tissue. *Proc Natl Acad Sci U S A*. **103(46)**, 17361-17365 (2006).

184 Markiewicz, A. Mesenchymal Phenotype of CTC-Enriched Blood Fraction and Lymph Node Metastasis Formation Potential. *PLoS One* **9(4)**, e93901 (2014).

185 Pierga, J. Y. Real-time quantitative PCR determination of urokinase-type plasminogen activator receptor (uPAR) expression of isolated micrometastatic cells from bone marrow of breast cancer patients. *Int. J. Cancer* **114**, 291–298 (2004).

186 Tan, M. Upregulation and activation of PKC alpha by ErbB2 through Src promotes breast cancer cell invasion that can be blocked by combined treatment with PKC alpha and Src inhibitors. *Oncogene* **25(23)**, 3286-3295 (2006).

187 Jo, M. Urokinase receptor primes cells to proliferate in response to epidermal growth factor. *Oncogene* **26(18)**, 2585-2594 (2007).

188 Li, C. RNAi-mediated downregulation of uPAR synergizes with targeting of HER2 through the ERK pathway in breast cancer cells. *Int J Cancer*. **127(7)**, 1507-1516 (2010).

189 Nagamine, Y. Transcriptional and posttranscriptional regulation of the plasminogen activator system. *Thromb Haemost*. **93(4)**, 661-675 (2005).

190 Benasciuti, E. MAPK and JNK transduction pathways can phosphorylate Sp1 to activate the uPA minimal promoter element and endogenous gene transcription. *Blood*. **104(1)**, 256-262 (2004).

191 Verde, P. An upstream enhancer and a negative element in the 5' flanking region of the human urokinase plasminogen activator gene. *Nucleic Acids Res*. **16(22)**, 10699-10716 (1988).

192 Vandenbunder, B. Expression of the transcription factor c-Ets1 correlates with the occurrence of invasive processes during normal and pathological development. *Invasion Metastasis*. **14(1-6)**, 198-209 (1994).

193 Bolon, I. Expression of c-ets-1, collagenase 1, and urokinase-type plasminogen activator genes in lung carcinomas. *Am J Pathol*. **147(5)**, 1298-1310 (1995).

194 Delannoy-Courdent, A. Expression of c-ets-1 and uPA genes is associated with mammary epithelial cell tubulogenesis or neoplastic scattering. *Int J Dev Biol*. **40(6)**, 1097-1108 (1996).

195 Chen, Z. Inhibition of vascular endothelial growth factor-induced endothelial cell migration by ETS1 antisense oligonucleotides. *Cancer Res*. **57(19)**, 2013-2019 (1997).

196 Watabe, T. The Ets-1 and Ets-2 transcription factors activate the promoters for invasion-associated urokinase and collagenase genes in response to epidermal growth factor. *Int J Cancer*. **77(1)**, 128-137 (1998).

197 Cirillo, G. Role of distinct mitogen-activated protein kinase pathways and cooperation between Ets-2, ATF-2, and Jun family members in human urokinase-type plasminogen activator gene induction by interleukin-1 and tetradecanoyl phorbol acetate. *Mol Cell Biol*. **19(9)**, 6240-6252 (1999).

198 Woodgett, J. R. Fos and jun: two into one will go. *Semin Cancer Biol*. **1(6)**, 389-397 (1990).

199 Angel, P. The role of Jun, Fos and the AP-1 complex in cell-proliferation and transformation. *Biochim Biophys Acta*. **1072(2-3)**, 129-157 (1991).

200 Rørth, P. Transcription factor PEA3 participates in the induction of urokinase plasminogen activator transcription in murine keratinocytes stimulated with epidermal growth factor or phorbol-ester. *Nucleic Acids Res*. **18(17)**, 5009-5017 (1990).

201 Lee, J. S. Okadaic acid-dependent induction of the urokinase-type plasminogen activator gene associated with stabilization and autoregulation of c-Jun. *J Biol Chem*. **269(4)**, 2887-2894 (1994).

202 Sakabe, T. Differential regulation of urokinase-type plasminogen activator expression by fluid shear stress in human coronary artery endothelial cells. *Am J Physiol Heart Circ Physiol*. **287(5)**, 2027-2034 (2004).

203 Besser, D. Elucidation of a signaling pathway induced by FGF-2 leading to uPA gene expression in NIH 3T3 fibroblasts. *Cell Growth Differ*. **6(8)**, 1009-1017 (1995).

204 Besser, D. Regulation of the urokinase-type plasminogen activator gene by the oncogene Tpr-Met involves GRB2. *Oncogene*. **14(6)**, 705-711 (1997).

205 Ried, S. Activation mechanisms of the urokinase-type plasminogen activator promoter by hepatocyte growth factor/scatter factor. *J Biol Chem*. **274(23)**, 16377-16386 (1999).

206 Dunn, S. E. Up-regulation of urokinase-type plasminogen activator by insulin-like growth factor-I depends upon phosphatidylinositol-3 kinase and mitogen-activated protein kinase kinase. *Cancer Res*. **61(4)**, 1367-1374 (2001).

207 Lengyel, E. Involvement of a mitogen-activated protein kinase signaling pathway in the regulation of urokinase promoter activity by c-Ha-ras. *J Biol Chem*. **270(39)**, 23007-23012 (1995).

208 Gum, R. Up-regulation of urokinase-type plasminogen activator expression by the HER2/neu proto-oncogene. *Anticancer Res*. **15(4)**, 1167-1172 (1995).

209 Miralles, F. UV irradiation induces the murine urokinase-type plasminogen activator gene via the c-Jun N-terminal kinase signaling pathway: requirement of an AP1 enhancer element. *Mol Cell Biol*. **18(8)**, 4537-4547 (1998).

210 Parra, M. The cJun N-terminal kinase (JNK) signaling pathway mediates induction of urokinase-type plasminogen activator (uPA) by the alkylating agent MNNG. *Blood*. **96(4)**, 1415-1424 (2000).

211 Lengyel, E. Stimulation of urokinase expression by TNF-alpha requires the activation of binding sites for the AP-1 and PEA3 transcription factors. *Biochim Biophys Acta*. **1268(1)**, 65-72 (1995).

212 Stacey, K. J. Regulation of urokinase-type plasminogen activator gene transcription by macrophage colony-stimulating factor. *Mol Cell Biol*. **15(6)**, 3430-3441 (1995).

213 Fowles, L. F. Regulation of urokinase plasminogen activator gene transcription in the RAW264 murine macrophage cell line by macrophage colony-stimulating

factor (CSF-1) is dependent upon the level of cell-surface receptor. *Biochem J*. **347**, 313-320 (2000).

214 Koziczak, M. E2F1-mediated transcriptional inhibition of the plasminogen activator inhibitor type 1 gene. *Eur J Biochem*. **268(18)**, 4969-4978 (2001).

215 Hansen, S. K. A novel complex between the p65 subunit of NF-kappa B and c-Rel binds to a DNA element involved in the phorbol ester induction of the human urokinase gene. *EMBO J*. **1(1)**, 205-213 (1992).

216 Hapke, S. Integrin alpha(v)beta(3)/vitronectin interaction affects expression of the urokinase system in human ovarian cancer cells. *J Biol Chem*. **276(28)**, 26349-26348 (2001).

217 von der Ahe, D. Macromolecular interaction on a cAMP responsive region in the urokinase-type plasminogen activator gene: a role of protein phosphorylation. *Nucleic Acids Res*. **18(8)**, 1991-1999 (1990).

218 Lee, J. S. Activation of cAMP-dependent protein kinase alters the chromatin structure of the urokinase-type plasminogen activator gene promoter. *Nucleic Acids Res*. **22(4)**, 569-575 (1994).

219 Menoud, P. A. Purification and cDNA cloning of a transcription factor which functionally cooperates within a cAMP regulatory unit in the porcine uPA gene. *Nucleic Acids Res*. **21(8)**, 1845-1852 (1993).

220 Soubt, M. K. Role of tissue-specific transcription factor LFB3 in a cyclic AMP-responsive enhancer of the urokinase-type plasminogen activator gene in LLC-PK1 cells. *Mol Cell Biol*. **18(8)**, 4698-4706 (1998).

221 Cannio, R. A cell-type specific and enhancer-dependent silencer in the regulation of the expression of the human urokinase plasminogen activator gene. *Nucleic Acids Res*. **19(9)**, 2303-2308 (1991).

222 Wang, W. Overexpression of urokinase-type plasminogen activator in pancreatic adenocarcinoma is regulated by constitutively activated RelA. *Oncogene*. **18(32)**, 4554-4563 (1999).

223 Hiendlmeyer, E. Beta-catenin up-regulates the expression of the urokinase plasminogen activator in human colorectal tumors. *Cancer Res*. **64(4)**, 1209-1214 (2004).

224 Pakneshan, P. Reversal of the hypomethylation status of urokinase (uPA) promoter blocks breast cancer growth and metastasis. *J Biol Chem*. **279(30)**, 31735-31744 (2004).

225 Guo, Y. Regulation of DNA methylation in human breast cancer. Effect on the urokinase-type plasminogen activator gene production and tumor invasion. *J Biol Chem*. **277(44)**, 41571-41579 (2002).

226 Casey, J. R. The structure of the urokinase-type plasminogen activator receptor gene. *Blood*. **84(4)**, 1151-1156 (1994).

227 Stewart, C. E. Characterisation of urokinase plasminogen activator receptor variants in human airway and peripheral cells. *BMC Mol Biol*. **10(75)**, 1-19 (2009).

228 Kristensen, P. Two alternatively spliced mouse urokinase receptor mRNAs with different histological localization in the gastrointestinal tract. *J Cell Biol*. **115(6)**, 1763-1771 (1991).

229 Pyke, C. An alternatively spliced variant of mRNA for the human receptor for urokinase plasminogen activator. *FEBS Lett*. **326(1-3)**, 69-74 (1993).

230 Wang, H. Transgenic mice demonstrate novel promoter regions for tissue-specific expression of the urokinase receptor gene. *Am J Pathol*. **163(2)**, 453-464 (2003).

231 Soravia, E. A conserved TATA-less proximal promoter drives basal transcription from the urokinase-type plasminogen activator receptor gene. *Blood*. **86(2)**, 624-635 (1995).

232 Dang, J. A region between -141 and -61 bp containing a proximal AP-1 is essential for constitutive expression of urokinase-type plasminogen activator receptor. *Eur J Biochem*. **264(1)**, 92-99 (1999).

233 Wang, Y. Identification of a novel nuclear factor-kappaB sequence involved in expression of urokinase-type plasminogen activator receptor. . *Eur J Biochem*. **267(11)**, 3248-3254 (2000).

234 Wang, H. The Kruppel-like KLF4 transcription factor, a novel regulator of urokinase receptor expression, drives synthesis of this binding site in colonic crypt luminal surface epithelial cells. *J Biol Chem*. **279(21)**, 22674-22683 (2004).

235 Lengyel, E. Requirement of an upstream AP-1 motif for the constitutive and phorbol ester-inducible expression of the urokinase-type plasminogen activator receptor gene. *J Biol Chem*. **271(38)**, 23176-23184 (1996).

236 Gum, R. Stimulation of urokinase-type plasminogen activator receptor expression by PMA requires JNK1-dependent and -independent signaling modules. *Oncogene*. **17(2)**, 213-225 (1998).

237 Lengyel, E. Elevated urokinase-type plasminogen activator receptor expression in a colon cancer cell line is due to a constitutively activated extracellular signal-regulated kinase-1-dependent signaling cascade. *Oncogene*. **14(21)**, 2563-2573 (1997).

238 Park, I. K. Sp1 mediates constitutive and transforming growth factor beta-inducible expression of urokinase type plasminogen activator receptor gene in human monocyte-like U937 cells. *Biochim Biophys Acta*. **1490(3)**, 302-310 (2000).

239 Hapke, S. beta(3)A-integrin downregulates the urokinase-type plasminogen activator receptor (u-PAR) through a PEA3/ets transcriptional silencing element in the u-PAR promoter. *Mol Cell Biol*. **21(6)**, 2118-2132 (2001).

240 Besta, F. Role of beta(3)-endonexin in the regulation of NF-kappaB-dependent expression of urokinase-type plasminogen activator receptor. *J Cell Sci*. **115**, 3879-3888 (2002).

241 Boyd, D. Determination of the levels of urokinase and its receptor in human colon carcinoma cell lines. *Cancer Res*. **48(11)**, 3112-3116 (1988).

242 Mohanam, S. Modulation of in vitro invasion of human glioblastoma cells by urokinase-type plasminogen activator receptor antibody. *Cancer Res*. **53(18)**, 4143-4147 (1993).

243 Schewe, D. M. Tumor-specific transcription factor binding to an activator protein-2/Sp1 element of the urokinase-type plasminogen activator receptor promoter in a first large series of resected gastrointestinal cancers. *Clin Cancer Res*. **9(6)**, 2267-2276 (2003).

244 Trisciuoglio, D. bcl-2 induction of urokinase plasminogen activator receptor expression in human cancer cells through Sp1 activation: involvement of ERK1/ERK2 activity. *J Biol Chem*. **279(8)**, 6737-6745 (2004).

245 Ginsburg, D. cDNA cloning of human plasminogen activator-inhibitor from endothelial cells. *J Clin Invest*. **78(6)**, 1673-1680 (1986).

246 Bosma, P. J. Different induction of two plasminogen activator inhibitor 1 mRNA species by phorbol ester in human hepatoma cells. *J Biol Chem*. **266(27)**, 17845-17849 (1991).

247 Descheemaeker, K. A. Interaction of AP-1-, AP-2-, and Sp1-like proteins with two distinct sites in the upstream regulatory region of the plasminogen activator inhibitor-1 gene mediates the phorbol 12-myristate 13-acetate response. *J Biol Chem*. **267(219)**, 15086-15091 (1992).

248 Arts, J. Role of c-Jun and proximal phorbol 12-myristate-13-acetate-(PMA)-responsive elements in the regulation of basal and PMA-stimulated plasminogen-activator inhibitor-1 gene expression in HepG2. *Eur J Biochem*. **241(2)**, 393-402 (1996).

249 Ding, H. Characterization of a helicase-like transcription factor involved in the expression of the human plasminogen activator inhibitor-1 gene. *DNA Cell Biol*. **15(6)**, 429-442 (1996).

250 Zhang, Q. Molecular cloning and characterization of P113, a mouse SNF2/SWI2-related transcription factor. *Gene*. **202(1-2)**, 31-37 (1997).

251 Riccio, A. Transforming growth factor beta 1-responsive element: closely associated binding sites for USF and CCAAT-binding transcription factor-nuclear factor I in the type 1 plasminogen activator inhibitor gene. *Mol Cell Biol*. **12(4)**, 1846-1855 (1992).

252 Dennler, S. Direct binding of Smad3 and Smad4 to critical TGF beta-inducible elements in the promoter of human plasminogen activator inhibitor-type 1 gene. *EMBO J*. **17(11)**, 3091-3010 (1998).

253 Song, C. Z. Smad4/DPC4 and Smad3 mediate transforming growth factor-beta (TGF-beta) signaling through direct binding to a novel TGF-beta-responsive element in the human plasminogen activator inhibitor-1 promoter. *J Biol Chem*. **273(45)**, 29287-29290 (1998).

254 Hua, X. Synergistic cooperation of TFE3 and smad proteins in TGF-beta-induced transcription of the plasminogen activator inhibitor-1 gene. *Genes Dev*. **12(19)**, 3084-3095 (1998).

255 Datta, P. K. Regulation of plasminogen activator inhibitor-1 expression by transforming growth factor-beta -induced physical and functional interactions between smads and Sp1. *J Biol Chem*. **275(51)**, 40014-40019 (2000).

256 Du, X. L. Hyperglycemia-induced mitochondrial superoxide overproduction activates the hexosamine pathway and induces plasminogen activator inhibitor-1 expression by increasing Sp1 glycosylation. *Proc Natl Acad Sci U S A*. **97(22)**, 12222-12226 (2000).

257 Goldberg, H. J. Glucosamine activates the plasminogen activator inhibitor 1 gene promoter through Sp1 DNA binding sites in glomerular mesangial cells. *Diabetes* **49(5)**, 863-871 (2000).

258 Chen, Y. Identification and localisation of a fatty acid response region in the human plasminogen activator inhibitor-1 gene. *Arterioscler Thromb Vasc Biol*. **20(12)**, 2696-2701 (2000).

259 Motojima, M. Sp1-like activity mediates angiotensin-II-induced plasminogen-activator inhibitor type-1 (PAI-1) gene expression in mesangial cells. *Biochem J*. **349**, 435-441 (2000).

260 Kooistra, T. Role of protein kinase C and cyclic adenosine monophosphate in the regulation of tissue-type plasminogen activator, plasminogen activator inhibitor-1, and platelet-derived growth factor mRNA levels in human endothelial cells. Possible involvement of proto-oncogenes c-jun and c-fos. *Arterioscler Thromb*. **11(4)**, 1042-1052 (1991).

261 Knudsen, H. A common response element mediates differential effects of phorbol esters and forskolin on type-1 plasminogen activator inhibitor gene expression in human breast carcinoma cells. *Eur J Biochem*. **220(1)**, 63-74 (1994).

262 Andreasen, P. A. Plasminogen activator inhibitors: hormonally regulated serpins. *Mol Cell Endocrinol*. **68(1)**, 1-19 (1990).

263 van Zonneveld, A. J. Type 1 plasminogen activator inhibitor gene: functional analysis and glucocorticoid regulation of its promoter. *Proc Natl Acad Sci U S A*. **85(15)**, 5525-5529 (1988).

264 Nordt, T. K. Augmentation of synthesis of plasminogen activator inhibitor type-1 in arterial endothelial cells by glucose and its implications for local fibrinolysis. *Arterioscler Thromb*. **13(12)**, 1822-1828 (1993).

265 Chen, Y. Q. Sp1 sites mediate activation of the plasminogen activator inhibitor-1 promoter by glucose in vascular smooth muscle cells. *J Biol Chem*. **273(14)**, 8225-8231 (1998).

266 Samad, F. Tissue factor gene expression in the adipose tissues of obese mice. *Proc Natl Acad Sci U S A*. **95(13)**, 7591-7596 (1998).

267 Hou, B. Tumor necrosis factor alpha activates the human plasminogen activator inhibitor-1 gene through a distal nuclear factor kappaB site. *J Biol Chem*. **279(18)**, 18127-18136 (2004).

268 Morange, P. E. Glucocorticoids and insulin promote plasminogen activator inhibitor 1 production by human adipose tissue. *Diabetes*. **48(4)**, 890-895 (1999).

269 Samad, F. Insulin continues to induce plasminogen activator inhibitor 1 gene expression in insulin-resistant mice and adipocytes. *Mol Med*. **6(8)**, 680-692 (2000).

270 Dawson, S. J. The two allele sequences of a common polymorphism in the promoter of the plasminogen activator inhibitor-1 (PAI-1) gene respond differently to interleukin-1 in HepG2 cells. *J Biol Chem*. **268(15)**, 10739-10745 (1993).

271 Eriksson, P. Allele-specific increase in basal transcription of the plasminogen-activator inhibitor 1 gene is associated with myocardial infarction. *Proc Natl Acad Sci U S A*. **92(6)**, 1851-1855 (1995).

272 Ryan, M. P. Complex regulation of plasminogen activator inhibitor type-1 (PAI-1) gene expression by serum and substrate adhesion. *Biochem J*. **314**, 1041-1046 (1996).

273 Fearns, C. Induction of plasminogen activator inhibitor 1 gene expression in murine liver by lipopolysaccharide. Cellular localisation and role of endogenous tumor necrosis factor-alpha. *Am J Pathol*. **150(2)**, 579-590 (1997).

274 Emeis, J. J. Interleukin 1 and lipopolysaccharide induce an inhibitor of tissue-type plasminogen activator in vivo and in cultured endothelial cells. *J Exp Med*. **163(5)**, 1260-1266 (1986).

275 Hopkins, W. E. Transcriptional regulation of plasminogen activator inhibitor type-1 mRNA in Hep G2 cells by epidermal growth factor. *Nucleic Acids Res*. **19(1)**, 163-168 (1991).

276 Ushiro, S. Heparin-binding epidermal growth factor-like growth factor: p91 activation induction of plasminogen activator/inhibitor, and tubular morphogenesis in human microvascular endothelial cells. *Jpn J Cancer Res*. **87(1)**, 68-77 (1996).

277 Pepper, M. S. Vascular endothelial growth factor (VEGF) induces plasminogen activators and plasminogen activator inhibitor-1 in microvascular endothelial cells. *Biochem Biophys Res Commun*. **181(2)**, 902-906 (1991).

278 Olofsson, B. Vascular endothelial growth factor B (VEGF-B) binds to VEGF receptor-1 and regulates plasminogen activator activity in endothelial cells. *Proc Natl Acad Sci U S A*. **95(20)**, 11709-11714 (1998).

279 Sandberg, T. Differential regulation of the plasminogen activator inhibitor-1 (PAI-1) gene expression by growth factors and progesterone in human endometrial stromal cells. *Mol Hum Reprod*. **3(9)**, 781-787 (1997).

280 Kunz, C. Differential regulation of plasminogen activator and inhibitor gene transcription by the tumor suppressor p53. *Nucleic Acids Res*. **23(18)**, 3710-3717 (1995).

281 Höckel, M. Tumor hypoxia: definitions and current clinical, biologic, and molecular aspects. *J Natl Cancer Inst*. **93(4)**, 266-276 (2001).

282 Wenger, R. H. Cellular adaptation to hypoxia: O2-sensing protein hydroxylases, hypoxia-inducible transcription factors, and O2-regulated gene expression. *FASEB J*. **16(10)**, 1151-1162 (2002).

283 Gertler, J. P. Ambient oxygen tension modulates endothelial fibrinolysis. *J Vasc Surg*. **18(6)**, 939-945 (1993).

284 Kietzmann, T. Induction of the plasminogen activator inhibitor-1 gene expression by mild hypoxia via a hypoxia response element binding the hypoxia-inducible factor-1 in rat hepatocytes. *Blood*. **94(12)**, 4177-4185 (1999).

285 Samoylenko, A. The upstream stimulatory factor-2a inhibits plasminogen activator inhibitor-1 gene expression by binding to a promoter element adjacent to the hypoxia-inducible factor-1 binding site. *Blood*. **97(9)**, 2657-2666 (2001).

286 Kietzmann, T. Regulation of the hypoxia-dependent plasminogen activator inhibitor 1 expression by MAP kinases. *Thromb Haemost*. **89(4)**, 666-673 (2003).

287 Zhang, Q. Crosstalk of hypoxia-mediated signaling pathways in upregulating plasminogen activator inhibitor-1 expression in keloid fibroblasts. *J Cell Physiol*. **199(1)**, 89-97 (2004).

288 Altus, M. S. Inhibition of protein synthesis in LLC-PK1 cells increases calcitonin-induced plasminogen-activator gene transcription and mRNA stability. *Biochem J*. **242(2)**, 387-392 (1987).

289 Altus, M. S. Protein synthesis inhibition stabilizes urokinase-type plasminogen activator mRNA. Studies in vivo and in cell-free decay reactions. *J Biol Chem*. **266(31)**, 21190-21196 (1991).

290 Ziegler, A. Protein kinase C down-regulation enhances cAMP-mediated induction of urokinase-type plasminogen activator mRNA in LLC-PK1 cells. *J Biol Chem*. **266(31)**, 21067-21074 (1991).

291 Ziegler, A. Ca2+ potentiates cAMP-dependent expression of urokinase-type plasminogen activator gene through a calmodulin- and protein kinase C-independent mechanism. *J Biol Chem*. **265(34)**, 21194-21201 (1990).

292 Wang, Y. Amiloride modulates urokinase gene expression at both transcription and post-transcription levels in human colon cancer cells. *Clin Exp Metastasis*. **13(3)**, 196-202 (1995).

293 Henderson, B. R. Dexamethasone decreases urokinase plasminogen activator mRNA stability in MAT 13762 rat mammary carcinoma cells. *Br J Cancer*. **67(1)**, 99-101 (1993).

294 Gaido, K. W. Post-transcriptional stabilization of urokinase plasminogen activator mRNA by 2,3,7,8-tetrachlorodibenzo-p-dioxin in a human keratinocyte cell line. *Toxicol Appl Pharmacol*. **133(1)**, 34-42 (1995).

295 Nambu, R. Multiple instability-regulating sites in the 3' untranslated region of the urokinase-type plasminogen activator mRNA. *Mol Cell Biol*. **14(7)**, 4920-4928 (1994).

296 Lagnado, C. A. AUUUA is not sufficient to promote poly(A) shortening and degradation of an mRNA: the functional sequence within AU-rich elements may be UUAUUUA(U/A)(U/A). *Mol Cell Biol*. **14(12)**, 7984-7995 (1994).

297 Zubiaga, A. M. The nonamer UUAUUUAUU is the key AU-rich sequence motif that mediates mRNA degradation. *Mol Cell Biol*. **15(4)**, 2219-2230 (1995).

298 Chen, C. Y. AU-rich elements: characterization and importance in mRNA degradation. *Trends Biochem Sci*. **20(11)**, 465-470 (1995).

299 Nambu, R. Enhanced stability of urokinase-type plasminogen activator mRNA in metastatic breast cancer MDA-MB-231 cells and LLC-PK1 cells down-regulated for protein kinase C--correlation with cytoplasmic heterogeneous nuclear ribonucleoprotein C. *Eur J Biochem*. **247(1)**, 169-174 (1997).

300 Tran, H. Stabilization of urokinase and urokinase receptor mRNAs by HuR is linked to its cytoplasmic accumulation induced by activated mitogen-activated protein kinase-activated protein kinase 2. *Mol Cell Biol*. **23(20)**, 7177-7188 (2002).

301 Han, Q. Rac1-MKK3-p38-MAPKAPK2 pathway promotes urokinase plasminogen activator mRNA stability in invasive breast cancer cells. *J Biol Chem*. **277(50)**, 48379-48385 (2002).

302 Tran, H. Facilitation of mRNA deadenylation and decay by the exosome-bound, DExH protein RHAU. *Mol Cell*. **13(1)**, 101-111 (2004).

303 Shetty, S. Protein synthesis and urokinase mRNA metabolism. *Mol Cell Biochem* **271**, 13-22 (2005).

304 Lund, L. R. Transcriptional and post-transcriptional regulation of the receptor for urokinase-type plasminogen activator by cytokines and tumour promoters in the human lung carcinoma cell line A549. *Biochem J*. **310**, 345-352 (1995).

305 Shetty, S. Regulation of urokinase receptor expression by phosphoglycerate kinase. *Am J Respir Cell Mol Biol*. **31(1)**, 100-106 (2004).

306 Wang, G. J. Posttranscriptional regulation of urokinase plasminogen activator receptor messenger RNA levels by leukocyte integrin engagement. *Proc Natl Acad Sci U S A*. **95(11)**, 6296-6301 (1998).

307 Montuori, N. Urokinase-type plasminogen activator up-regulates the expression of its cellular receptor through a post-transcriptional mechanism. *FEBS Lett*. **508(3)**, 379-384 (2001).

308 Montuori, N. Urokinase-mediated posttranscriptional regulation of urokinase-receptor expression in non small cell lung carcinoma. *Int J Cancer*. **105(3)**, 353-360 (2003).

309 Westerhausen, D. R. J. Multiple transforming growth factor-beta-inducible elements regulate expression of the plasminogen activator inhibitor type-1 gene in Hep G2 cells. *J Biol Chem*. **266(2)**, 1092-1100 (1991).

310 Fattal, P. G. Post-transcriptional regulation of expression of plasminogen activator inhibitor type 1 mRNA by insulin and insulin-like growth factor 1. *J Biol Chem*. **267(18)**, 12412-12415 (1992).

311 Heaton, J. H. Cyclic nucleotide regulation of type-1 plasminogen activator-inhibitor mRNA stability in rat hepatoma cells. Identification of cis-acting sequences. *J Biol Chem*. **273(23)**, 14261-14268 (1998).

312 Tillmann-Bogush, M. Cyclic nucleotide regulation of PAI-1 mRNA stability. Identification of cytosolic proteins that interact with an a-rich sequence. *J Biol Chem*. **274(2)**, 1172-1179 (1999).

313 Yeh, L. C. Regulation of expression of plasminogen activator inhibitor-1 in cultured rat osteoblastic cells by osteogenic protein-1 (BMP-7). *J Cell Biochem Suppl*. **36**, 46-54 (2001).

314 van Leeuwen, R. T. Angiotensin II increases plasminogen activator inhibitor type 1 and tissue-type plasminogen activator messenger RNA in cultured rat aortic smooth muscle cells. *Circulation*. **90(1)**, 362-368 (1994).

315 Takeda, K. Critical role of Rho-kinase and MEK/ERK pathways for angiotensin II-induced plasminogen activator inhibitor type-1 gene expression. *Arterioscler Thromb Vasc Biol*. **21(5)**, 868-873 (2001).

316 Shi, R. J. Post-transcriptional regulation of endothelial cell plasminogen activator inhibitor-1 expression during R. rickettsii infection. *Microb Pathog*. **28(3)**, 127-133 (2000).

317 Lee, Y. MicroRNA genes are transcribed by RNA polymerase II. *EMBO J*. **23(20)**, 4051-4060 (2004).

318 Gregory, R. I. The Microprocessor complex mediates the genesis of microRNAs. *Nature*. **432(7014)**, 235-240 (2004).

319 Han, J. The Drosha-DGCR8 complex in primary microRNA processing. *Genes Dev*. **18(24)**, 3016-3027 (2004).

320 Yi, R. Exportin-5 mediates the nuclear export of pre-microRNAs and short hairpin RNAs. *Genes Dev*. **17(24)**, 3011-3016 (2003).

321 Bernstein, E. Role for a bidentate ribonuclease in the initiation step of RNA interference. *Nature*. **409(6818)**, 363-366 (2001).

322 Gregory, R. I. Human RISC couples microRNA biogenesis and posttranscriptional gene silencing. *Cell*. **123(4)**, 631-640 (2005).

323 Brennecke, J. Principles of microRNA-target recognition. *PLoS Biol*. **3(3)**, 1-15 (2005).

324 Kiriakidou, M. An mRNA m7G cap binding-like motif within human Ago2 represses translation. *Cell*. **129(6)**, 1141-1151 (2007).

325 Thermann, R. Drosophila miR2 induces pseudo-polysomes and inhibits translation initiation. *Nature*. **447(7146)**, 875-878 (2007).

326 Mathonnet, G. MicroRNA inhibition of translation initiation in vitro by targeting the cap-binding complex eIF4F. *Science*. **317(5845)**, 1764-1767 (2007).

327 Bagga, S. Regulation by let-7 and lin-4 miRNAs results in target mRNA degradation. *Cell*. **122(4)**, 553-563 (2005).

328 Wu, L. MicroRNAs direct rapid deadenylation of mRNA. *Proc Natl Acad Sci U S A*. **103(11)**, 4034-4039 (2006).

329 Behm-Ansmant, I. mRNA degradation by miRNAs and GW182 requires both CCR4:NOT deadenylase and DCP1:DCP2 decapping complexes. *Genes Dev*. **20(14)**, 1885-1898 (2006).

330 Li, X. F. Downregulation of miR-193b contributes to enhance urokinase-type plasminogen activator (uPA) expression and tumor progression and invasion in human breast cancer. *Oncogene* **28(44)**, 3937-3948 (2009).

331 Iliopoulos, D. Inhibition of miR-193a expression by Max and RXR α activates K-Ras and PLAU to mediate distinct aspects of cellular transformation. *Cancer Res*. **71(15)**, 5144-5153 (2011).

332 Noh, H. Impaired MicroRNA Processing Facilitates Breast Cancer Cell Invasion by Upregulating Urokinase-Type Plasminogen Activator Expression. *Genes Cancer*. **2(2)**, 140-150 (2011).

333 Hu, Q. Interleukin enhancer-binding factor 3 promotes breast tumor progression by regulating sustained urokinase-type plasminogen activator expression. *Oncogene* **32(34)**, 3933-3943 (2013).

334 Xie, C. CFTR suppresses tumor progression through miR-193b targeting urokinase plasminogen activator (uPA) in prostate cancer. *Oncogene* **32(18)**, 2282-2291 (2013).

335 Salvi, A. Effects of miR-193a and sorafenib on hepatocellular carcinoma cells. *Mol Cancer*. **12(162)**, 1-15 (2013).

336 Salvi, A. MicroRNA-23b mediates urokinase and c-met downmodulation and a decreased migration of human hepatocellular carcinoma cells. *FEBS J*. **276(11)**, 2966-2982 (2009).

337 Au Yeung, C. L. Human papillomavirus type 16 E6 induces cervical cancer cell migration through the p53/microRNA-23b/urokinase-type plasminogen activator pathway. *Oncogene* **30(21)**, 2401-2410 (2011).

338 Hannafon, B. N. Exosome-mediated microRNA signaling from breast cancer cells is altered by the anti-angiogenesis agent docosahexaenoic acid (DHA). *Mol Cancer*. **14(1)** (2015).

339 Li, C. MiR-10a and miR-181c regulate collagen type I generation in hypertrophic scars by targeting PAI-1 and uPA. *FEBS Lett*. **589(3)**, 380-389 (2015).

340 Al-Ahmadi, W. miR-29a inhibition normalizes HuR over-expression and aberrant AU-rich mRNA stability in invasive cancer. *J Pathol*. **230(1)**, 28-38 (2013).

341 Lee, S. J. Over-expression of miR-145 enhances the effectiveness of HSVtk gene therapy for malignant glioma. *Cancer Lett*. **320(1)**, 72-80 (2012).

342 Falkenberg, N. MiR-221/-222 differentiate prognostic groups in advanced breast cancers and influence cell invasion. *Br J Cancer*. **190(10)**, 2714-2723 (2013).

343 Alfano, D. Urokinase receptor and CXCR4 are regulated by common microRNAs in leukaemia cells. *J Cell Mol Med*. **19(9)**, 2262-2272 (2015).

344 Falkenberg, N. Secreted uPAR isoform 2 (uPAR7b) is a novel direct target of miR-221. *Oncotarget*. **6(10)**, 8103-8114 (2015).

345 Sasayama, T. MicroRNA-10b is overexpressed in malignant glioma and associated with tumor invasive factors, uPAR and RhoC. *Int J Cancer*. **125(6)**, 1407-1413 (2009).

346 Sun, L. MicroRNA-10b induces glioma cell invasion by modulating MMP-14 and uPAR expression via HOXD10. *Brain Res*. **1389**, 9-18 (2011).

347 Liao, C. G. miR-10b is overexpressed in hepatocellular carcinoma and promotes cell proliferation, migration and invasion through RhoC, uPAR and MMPs. *J Transl Med*. **12(1)** (2014).

348 Martin, E. C. miR-155 induced transcriptome changes in the MCF-7 breast cancer cell line leads to enhanced mitogen activated protein kinase signaling. *Genes Cancer*. **5(9-10)**, 353-364 (2014).

349 Hwang, S. MicroRNA-146a suppresses metastatic activity in brain metastais. *Mol. Cells* **34(3)**, 329-334 (2012).

350 Patel, N. MicroRNA-30c promotes human adipocyte differentiation and co-represses PAI-1 and ALK2. *Biochem J*. **434(3)**, 473-482 (2011).

351 Karbiener, M. MicroRNA-30c promotes human adipocyte differentiation and co-represses PAI-1 and ALK2. *RNA Biol*. **8(59)**, 850-860 (2011).

352 Marchand, A. miR-421 and miR-30c inhibit SERPINE 1 gene expression in human endothelial cells. *PLoS One*. **7(8)**, 1-9 (2012).

353 Zhu, E. D. miR-30b, Down-Regulated in Gastric Cancer, Promotes Apoptosis and Suppresses Tumor Growth by Targeting Plasminogen Activator Inhibitor-1. *PloS One*. **9(8)**, 1-12 (2014).

354 Umemura, K. Roles of microRNA-34a in the pathogenesis of placenta accreta. *J Obstet Gynaecol Res*. **39(1)**, 67-74 (2013).

355 Savarimuthu Francis, S. M. MicroRNA-34c is associated with emphysema severity and modulates SERPINE1 expression. *BMC Genomics*. **15(88)**, 1-8 (2014).

356 Kang, H. J. Involvement of miR-34c in high glucose-insulted mesenchymal stem cells leads to inefficient therapeutic effect on myocardial infarction. *Cell Signal*. **27(11)**, 2241-2251 (2015).

357 Rio, D. C. Reverse transcription-polymerase chain reaction. *Cold Spring Harb Protoc*. **2014(11)**, 1207-1216 (2014).

358 Sambrook, J. Agarose gel electrophoresis. *CSH Protoc*. **2006(1)** (2006).

359 Livak, K. J. Analysis of relative gene expression data using real-time quantitative PCR and the 2(-Delta Delta C(T)) Method. *Methods*. **25(4)**, 402-408 (2001).

360 Heiner, C. R. Sequencing multimegabase-template DNA with BigDye terminator chemistry. *Genome Res*. **8(5)**, 557-561 (1998).

361 Irizarry, R. A. Summaries of Affymetrix GeneChip probe level data. *Nucleic Acids Res*. **31(4)**, 1-8 (2003).

362 Irizarry, R. A. Exploration, normalization, and summaries of high density oligonucleotide array probe level data. *Biostatistics*. **4(2)**, 249-264 (2003).

363 Bolstad, B. M. A comparison of normalization methods for high density oligonucleotide array data based on variance and bias. *Bioinformatics*. **19(2)**, 185-193 (2003).

364 Benjamini, Y. Controlling the False Discovery Rate: A Practical and Powerful Approach to Multiple Testing. *J.R. Statist. Soc. B* **57(1)**, 289-300 (1995).

365 Rønne, E. Cell-induced potentiation of the plasminogen activation system is abolished by a monoclonal antibody that recognizes the NH2-terminal domain of the urokinase receptor. *FEBS Lett*. **288(1-2)**, 233-236 (1991).

366 Sambrook, J. SDS-Polyacrylamide Gel Electrophoresis of Proteins. *CSH Protoc*. **2006(4)** (2006).

367 Atienza, J. M. Dynamic monitoring of cell adhesion and spreading on microelectronic sensor arrays. *J Biomol Screen*. **10(8)**, 795-805 (2005).

368 Jørgensen, S. Robust one-day in situ hybridization protocol for detection of microRNAs in paraffin samples using LNA probes. *Methods*. **52(4)**, 375-381 (2010).

369 Nielsen, B. S. High levels of microRNA-21 in the stroma of colorectal cancers predict short disease-free survival in stage II colon cancer patients. *Clin Exp Metastasis*. **28(1)**, 27-38 (2011).

370 Rhodes, D. R. ONCOMINE: a cancer microarray database and integrated data-mining platform. *Neoplasia*. **6(1)**, 1-6 (2004).

371 Reinhold, W. C. CellMiner: a web-based suite of genomic and pharmacologic tools to explore transcript and drug patterns in the NCI-60 cell line set. *Cancer Res*. **72(14)**, 3499-3511 (2012).

372 Betel, D. The microRNA.org resource: targets and expression. *Nucleic Acids Res*. **36**, 149-153 (2008).

373 Enright, A. J. MicroRNA targets in Drosophila. *Genome Biol*. **5(1)**, 1-14 (2003).

374 Lewis, B. P. Prediction of mammalian microRNA targets. *Cell*. **115(7)**, 787-798 (2003).

375 Pruitt, K. D. NCBI reference sequences (RefSeq): a curated non-redundant sequence database of genomes, transcripts and proteins. *Nucleic Acids Res*. **35**, 32-36 (2007).

376 Madden, S. F. BreastMark: an integrated approach to mining publicly available transcriptomic datasets relating to breast cancer outcome. *Breast Cancer Res*. **15(4)**, 1-14 (2013).

377 Chen, E. Y. Enrichr: interactive and collaborative HTML5 gene list enrichment analysis tool. *BMC Bioinformatics*. **14** (2013).

378 Ludbrook, J. Analysis of 2 x 2 tables of frequencies: matching test to experimental design. *Int J Epidemiol*. **37(6)**, 1430-1435 (2008).

379 Dunnett, C. W. A multiple comparison procedure for comparing several tratements with a control. *Journal of the American Statistical Association* **50(272)**, 1096-1121 (1955).

380 Meng, S. HER-2 gene amplification can be acquired as breast cancer progresses. *Proc Natl Acad Sci U S A*. **101(25)**, 9393-9398 (2004).

381 Nassar, A. Correlation of HER2 overexpression with gene amplification and its relation to chromosome 17 aneuploidy: a 5-year experience with invasive ductal and lobular carcinomas. *Int J Clin Exp Pahol*. **7(9)**, 6254-6261 (2014).

382 Mestdagh, P. A novel and universal method for microRNA RT-qPCR data normalization. *Genome Biol*. **10(6)**, 1-10 (2009).

383 Betel, D. Comprehensive modeling of microRNA targets predicts functional non-conserved and non-canonical sites. *Genome Biol*. **11(8)**, 1-14 (2010).

384 Yamashita, D. miR-340 suppresses the stem-like cell function of glioma-initiating cells by targeting tissue plasminogen activator. *Cancer Res*. **75(6)**, 1123-1133 (2015).

385 Zhou, J. microRNA-340-5p Functions Downstream of Cardiotrophin-1 to Regulate Cardiac Eccentric Hypertrophy and Heart Failure via Target Gene Dystrophin. *Int Heart J*. **56(4)**, 454-458 (2015).

386 Guerau-de-Arellano, M. Micro-RNA dysregulation in multiple sclerosis favours pro-inflammatory T-cell-mediated autoimmunity. *Brain*. **134**, 3578-3589 (2011).

387 Wu, Z. S. miR-340 inhibition of breast cancer cell migration and invasion through targeting of oncoprotein c-Met. *Cancer* **117(13)**, 2842-2852 (2011).

388 Takeyama, H. Decreased miR-340 expression in bone marrow is associated with liver metastasis of colorectal cancer. *Mol Cancer Ther*. **13(4)**, 976-985 (2014).

389 Zhou, X. MicroRNA-340 suppresses osteosarcoma tumor growth and metastasis by directly targeting ROCK1. *Biochem Biophys Res Commun*. **437(4)**, 653-658 (2013).

390 Cai, H. Combined microRNA-340 and ROCK1 mRNA profiling predicts tumor progression and prognosis in pediatric osteosarcoma. *Int J Mol Sci*. **15(1)**, 560-573 (2014).

391 Huang, D. miR-340 suppresses glioblastoma multiforme. *Oncotarget*. **6(11)**, 9257-9270f (2015).

392 Das, S. Modulation of neuroblastoma disease pathogenesis by an extensive network of epigenetically regulated microRNAs. *Oncogene* **32(24)**, 2927-2936 (2013).

393 Sun, Y. miR-124, miR-137 and miR-340 regulate colorectal cancer growth via inhibition of the Warburg effect. *Oncol Rep*. **28(4)**, 1346-1352 (2012).

394 Shi, L. miR-340 Reverses Cisplatin Resistance of Hepatocellular Carcinoma Cell Lines by Targeting Nrf2-dependent Antioxidant Pathway. *Asian Pac J Cancer Prev*. **15(23)**, 10439-10444 (2014).

395 Fernandez, S. miR-340 inhibits tumor cell proliferation and induces apoptosis by targeting multiple negative regulators of p27 in non-small cell lung cancer. *Oncogene* **34(25)**, 3240-3250 (2014).

396 Li, X. miR-340 inhibits glioblastoma cell proliferation by suppressing CDK6, cyclin-D1 and cyclin-D2. *Biochem Biophys Res Commun*. **460(3)**, 670-677 (2015).

397 Wells, J. E. Deregulated expression of connective tissue growth factor (CTGF/CCN2) is linked to poor outcome in human cancer. *Int J Cancer*. **137(3)**, 504-511 (2015).

398 Knipe, R. S. The Rho kinases: critical mediators of multiple profibrotic processes and rational targets for new therapies for pulmonary fibrosis. *Pharmacol Rev*. **67(1)**, 103-117 (2015).

399 Liu, F. Mechanosignaling through YAP and TAZ drives fibroblast activation and fibrosis. *Am J Physiol Lung Cell Mol Physiol*. **308(4)**, 344-357 (2015).

400 Walker, R. A. The complexities of breast cancer desmoplasia. *Breast Cancer Res*. **3(3)**, 143-145 (2001).

401 Mahadevan, D. Tumor-stroma interactions in pancreatic ductal adenocarcinoma. *Mol Cancer Ther*. **6(4)**, 1186-1197 (2007).

402 Cox, T. R. LOX-mediated collagen crosslinking is responsible for fibrosis-enhanced metastasis. *Cancer Res*. **73(6)**, 1721-1732 (2013).

403 Kodaka, M. The mammalian Hippo pathway: regulation and function of YAP1 and TAZ. *Cell Mol Life Sci*. **72(2)**, 285-306 (2015).

404 Carbery, I. D. Targeted Genome Modification in Mice Using Zinc-Finger Nucleases. *Genetics*. **186(2)**, 451-459 (2010).

405 Huang, S. Urokinase plasminogen activator/urokinase-specific surface receptor expression and matrix invasion by breast cancer cells requires constitutive p38alpha mitogen-activated protein kinase activity. *J Biol Chem*. **275(16)**, 12266-12272 (2000).

406 Trisciuoglio, D. bcl-2 induction of urokinase plasminogen activator receptor expression in human cancer cells through Sp1 activation: involvement of ERK1/ERK2 activity.\. *J Biol Chem*. **279(8)**, 6737-6745 (2004).

407 Lee, J. A. Forty years later and the role of plasminogen activator inhibitor type 2/SERPINB2 is still an enigma. *Semin Thromb Hemost*. **37(4)**, 395-407 (2011).

408 Duggan, C. Plasminogen activator inhibitor type 2 in breast cancer. *Br J Cancer*. **76(5)**, 622-627 (1997).

409 Jing, Q. Involvement of microRNA in AU-rich element-mediated mRNA instability. *Cell*. **120(5)**, 623-634 (2005).

410 Chen, C. Real-time quantification of microRNAs by stem–loop RT–PCR. *Nucleic Acids Res*. **33(20)**, 1-9 (2005).

411 Cox, T. R. The hypoxic cancer secretome induces pre-metastatic bone lesions through lysyl oxidase. *Nature*. **522(7554)**, 106-110 (2015).

412 Jiang, Y. Evaluation of genetic variants in microRNA biosynthesis genes and risk of breast cancer in Chinese women. *Int J Cancer*. **133(9)**, 2216-2224 (2013).

413 Avery-Kiejda, K. A. The expression of Dicer and Drosha in matched normal tissues, tumours and lymph node metastases in triple negative breast cancer. *BMC Cancer*. **14(253)**, 2407-2414 (2014).

414 Zhi, X. YAP Promotes Breast Cell Proliferation and Survival Partially through Stabilizing the KLF5 Transcription Factor. *Am J Pathol*. **180(6)**, 2452-2461 (2012).

415 Lamar, J. M. The Hippo pathway target, YAP, promotes metastasis through its TEAD-interaction domain. *Proc Natl Acad Sci U S A*. **109(37)**, 2441-2450 (2012).

416 Koziczak, M. Pocket protein-independent repression of urokinase-type plasminogen activator and plasminogen activator inhibitor 1 gene expression by E2F1. *Mol Cell Biol*. **20(6)**, 2014-2022 (2000).

417 Park, C. Y. Analysis of microRNA knockouts in mice. *Hum Mol Genet*. **19(R2)**, 169-175 (2010).

418 Almholt, K. Extracellular Proteolysis in Transgenic Mouse Models of Breast Cancer. *J Mammary Gland Biol Neoplasia*. **12**, 83-97 (2007).

419 Du, Z. Introduction of oncogenes into mammary glands in vivo with an avian retroviral vector initiates and promotes carcinogenesis in mouse models. *Proc Natl Acad Sci U S A*. **103(46)**, 17396-17401 (2006).

10. ACKNOWLEDGEMENTS

The accomplishment of this project has been possible thank to the involvement and help of several people. Firstly, I would like to thank our collaborators Dr. Paul Span (Radboud University Nijmegen Medical Centre) who kindly provided the DNA and cDNA samples of the unselected cross-section of primary breast cancer patients and Dr. Stephen Madden (NCBI, Dublin) for the microarray data analysis. Some experiments were performed by the IFOM facilities including qPCR, sequencing, microarray, transgenic, imaging, cell biology and tissue processing units. A special thank goes to the "the foster" Elisa Allievi who together with Ambra Belpietro and Eleonora Verga have been much more than the Transgenic Facility's girls. Furthermore, I would like to say that our laboratory day life would have not been so confortable without the IFOM services including IT, kitchen, warehouse, maintenance and animal house services.

This educational path was possible and successful thanks to my supervisor Dr. Nicolai Sidenius who believed in me and gave me the opportunity to develop this project suitable to my skills even though it was far from his research interests. I would like also to thank my PhD advisors Dr. Ugo Cavallaro (IEO, Milan) who followed my project and my progress during this period and Dr. Thomas Bugge (NIH, Bethesda, MD) especially for his suggestions about the generation of the Mir340 knock out mouse model. Likewise I am grateful to my PhD examiners Dr. Pasquale Verde (IGB, Naples) and Dr. Stefano Casola (IFOM, Milan) for the thesis correction and their precious suggestions about the project. In particular, Dr. Stefano Casola followed my career and personal scientific issues beyond its role of internal PhD examiner. I would like to thank the SEMM office people, Dr. Francesca Fiore and Dr. Veronica Viscardi who always took care of PhD students, helping us with bureaucracy issues and PhD deadlines.

Finally, I would thank all the people who made these four years very special. First of all people belonging to my group like Gian Maria who made every single moment of the laboratory life amazing and my buddy Valentina De Lorenzi who always supported me and whose company I always enjoyed. The lab F members especially my personal bioinformatics Federica Zanardi and my travel buddies Valentina Petrocelli e Lara Sicouri with whom I shared every moment of this PhD. I would also thank my PhD classmates, especially Roberto Cuttano, Francis Kobia and Emiliana Tognon who spent loads of time with me in library making the thesis writing much more enjoyable. Finally, I would thank those people who have always been part of my life, my family and my best friends Manuela, Andrea and Rosangela. Last but not least, a big thank to the most important gift that this experience gave to me, my boyfriend Andrea Piontini for the *in vivo* experiment training and because he lovely stands by me every day in spite of my complicated personality.